Atomistic Simulations
for Industrial Applications

Volker Eyert

Materials Design Inc.

8 October 2014

Agenda

▶ Company Profile Materials Design, Inc.

- Products and Services: Software and Consulting

▶ Challenges and Solutions

- Capabilities of the MedeA® software environment

▶ Current trends in materials research

- Thermo-mechanical properties, material fatigue, ageing effects
- Battery materials
- Electronic and thermal conductivity, thermoelectricity

▶ Summary and Perspectives

Company Profile

materials design

▶ Founded by scientists in 1998

▶ Over 400 customers in industry, universities, and government laboratories including over 50 major companies worldwide

▶ Products: **MedeA**® software, support and consulting services

▶ Global: Offices in San Diego, Angel Fire, Paris and Stockholm

▶ Business partners: Japan, Korea, China, Taiwan, Singapore, and India

▶ Core competence in

- Computational chemistry & physics
- Materials science & chemical engineering
- Materials property databases & software engineering

Customers

Energy	Metals & Alloys	Chemicals	Oil & Gas
Electronics	Automotive & Aerospace	Glass & Ceramics	Mining & Drilling

Universities and Government R&D Laboratories

Customers

12 world largest companies by revenue

Ranking	Name	Industry	Revenue (USD billions)	FY	Capitalization (USD billions)	Employees	Listing	Headquarters	CEO	Ref(s)
1	Exxon Mobil	Oil and gas	$491	December 31, 2013	$438	76,900	NYSE: XOM	Irving, Texas	Rex W. Tillerson	[2]
2	Sinopec Group	Oil and gas	$486	December 31, 2013		401,000	-	Beijing	Wang Tianpu	[3]
3	Royal Dutch Shell	Oil and gas	$478	December 31, 2013	$243	90,000	LSE: RDSA	The Hague; London	Ben van Beurden	[4]
4	Wal-Mart Stores, Inc	Retail	$476	January 31, 2014	$203	2,200,000	NYSE: WMT	Bentonville, Arkansas	Doug McMillon	[5]
5	China National Petroleum Corporation	Oil and gas	$455	December 31, 2013		1,668,072	—	Beijing	Zhou Jiping	[6]
6	BP	Oil and gas	$379	December 31, 2013	$89	83,900	LSE: BP	London	Bob Dudley	[7]
7	Saudi Aramco	Oil and gas	$365	2011		54,041	—	Dhahran	Khalid A. Al-Falih	[8]
8	State Grid Corporation of China	Electric utility	$338	2013		1,564,000	—	Beijing	Liu Zhenya	[9]
9	Vitol	Commodities	$307	2013		5,441	—	Rotterdam; Geneva	Ian Taylor	[10]
10	Volkswagen Group	Automotive	$263	December 31, 2013	$77	572,800	ISIN: DE0007664005	Wolfsburg	Martin Winterkorn	[11]
11	Total	Oil and gas	$253	December 31, 2013	$120	98,799	Euronext: FP	Courbevoie	Christophe de Margerie	[12]
12	Toyota	Automotive	$249	March 31, 2014	$149	326,000	TYO: 7203; NYSE: TM	Toyota, Aichi	Akio Toyoda	[13]

Products and Services

▶ **MedeA® software**

- Comprehensive atomistic modeling environment with leading technology
- Installation, training, online support, and maintenance
- Scientific/technological interactions
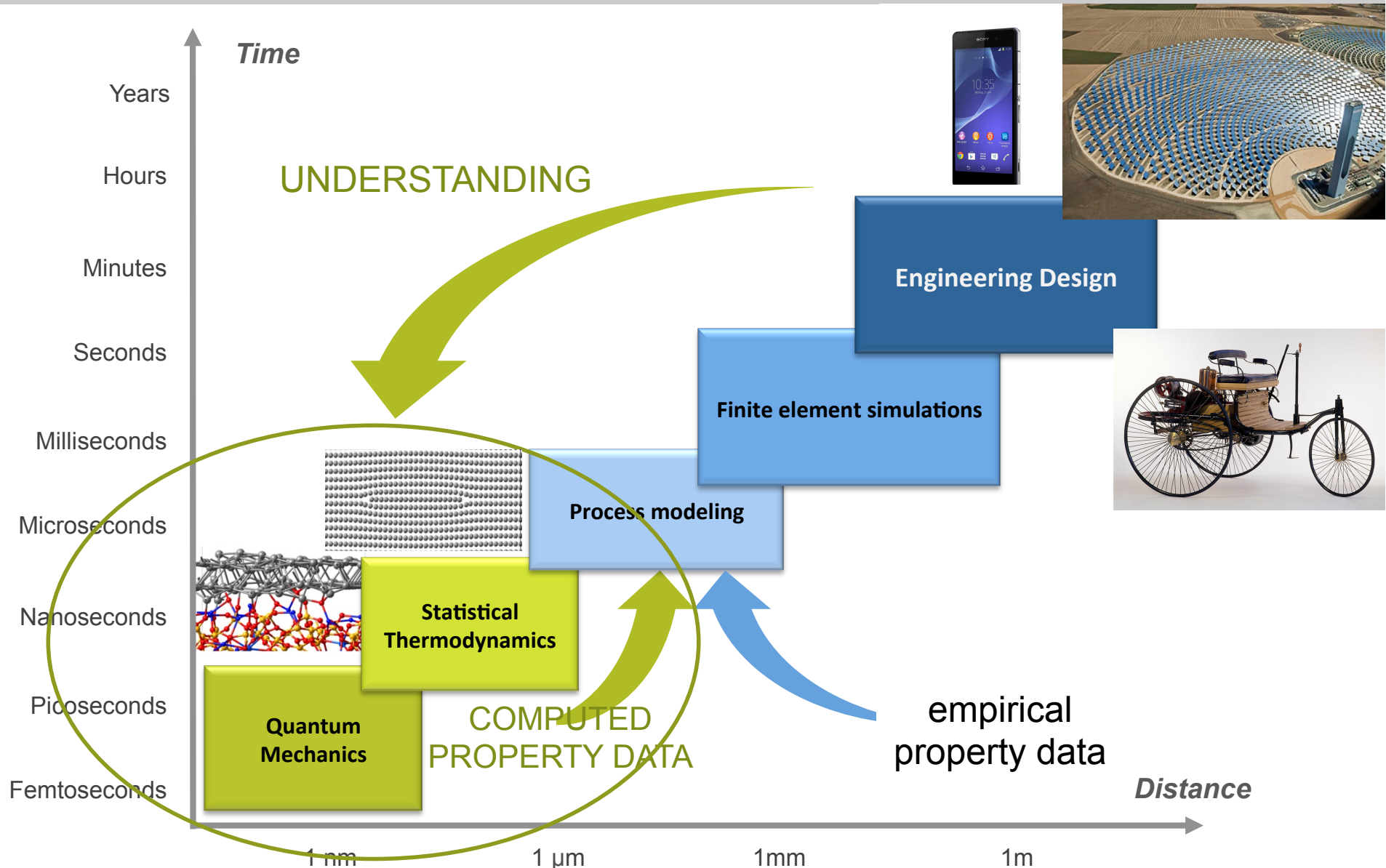- Yearly users group meetings (Philadelphia, Oct 21-23, 2014)

▶ **Contract research**

- Solution of specific industrial problems
- Leverages expertise and resources of MD's scientists
- Publicly funded programs

▶ **Technology partnerships**

- Development of customized modeling capabilities (e.g. Toyota)

Technology Positioning

Time

- Years
- Hours — UNDERSTANDING
- Minutes
- Seconds
- Milliseconds
- Microseconds
- Nanoseconds
- Picoseconds
- Femtoseconds

Engineering Design

Finite element simulations

Process modeling

Statistical Thermodynamics

Quantum Mechanics

COMPUTED PROPERTY DATA

empirical property data

Distance

1 nm   1 µm   1mm   1m

Goal of Atomistic Simulations

MedeA®: Software for Efficient R&D

Understanding on the level of electrons and atoms
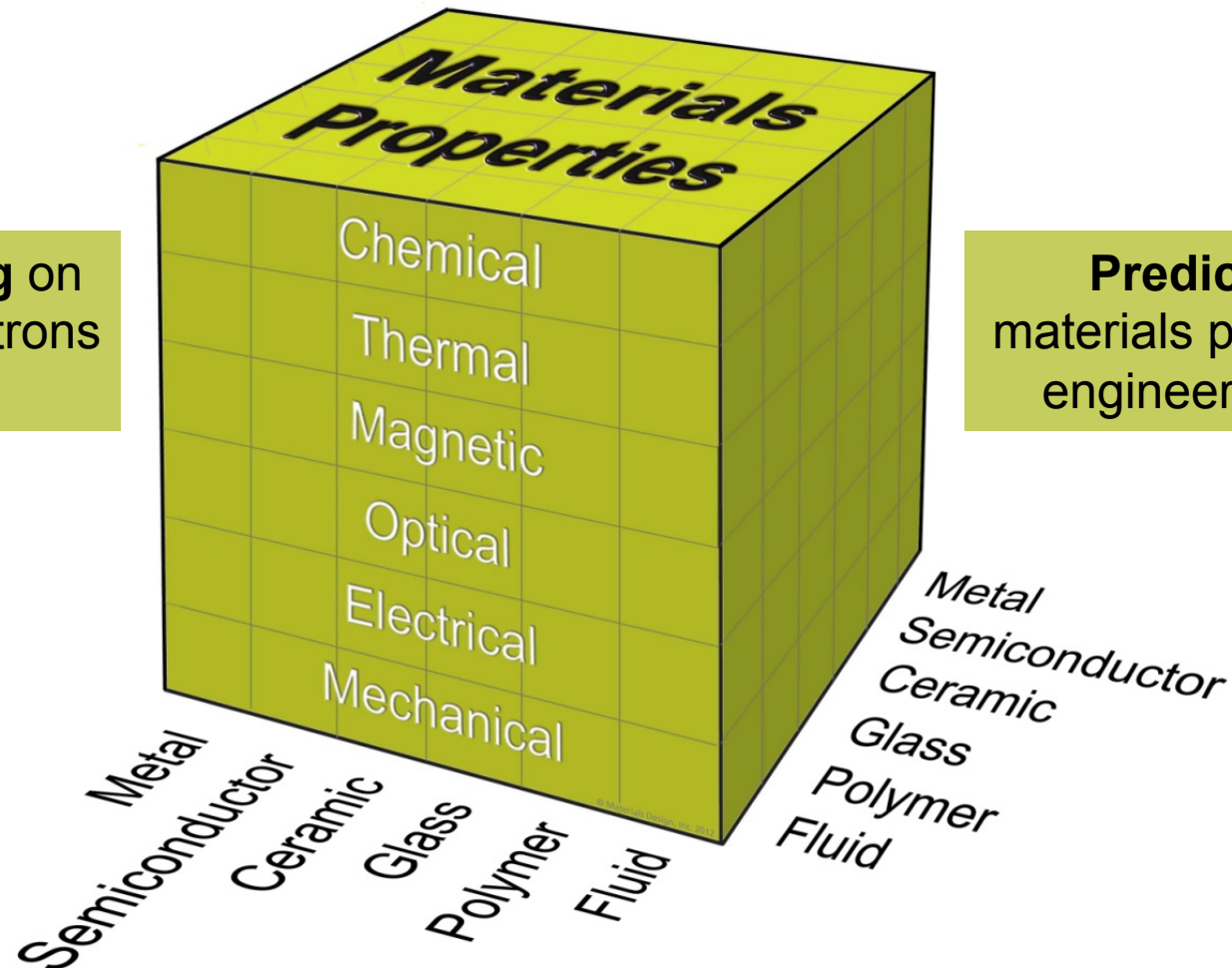
Prediction of materials properties of engineering value

© Materials Design, Inc. 2014

Materials **E**xploration and **De**sign **A**nalysis

MedeA® Software

MODELING & ANALYSIS

Builders: crystals, defects, interfaces, surfaces, molecules, nanostructures, polymers, amorphous materials

Analysis: geometry, band structures and DOS, electron and spin density, potential, Fermi surface, phonons, transition states, dynamics trajectories

Job Server

DATABASES

Experimental and Computed Structure and Property Data

ICSD	NIST Crystal Data	Pauling	Pearson	Computed

Task Servers

Mechanical   Thermal   Chemical   Kinetic   Electric   Optic   Magnetic

COMPUTATION OF PROPERTIES

ab initio QM - **VASP**	Semi-empirical - **MOPAC**	Monte Carlo - **GIBBS**	Mol. dynamics - **LAMMPS**
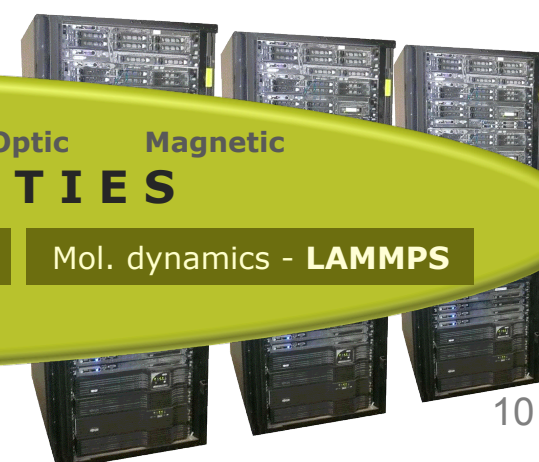
Electronic Properties

Accurate Band Structures

Ge
Energy Band Structure and Density of States
spin-orbit relativistic, HSE06 hybrid functional, VASP 5.2
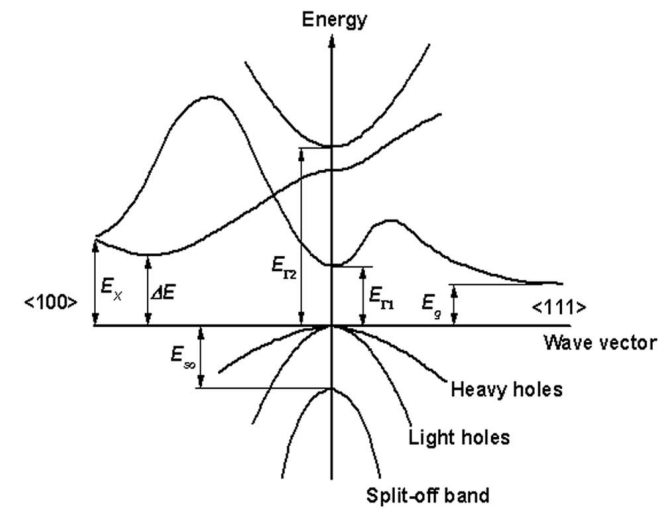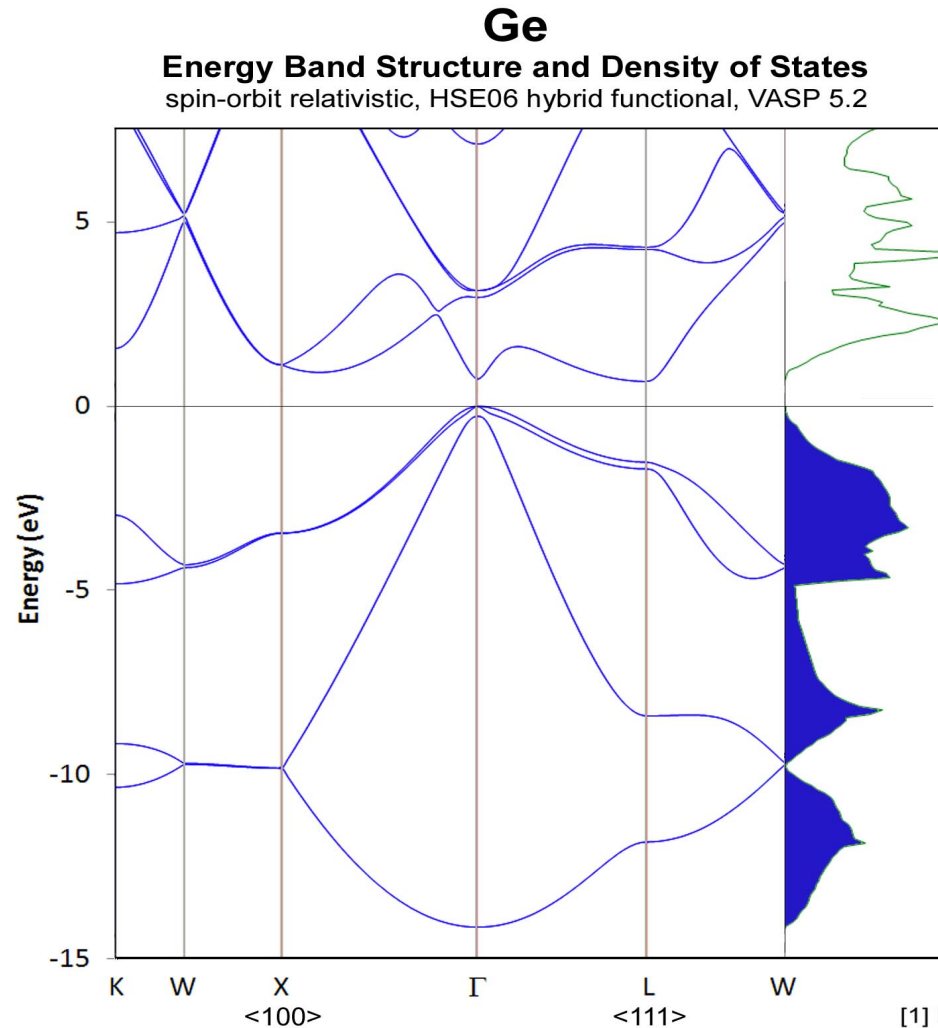
Expt. [1]		Computed
300 K	E_g = 0.66 eV	0.66
	E_x = 1.2 eV	1.12
	$E_{\Gamma 1}$ = 0.8 eV	0.73
	$E_{\Gamma 2}$ = 3.22 eV	3.14
	ΔE = 0.85 eV	0.91
	E_{so} = 0.29 eV	0.29

[1] http://www.ioffe.rssi.ru/SVA/NSM/ Semicond/Ge/bandstr.html

Note: Standard LDA or GGA predicts Ge to be metallic

Accuracy of Computed Band Gaps
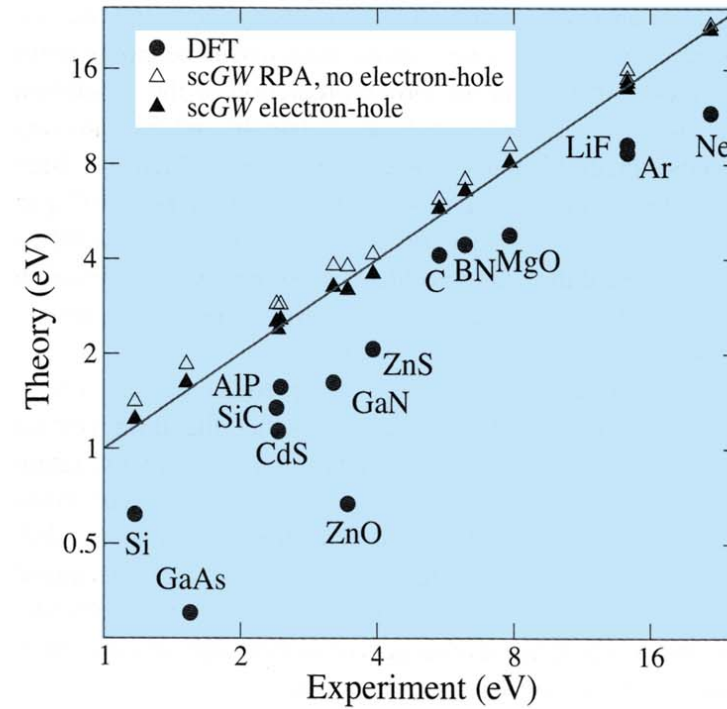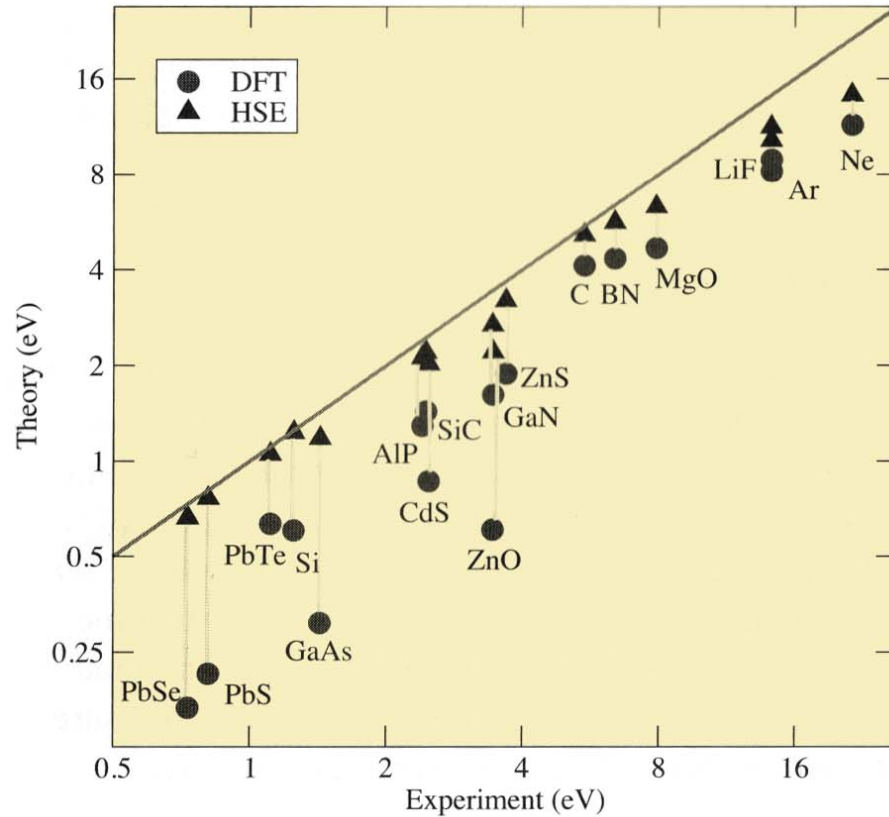
Performance of VASP 5.2 as reviewed by
J. Hafner, J. Phys.: Condens. Matter **22**, 384205 (2010)

Design of III-V Alloys

▶ Which III-V alloy has a band gap around 0.5 eV and the largest Γ-L separation?
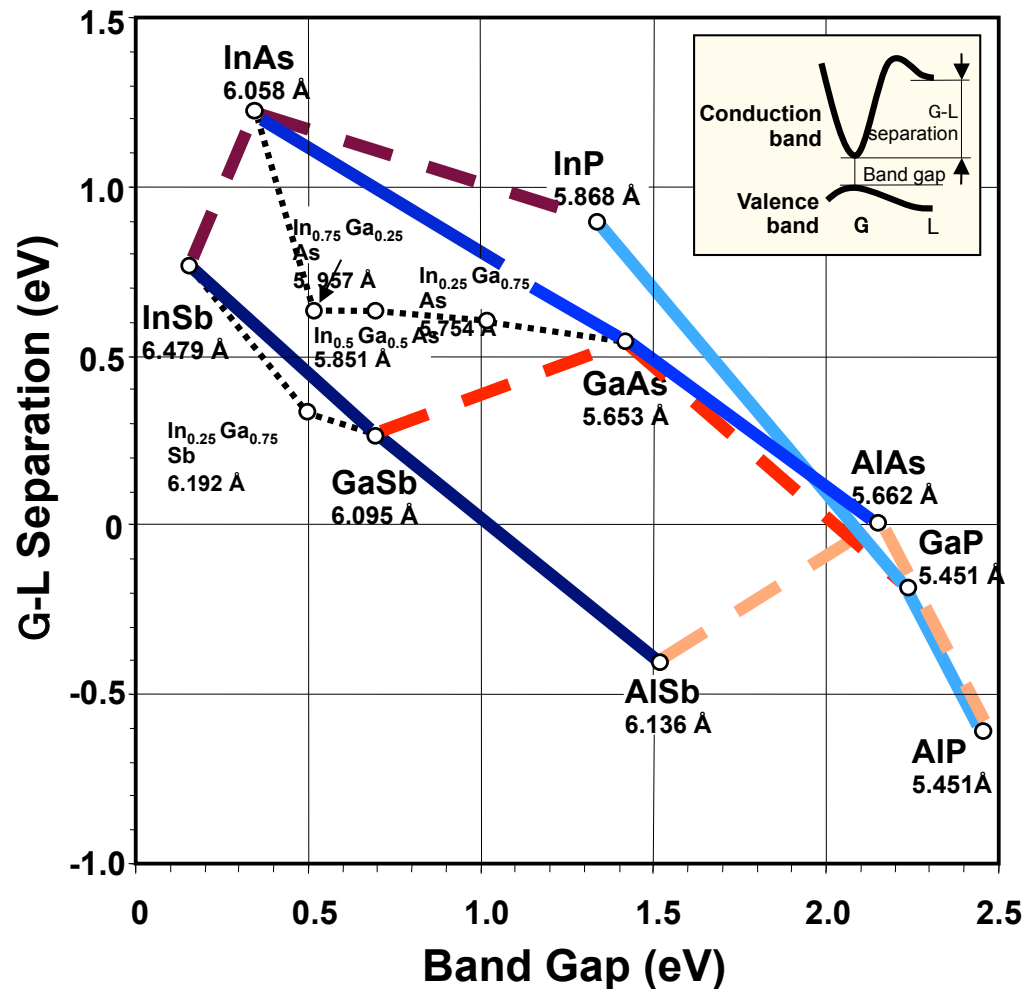
AX with
A = Al,Ga,In
X = P, As, Sb

Geller et al.,
Appl. Phys. Lett.
79, 368 (2001)

Computations: Source of Reliable Data

Band structure engineering
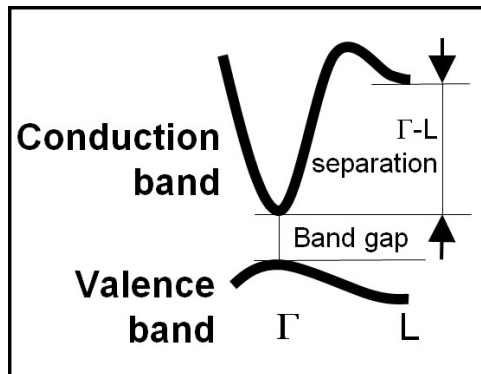
The $\Gamma-L$ and $\Gamma-X$ separations (cf. Table I) show an overall better performance of sX compared with LDA. A remarkable case is the $\Gamma-L$ separation in InAs. The most often reported experimental value is 0.74 eV,[15] whereas sX gives 1.21 eV. Recent measurements, by using improved techniques, resulted in a revised value of 1.10 ± 0.05 eV.[17] A systematic investigation of effective masses reveals a similar picture, namely, that sX improves the overall agreement with experiment. In particular, the performance of sX in predicting m_c^{Γ} is rather remarkable (cf. Table II). Never-

Geller et al., Appl. Phys. Lett. **79**, 368 (2001)

Elastic Properties, Phonons

Aluminum Nitride
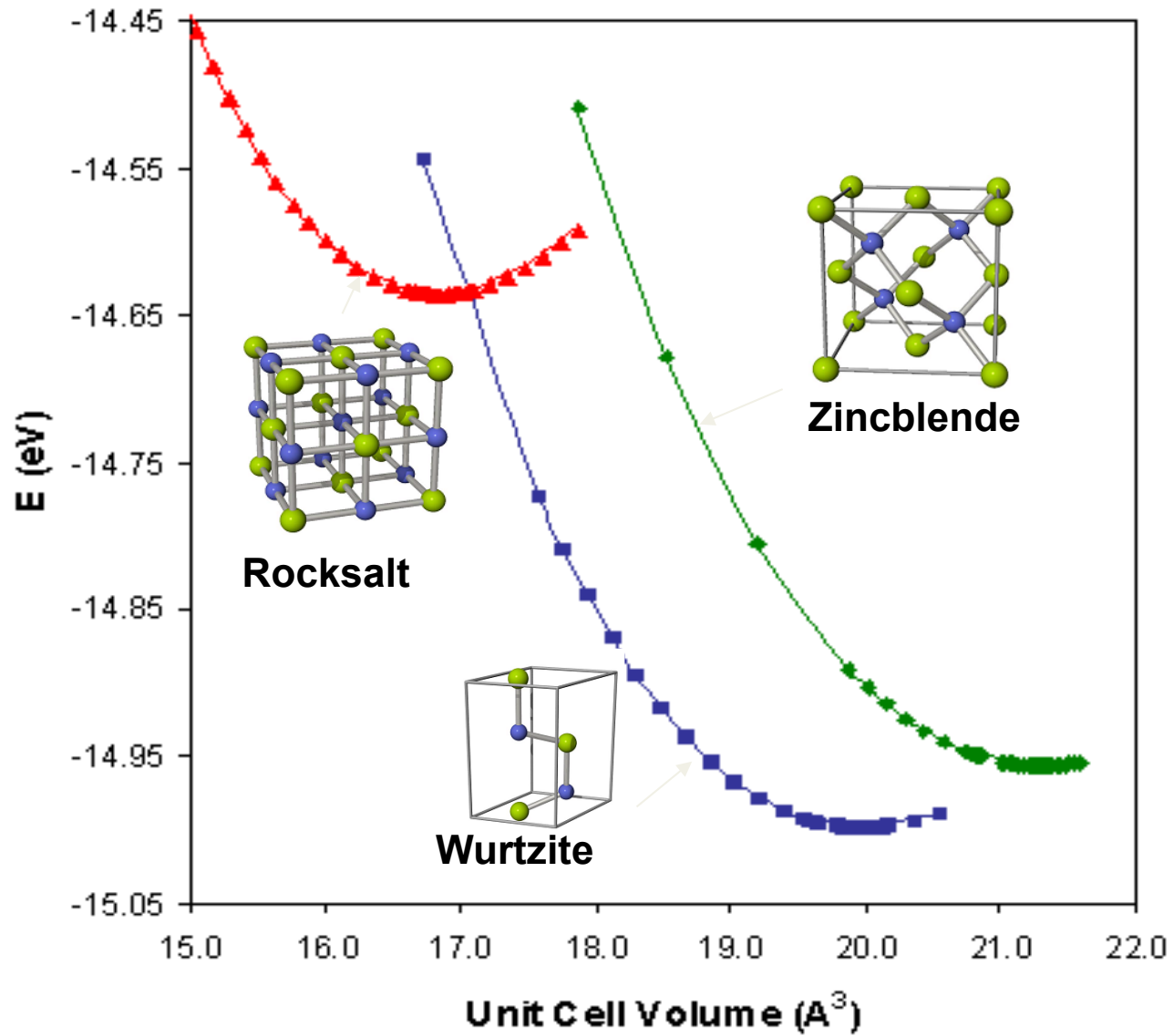
Aluminum Nitride

(GPa)	Expt[1]	Expt[2]	Calculated
C_{11}	345	411	375
C_{12}	125	149	130
C_{13}	120	99	100
C_{33}	395	389	347
C_{44}	118	125	113
C_{66}	110	131	122
B	202	212	195

1. K.Tsubouchi, N. Mikoshiba, IEEE Trans. Sonics Ultrason. **SU-32**, 634 (1985)

2. L.E. McNeil, M. Grimsditch, R.H. French, J. Am. Ceram. Soc. **76**, 1132 (1993)

α-Al$_2$O$_3$

Elastic coefficients of corundum, Al$_2$O$_3$. All values in GPa.
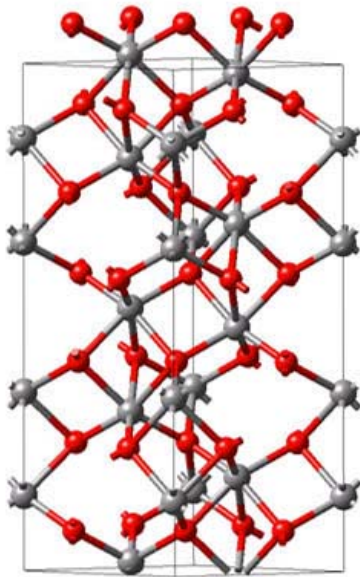
	Expt. [a]	Computed [b]
C_{11}	497.3	495
C_{12}	162.8	171
C_{13}	116.0	130
C_{14}	-21.9	+20
C_{33}	500.9	486
C_{44}	146.8	148

a) T. Goto, O. Anderson, I. Ohno, and S. Yamamoto, J. Geophys. Res. **94**, 7588 (1989)
b) J. R. Gladden, J. D. Maynard, J. H. So, P. Saxe, and Y. Le Page, Appl. Phys. Lett. **85**, 392 (2004)

Elastic coefficients of corundum, Al_2O_3. All values in GPa.
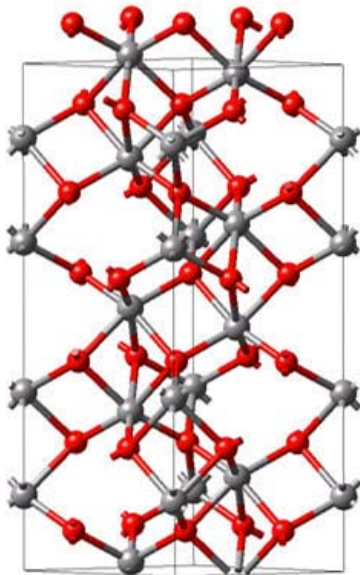
	Expt. [a]	Computed [b]	Expt. [b]	
			Sample 1	Sample 2
C_{11}	497.3	495	495.6	497.4
C_{12}	162.8	171	160.2	158.3
C_{13}	116.0	130	117.0	121.0
C_{14}	-21.9	+20	+22.1	+23.0
C_{33}	500.9	486	501.0	505.8
C_{44}	146.8	148	147.0	145.3

a) T. Goto, O. Anderson, I. Ohno, and S. Yamamoto, J. Geophys. Res. **94**, 7588 (1989)
b) J. R. Gladden, J. D. Maynard, J. H. So, P. Saxe, and Y. Le Page, Appl. Phys. Lett. **85**, 392 (2004)

α-Al_2O_3

Analyze Phonons of Graphene
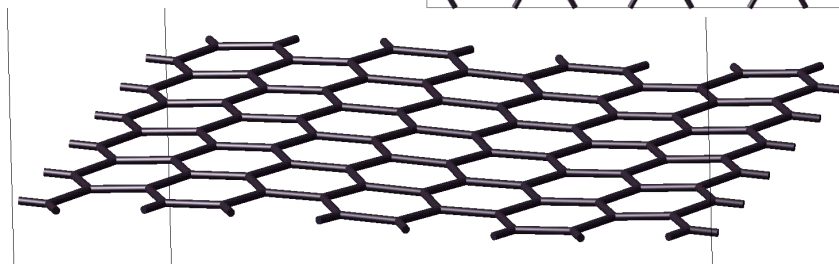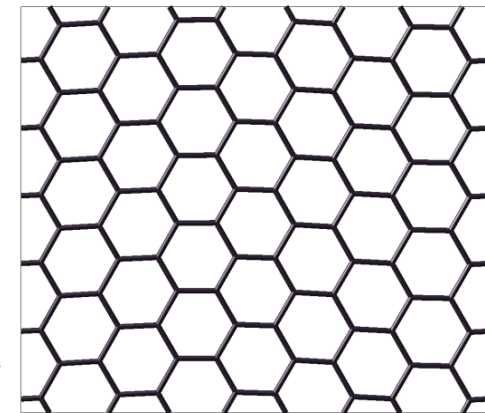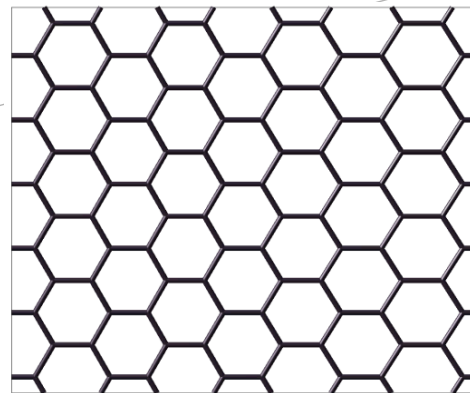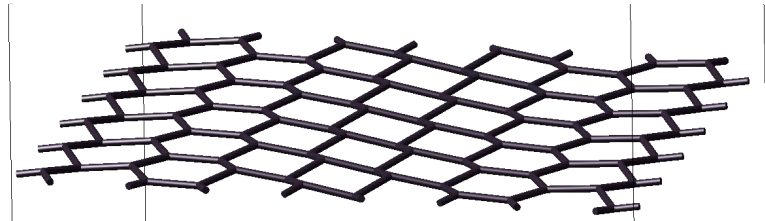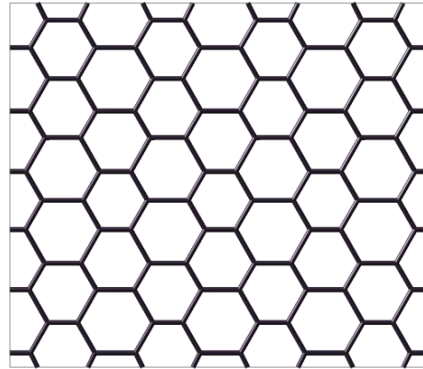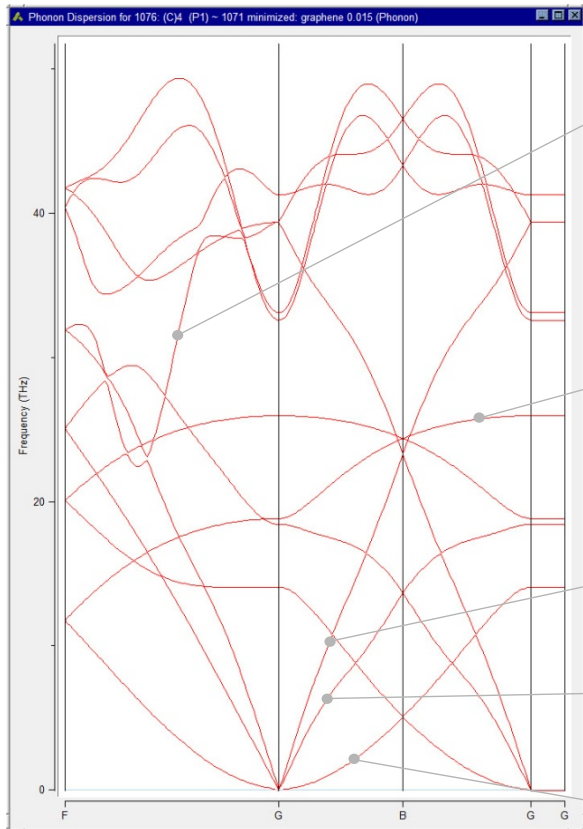
Hydrogen Storage

Hydrogen in $LaNi_5H_n$ and $LaCo_5H_n$

Hydrogen site energetics in $LaNi_5H_n$ and $LaCo_5H_n$: Toward predicting hydrides

J. F. Herbst[a] and L. G. Hector, Jr.

Materials and Processes Laboratory, General Motors Research and Development Center,
Mail Code 480-106-224, 30500 Mound Road, Warren, Michigan 48090-9055

We have investigated the energetics of hydrogen site occupation in $LaNi_5H_n$ (hexagonal $P6_3mc$ structure) and $LaCo_5H_n$ (orthorhombic $Cmmm$ structure) via calculation of the site-dependent enthalpies of hydride formation ΔH. For each structure ΔH was determined for a broad variety of hydrogen configurations. In $LaNi_5H_n$ ($LaCo_5H_n$) we find that the minimum ΔH occurs for hydrogen filling of the $2b6c_16c_2$ ($4e4h$) sites, precisely those identified by neutron diffraction. Hydrogen-richer hydrides are predicted for both structures, in qualitative agreement with experiments performed at higher pressures. © 2004 American Institute of Physics.
[DOI: 10.1063/1.1808503]

Herbst, Hector, Appl. Phys. Lett. **85**, 3465 (2004)

Hydrogen in $LaNi_5H_n$ and $LaCo_5H_n$
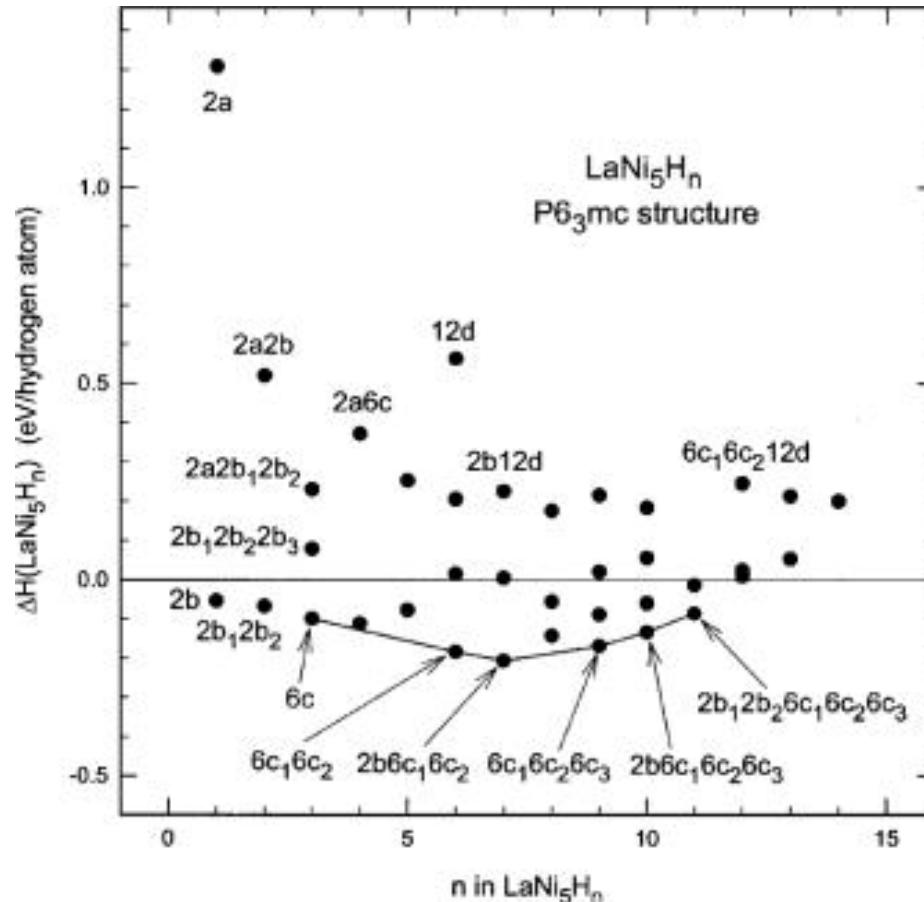
▶ **Enthalpy of hydride formation in $LaNi_5H_n$**

- $\Delta H (LaNi_5H_n) = E (LaNi_5H_n) - E(LaNi_5) - \frac{1}{2} n E(H_2)$

- $\Delta H_{min} = - 40$ kJ/molH$_2$ for H at $2b6c_16c_2$

- agrees with

  - neutron data

  - calorimetry:

    $\Delta H_{min} = - (32/37)$ kJ/molH$_2$

Herbst, Hector, Appl. Phys. Lett. **85**, 3465 (2004)

Hydrogen in $LaNi_5H_n$ and $LaCo_5H_n$
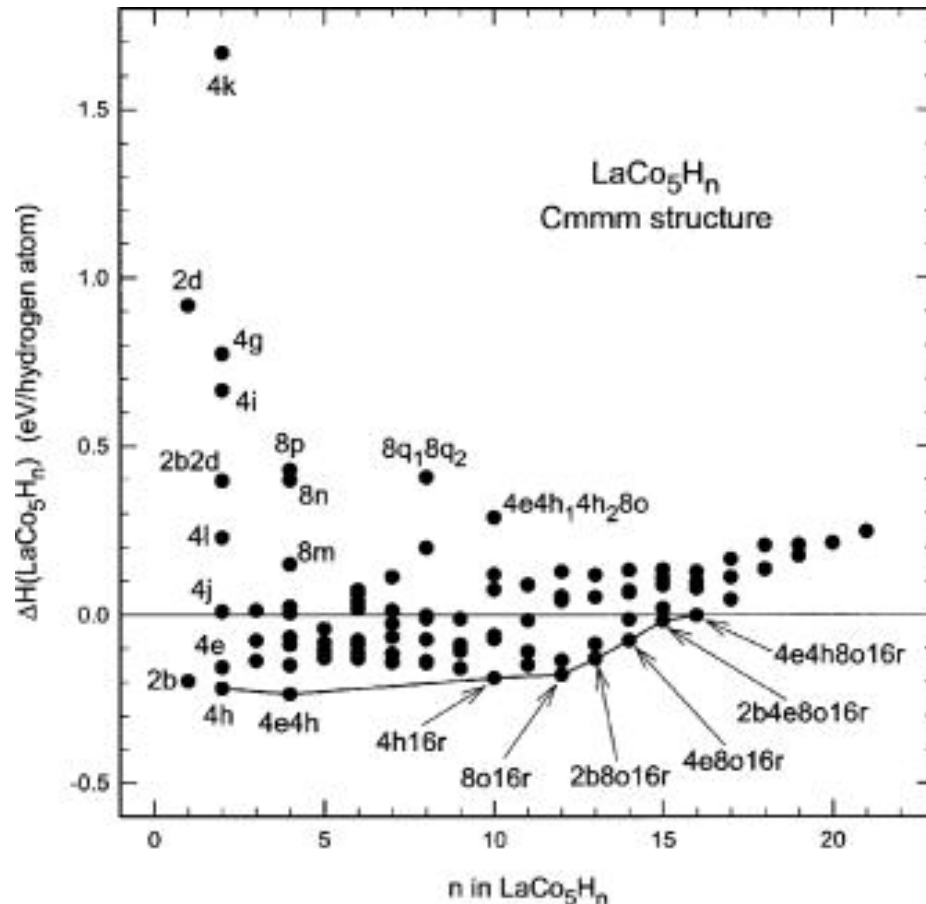
▶ **Enthalpy of hydride formation in $LaCo_5H_n$**

- $\Delta H (LaCo_5H_n) = E (LaCo_5H_n) - E(LaCo_5) - \frac{1}{2} n\, E(H_2)$

- $\Delta H_{min} = -45.6$ kJ/molH$_2$ for H at 4e4h

- agrees with
  - neutron data
  - calorimetry:

    $\Delta H_{min} = -45.2$ kJ/molH$_2$

Herbst, Hector, Appl. Phys. Lett. **85**, 3465 (2004)

Diffusion of H in Ni

Diffusion Coefficients

1. Transition state approach

▶ Compute initial and final structures (minimization)

▶ Search transition state (TSS)

▶ Compute phonon dispersion and phonon density of states

▶ Apply Eyring's transition state theory to get jump rates

▶ Use kinetic Monte Carlo for networks

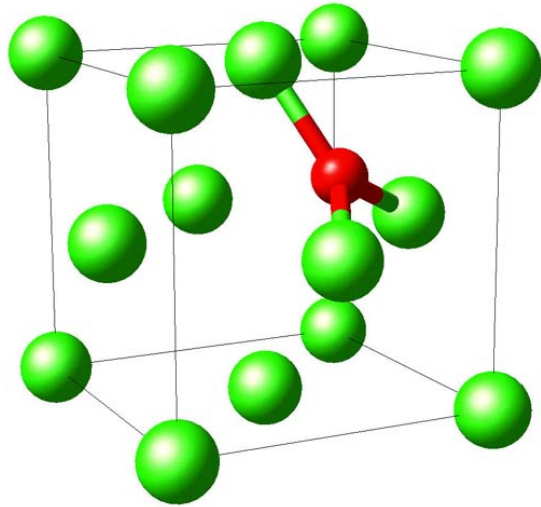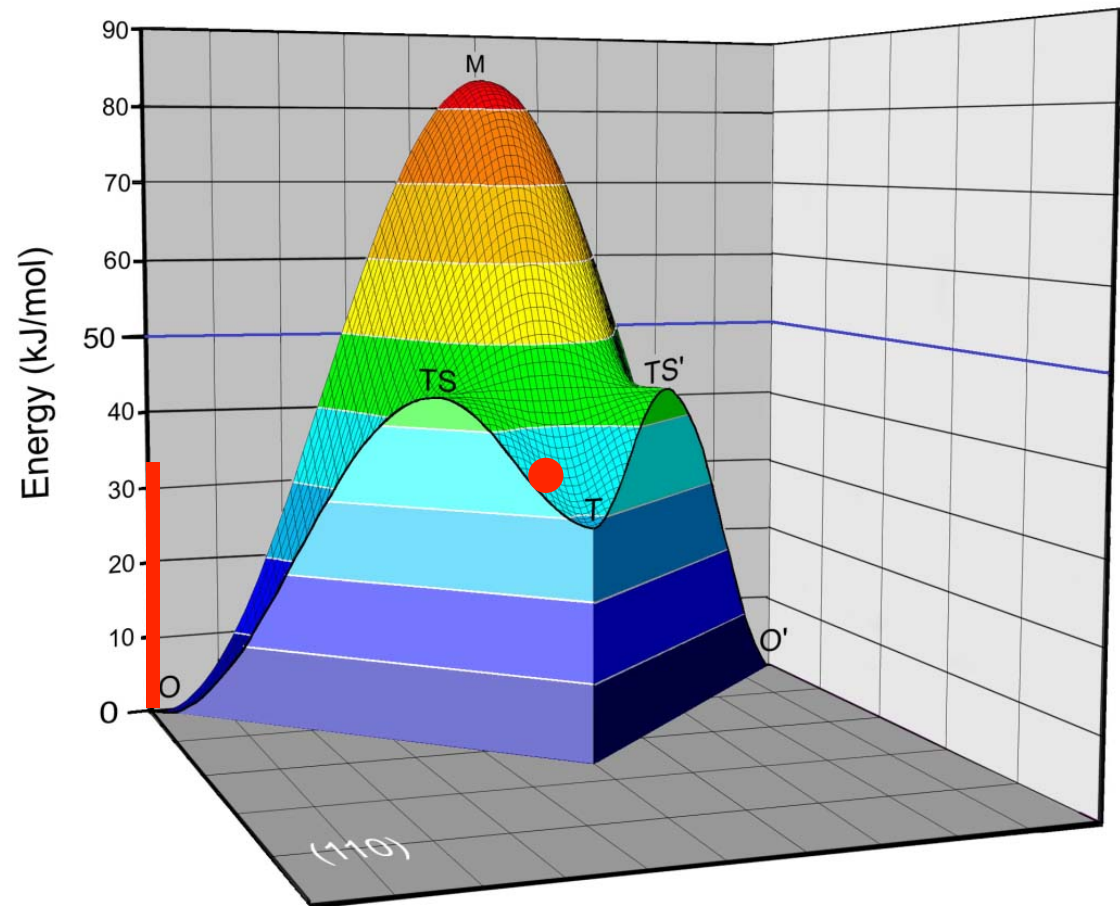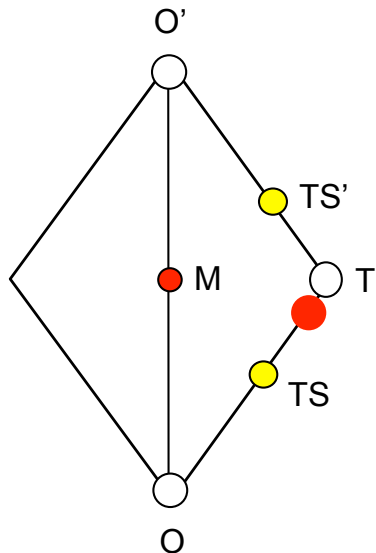**2. Mean square displacement (MSD) from molecular dynamics**

Diffusion of Interstitial Impurities
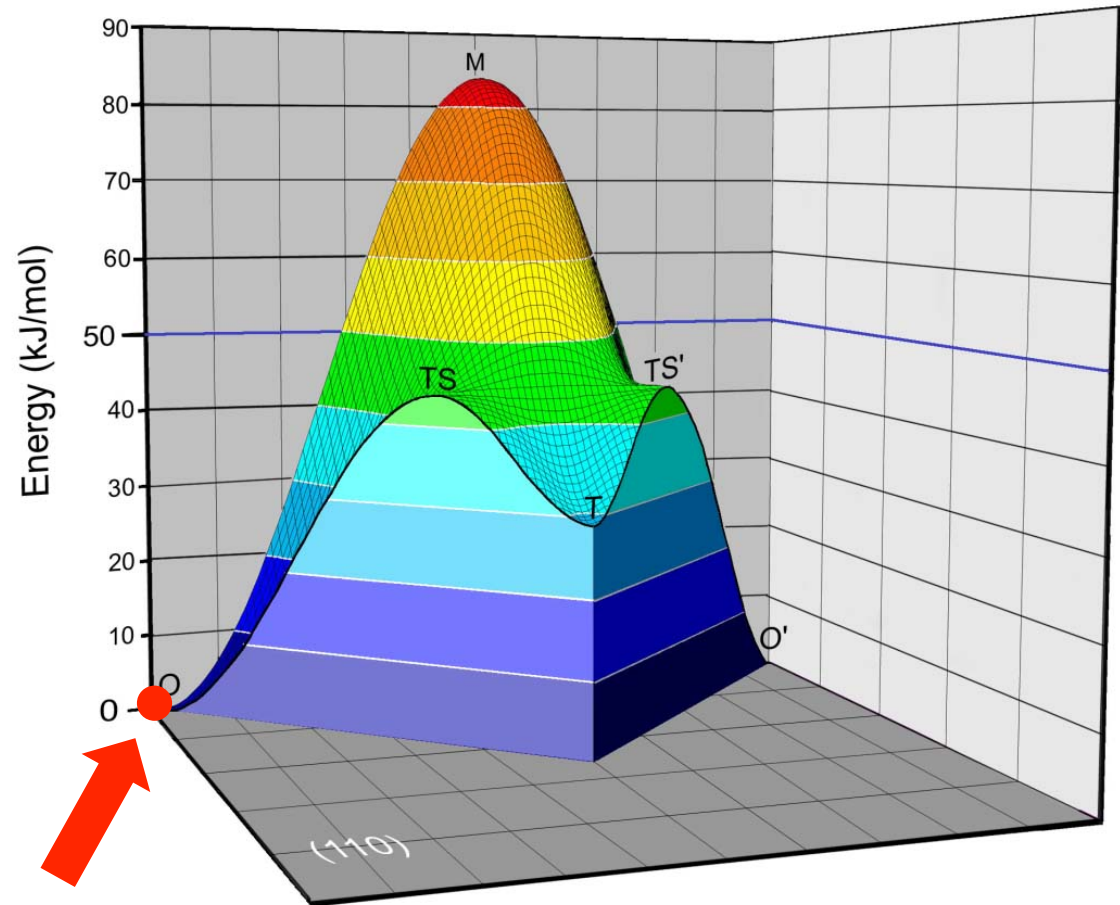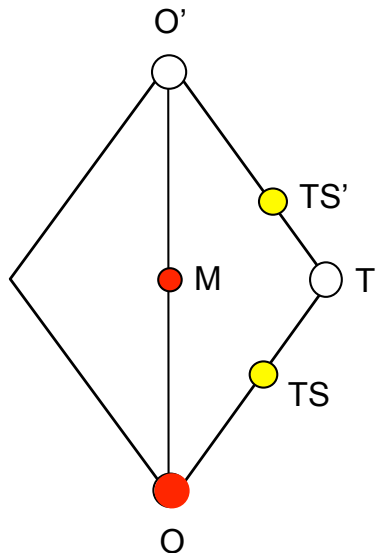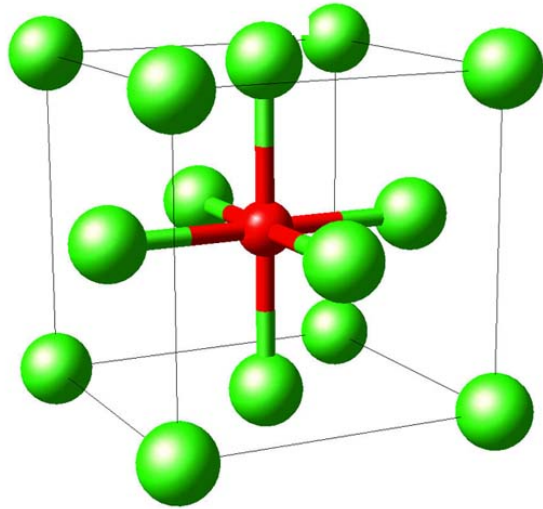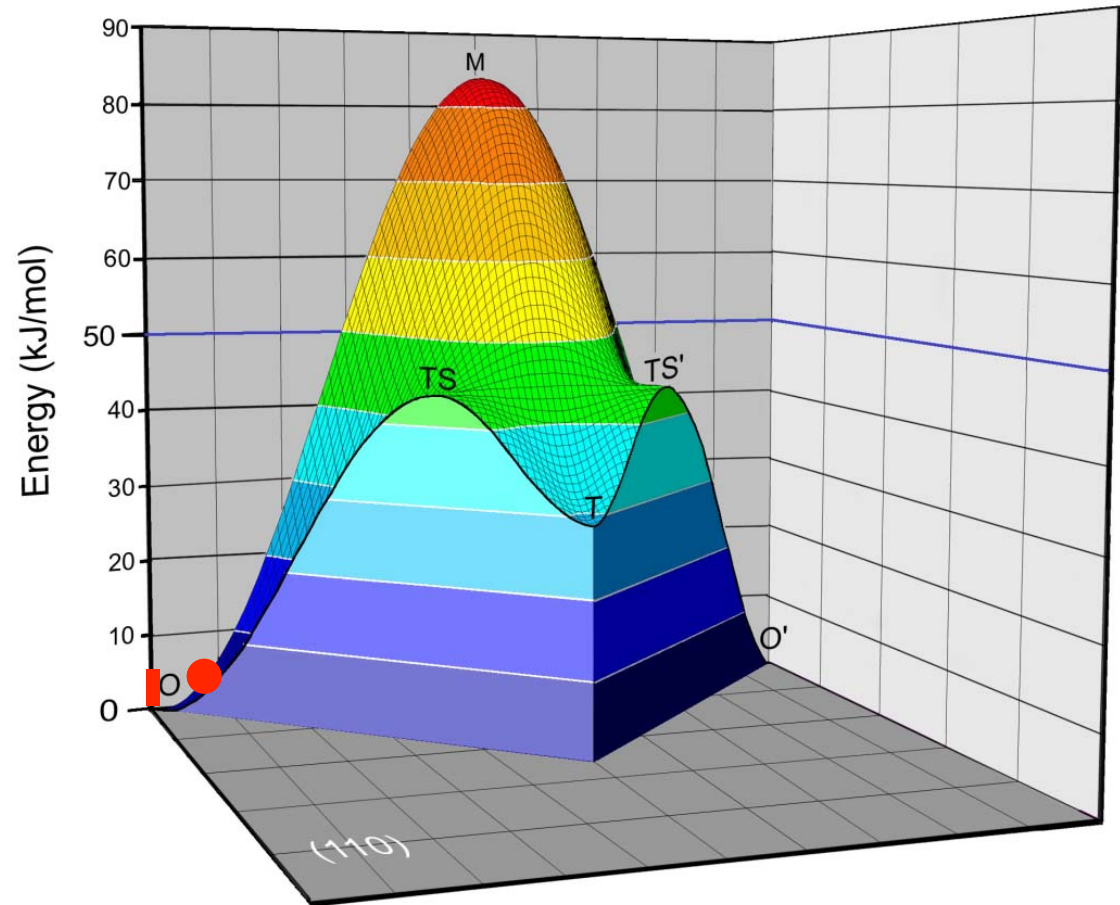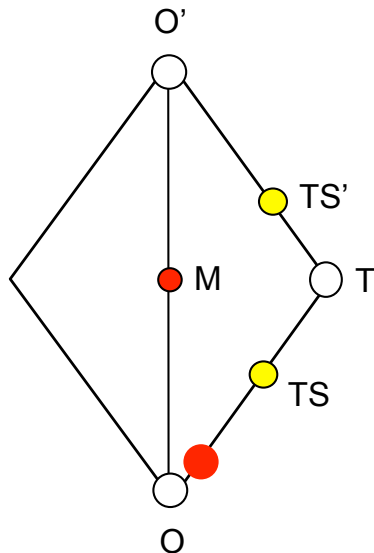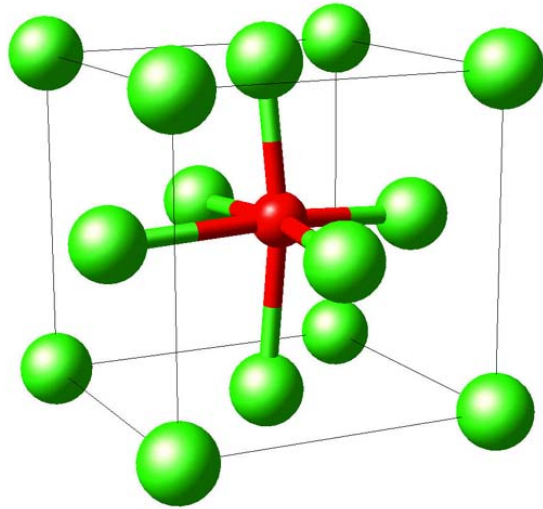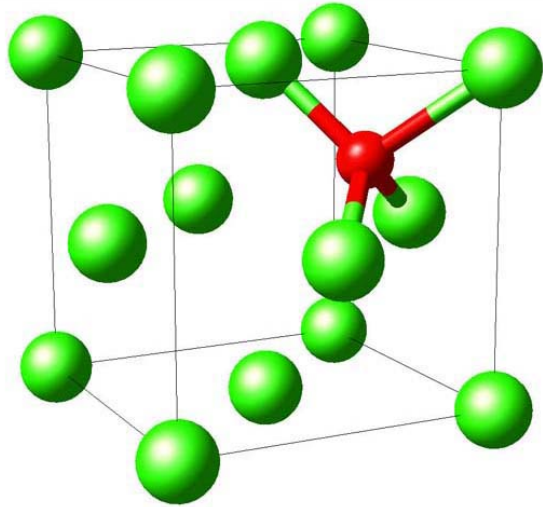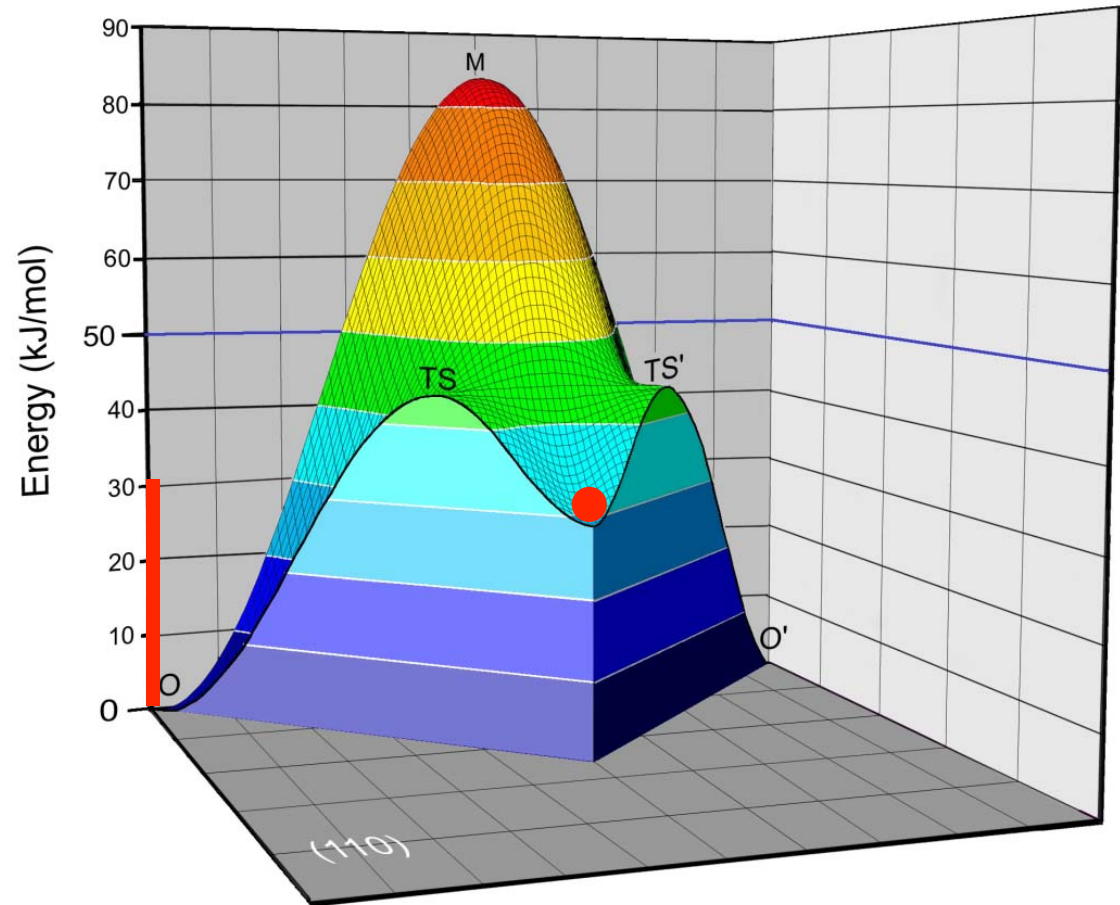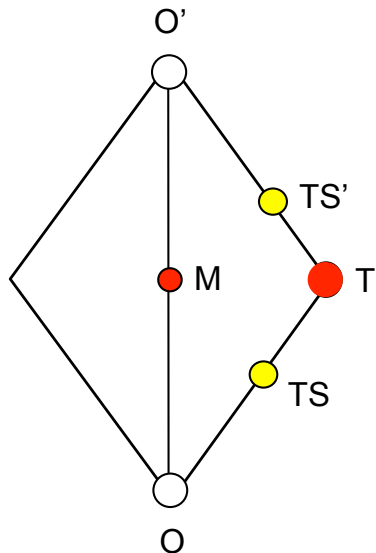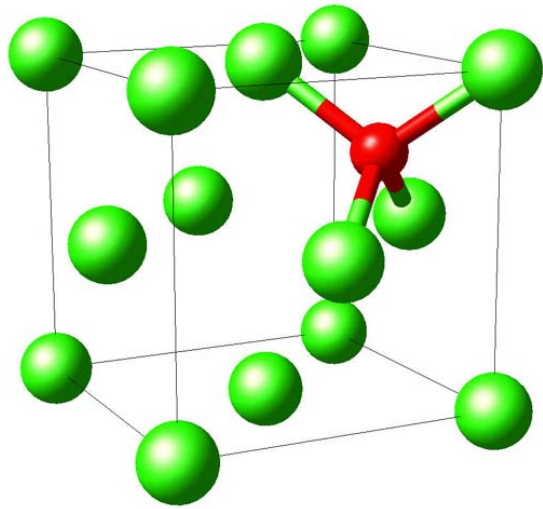
Diffusion of Interstitial Impurities
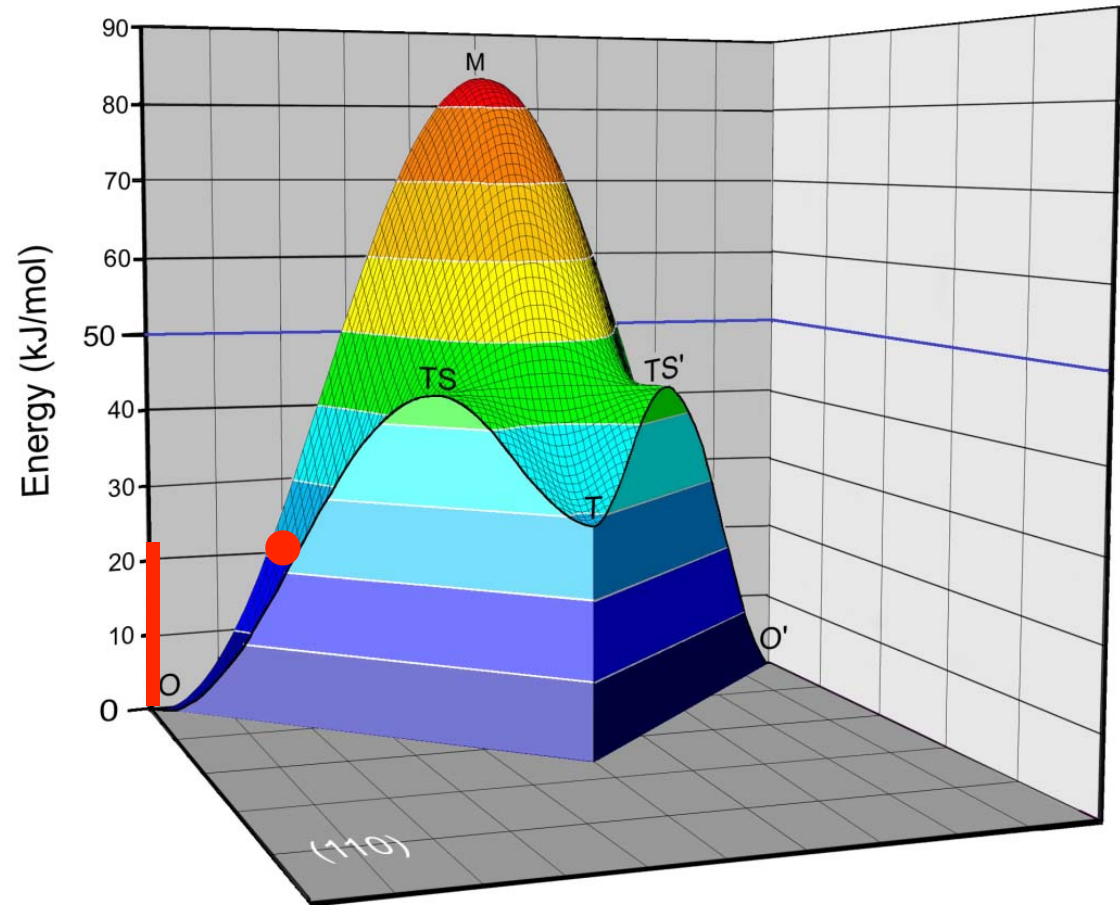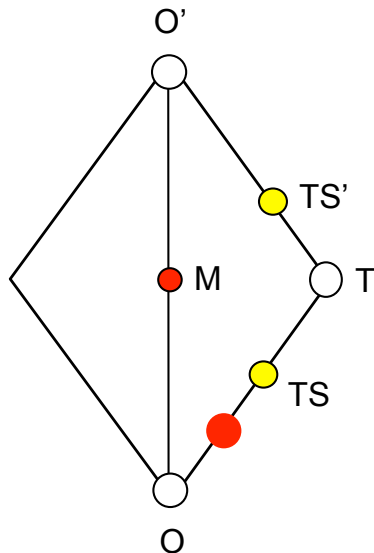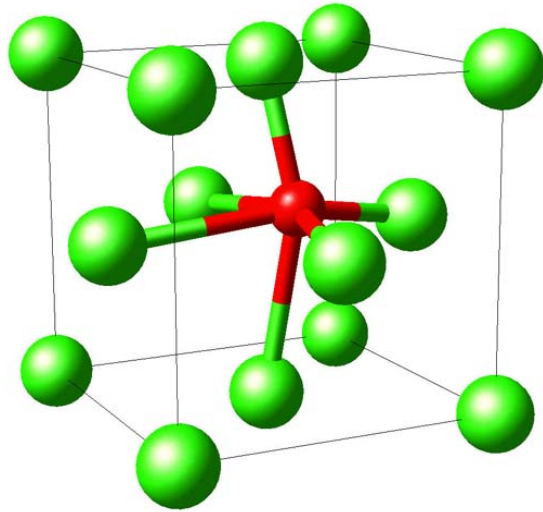
Diffusion of Interstitial Impurities
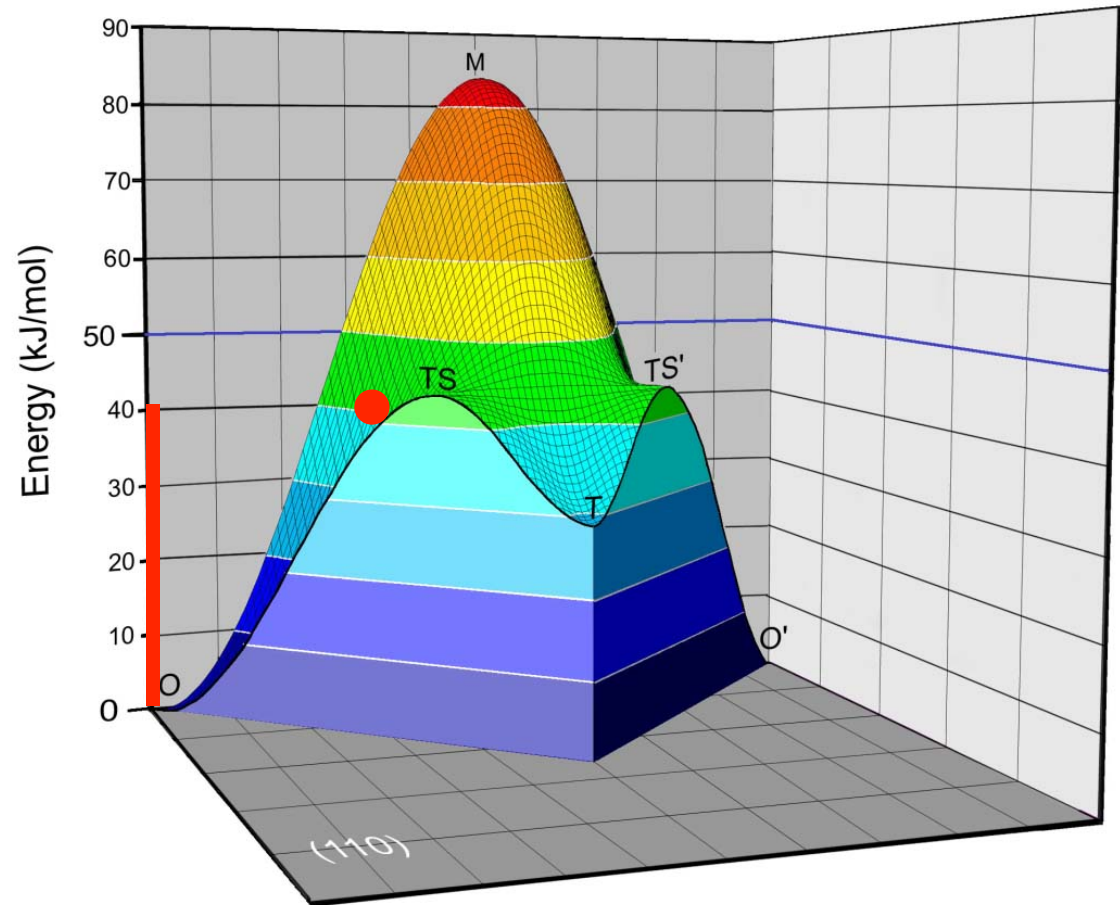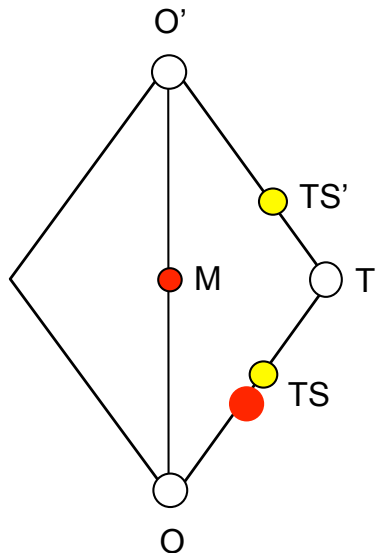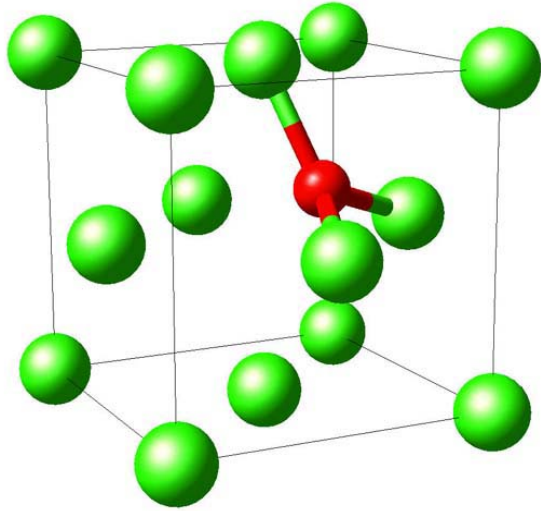
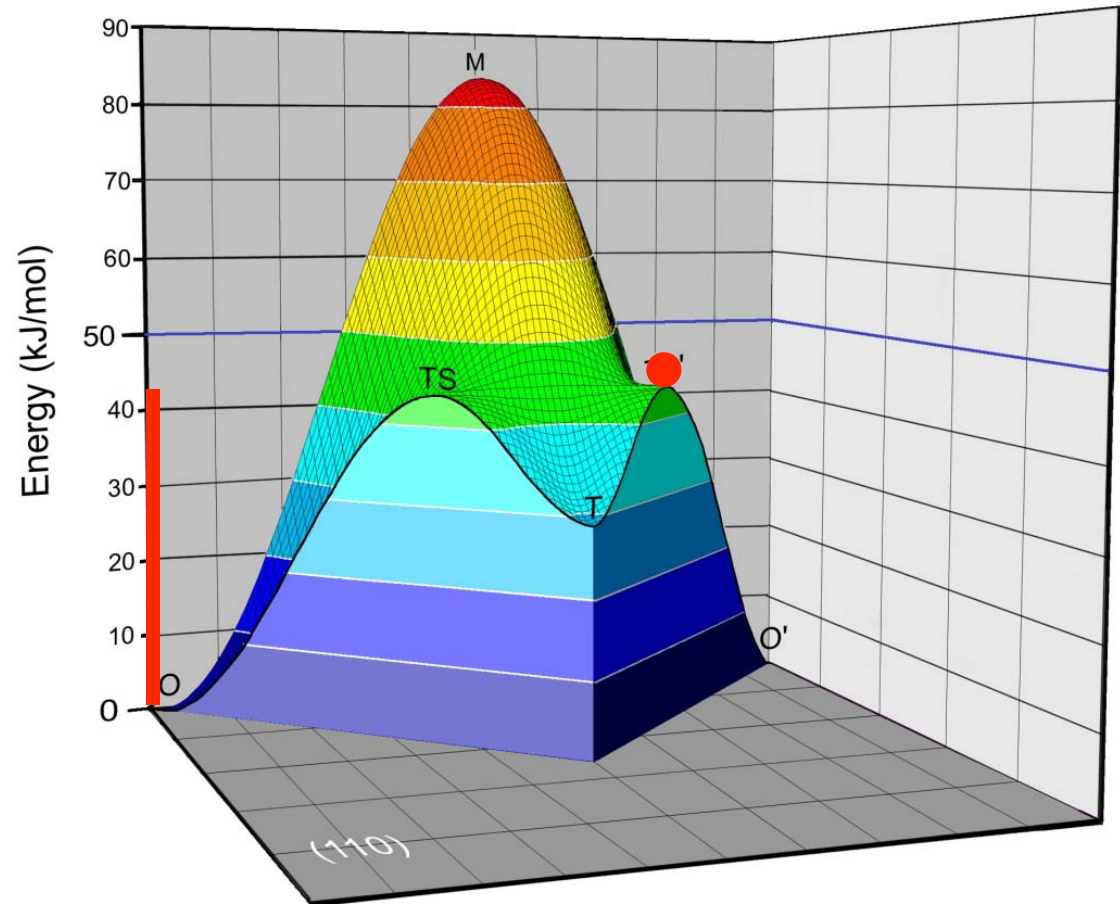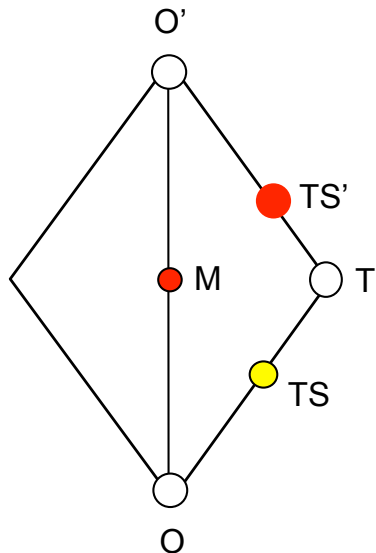# Diffusion of Interstitial Impurities
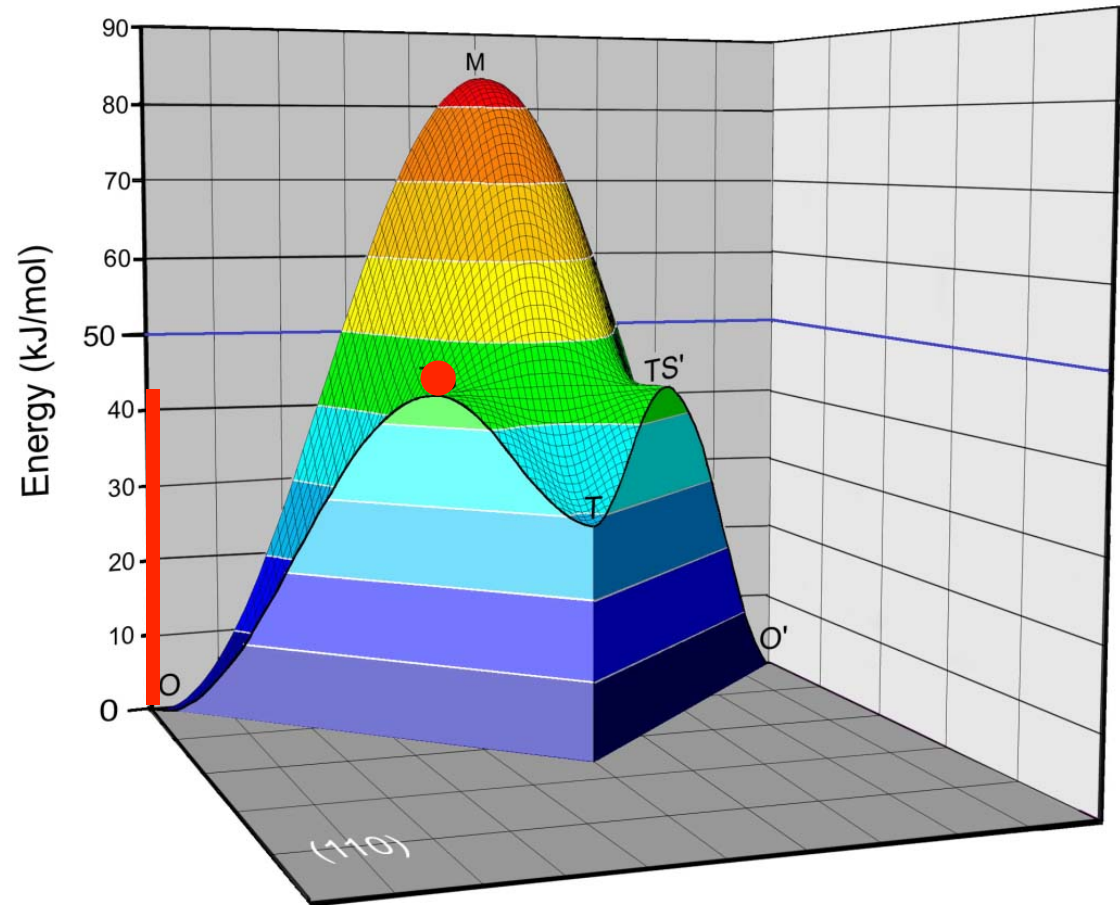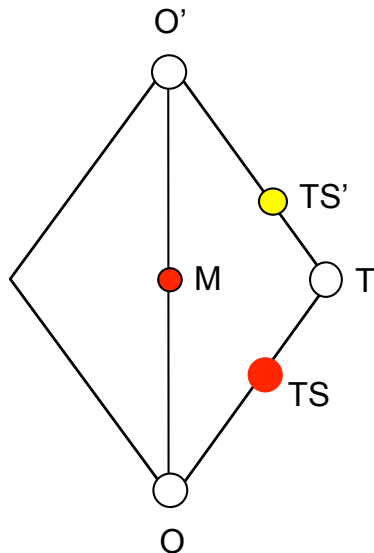
Diffusion of Interstitial Impurities

Diffusion of Interstitial Impurities

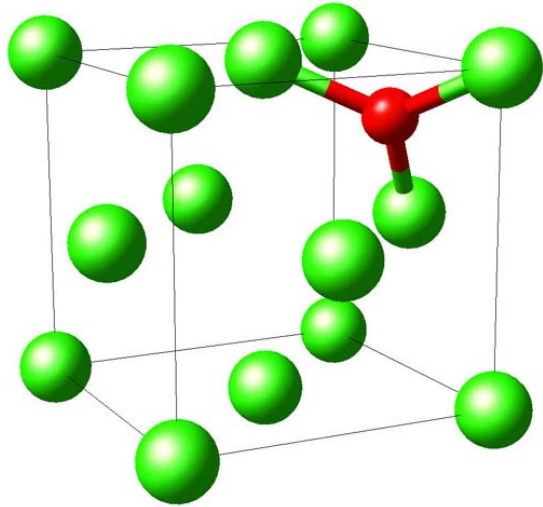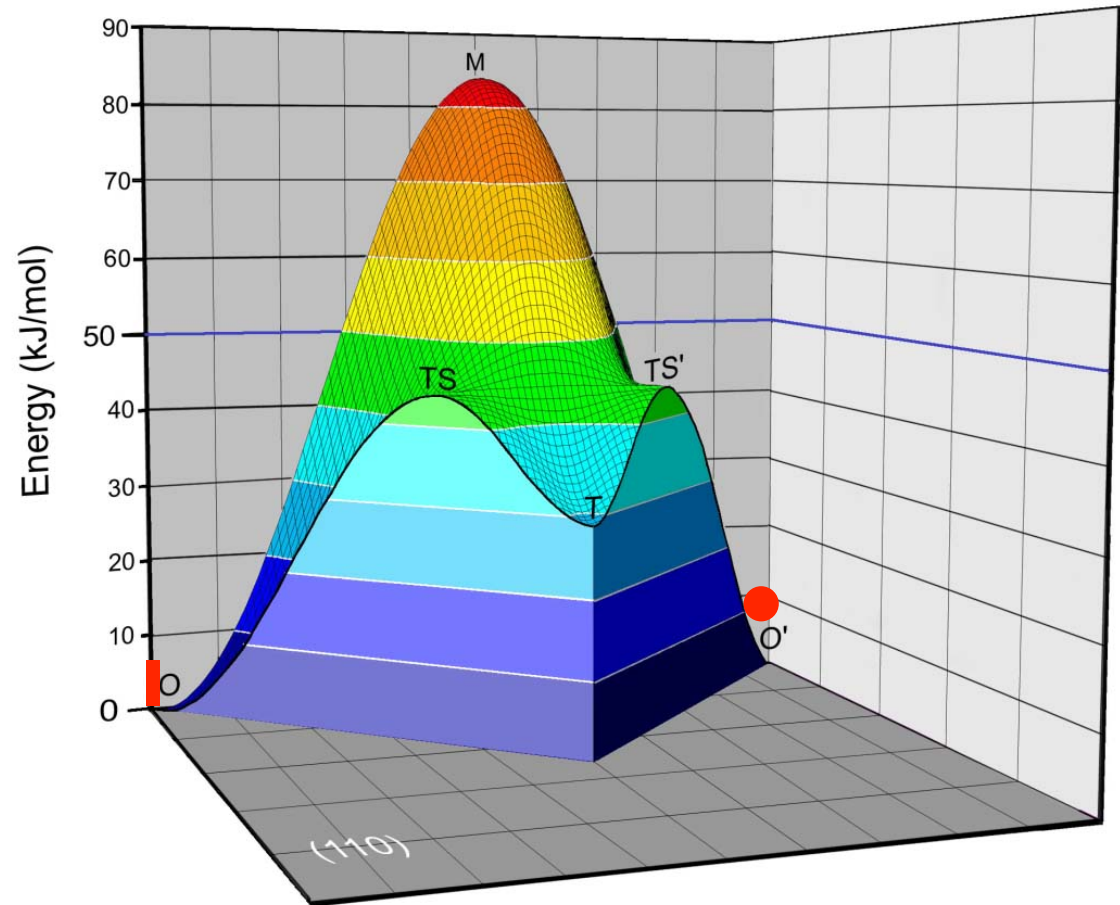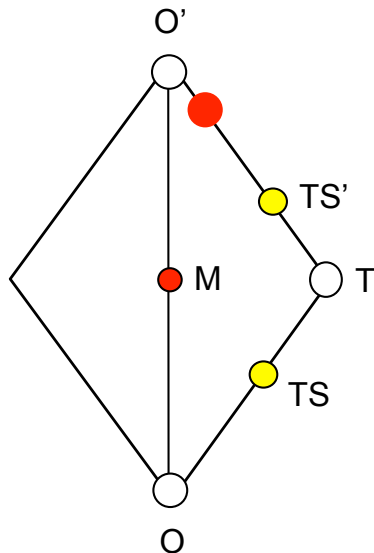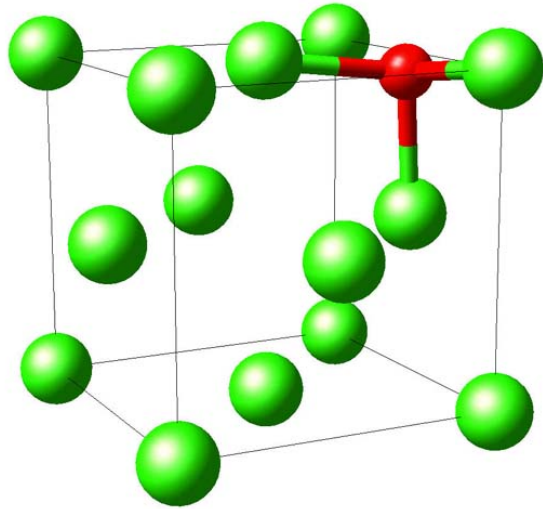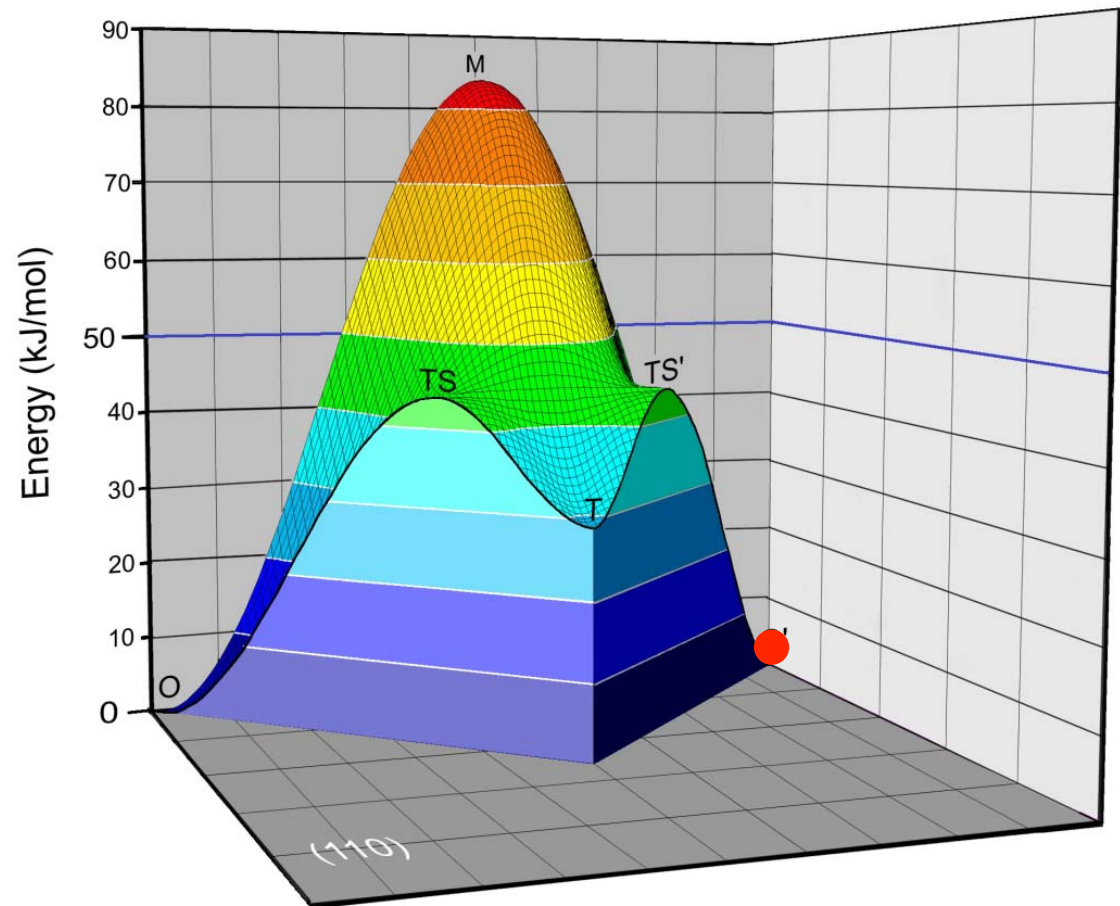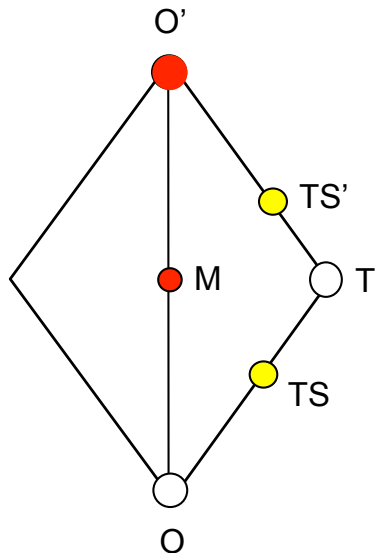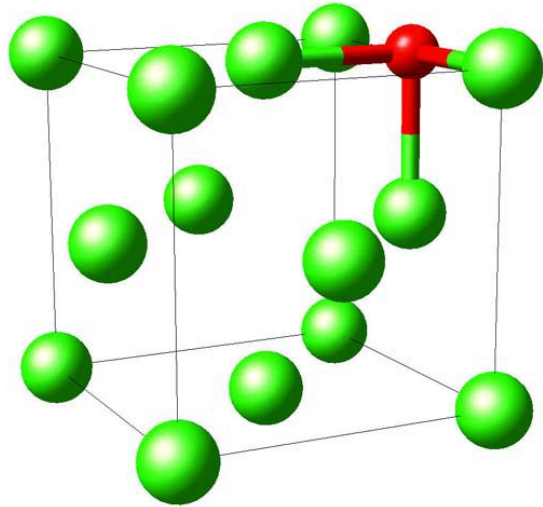# Diffusion of Interstitial Impurities

Diffusion of Interstitial Impurities

Diffusion of Interstitial Impurities

Diffusion: Hydrogen in Ni

Diffusivity of H, D, and T in fcc Ni
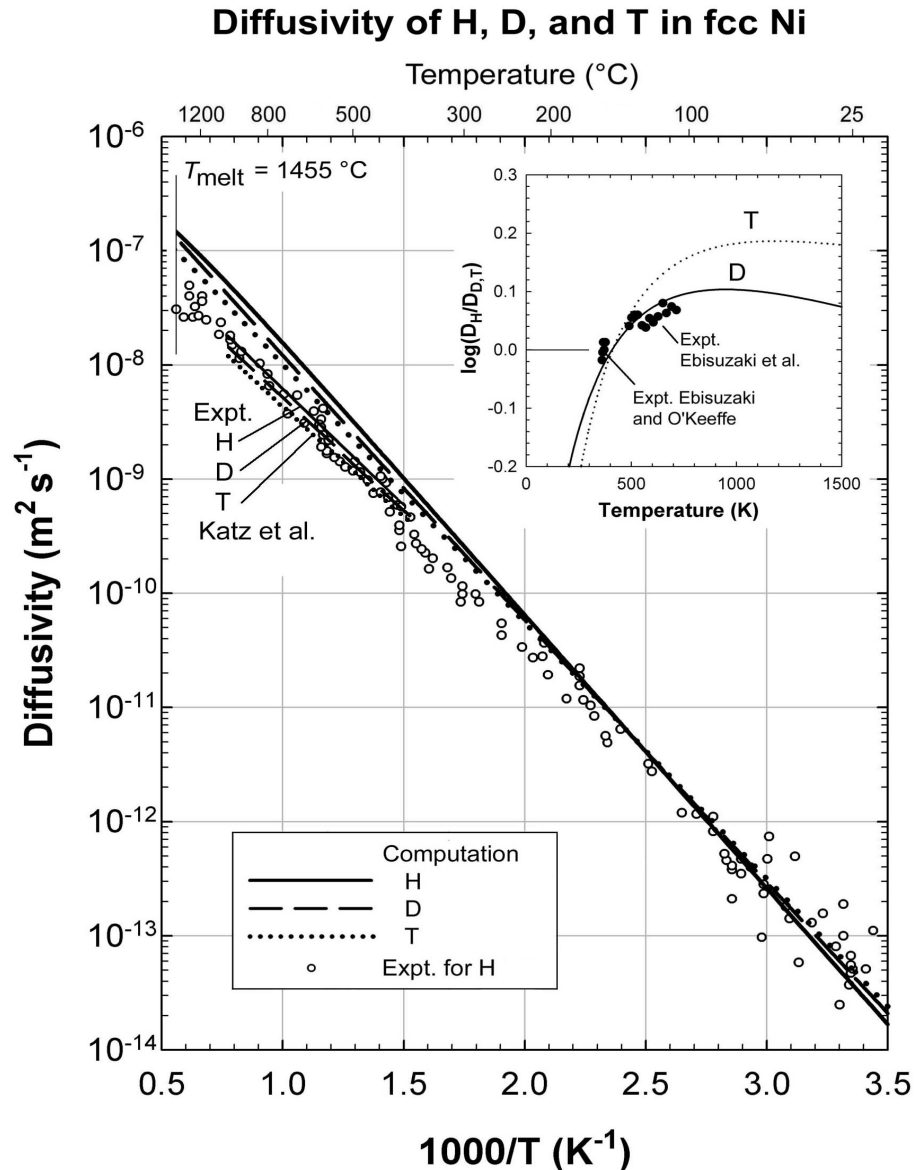
The diffusion coefficient of H in Ni computed from first-principles has similar accuracy as experimental data at ambient and medium temperatures

Isotope effects are well explained and quantitatively described

Computational approach:
Eyring transition state theory
Ab initio phonons for entire supercell thermal expansion from quasi harmonic approximation

E. Wimmer, W. Wolf, J. Sticht, P. Saxe, C. B. Geller, R. Najafabadi, and G. A. Young, "Temperature-dependent diffusion coefficients from *ab initio* computations: Hydrogen, deuterium, and tritium in nickel", Phys. Rev. B **77**, 134305 (2008)

Grain Boundaries

Development of Fracture Mechanics Method to Evaluate Iodine Stress

Corrosion Cracking of Zirconium Alloys

T.M. Angeliu, B. Kallenburg, D.B. Knorr and J.D. Ballard*

Knolls Atomic Power Laboratory

PO Box 1072, Schenectady, NY 12301-1072

Tel: (518) 395-7865, Fax: (518)-395-4422, Email: ballajd@kapl.gov
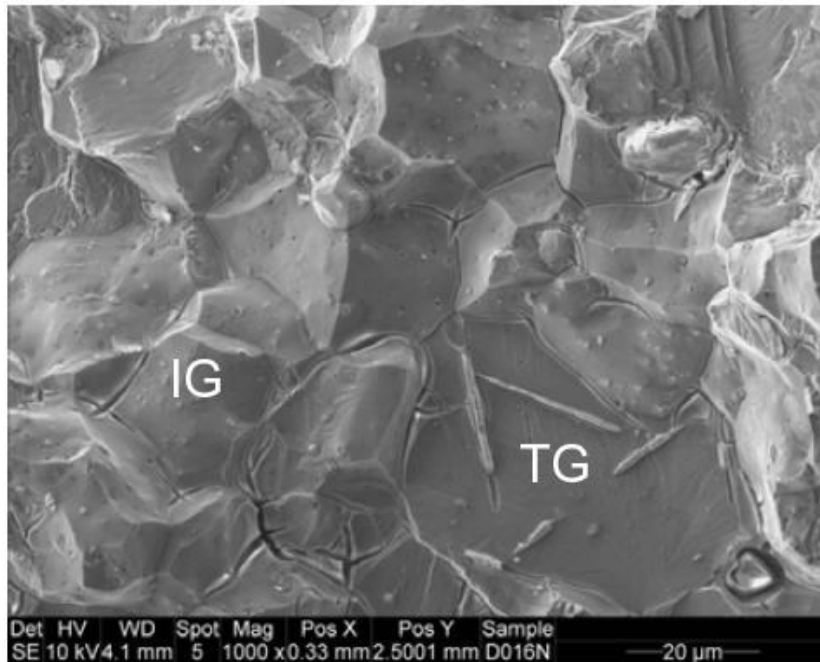
Intergranular cracking more prevalent as both temperature and iodine concentration increased

Possible mechanism:

Iodine in grain boundary diffuses to crack tip and lowers work of separation

Maximum Stress

**Grain boundary
of hcp metal**

Alloying Atoms at Interfaces

hcp - Zr

Grain 1 **Grain 2**
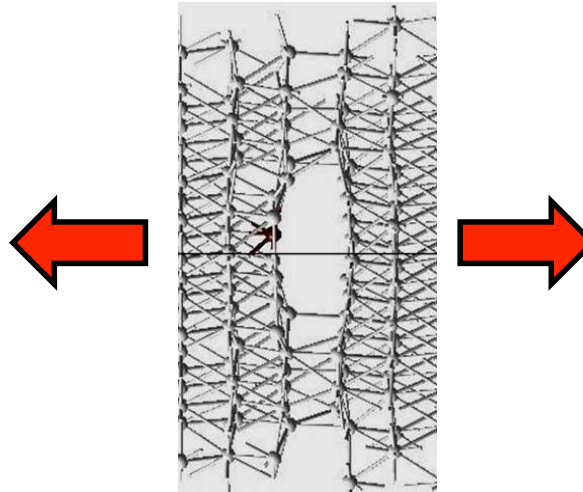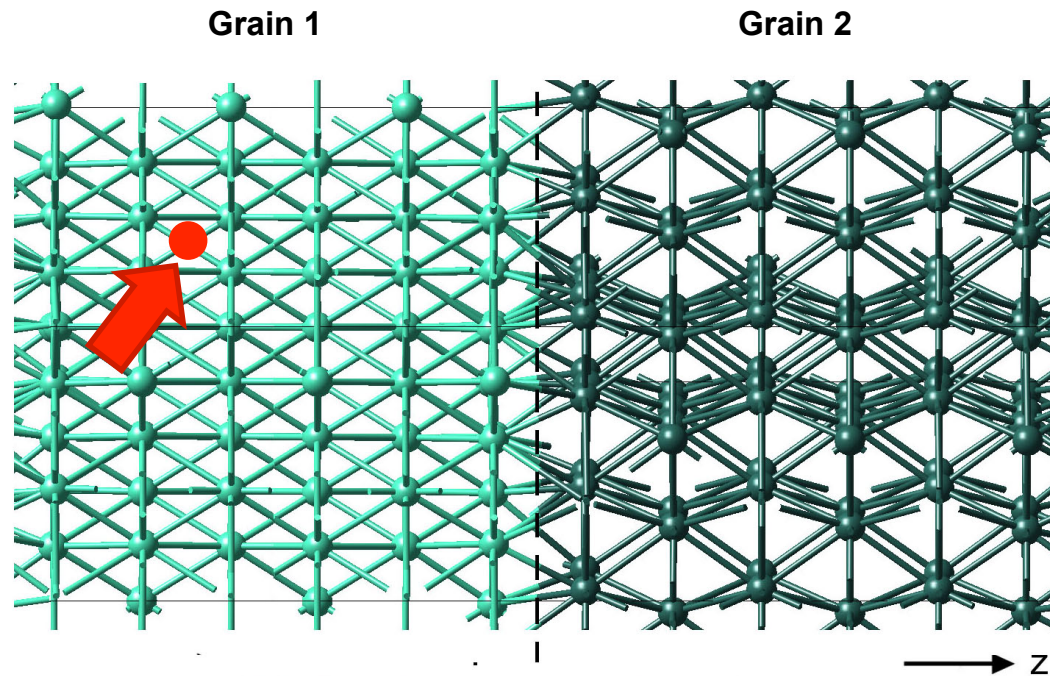
Zr(0001)/Zr(0001) Σ7
twist grain boundary

Alloying Atoms at Interfaces
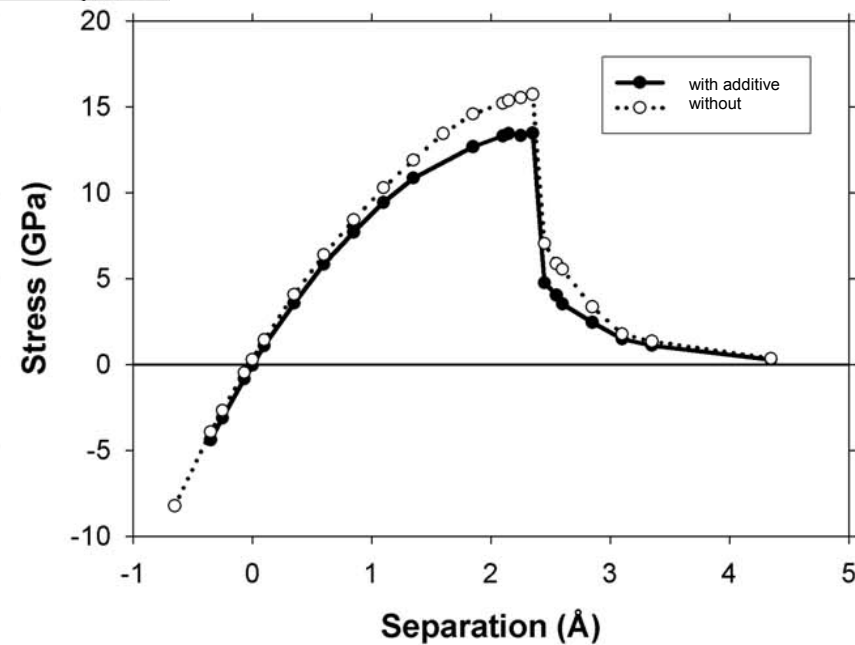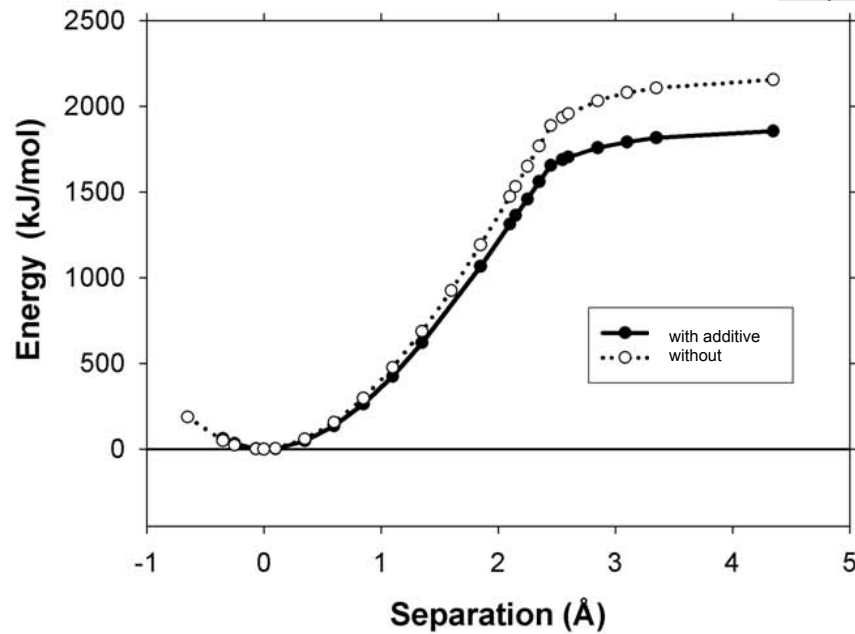
hcp - Zr

Grain 1   Grain 2
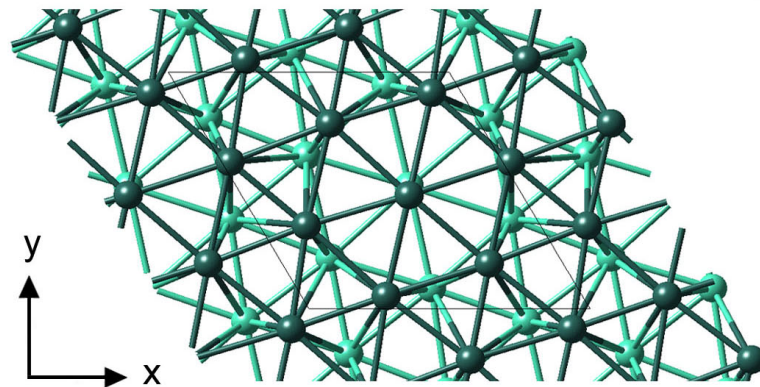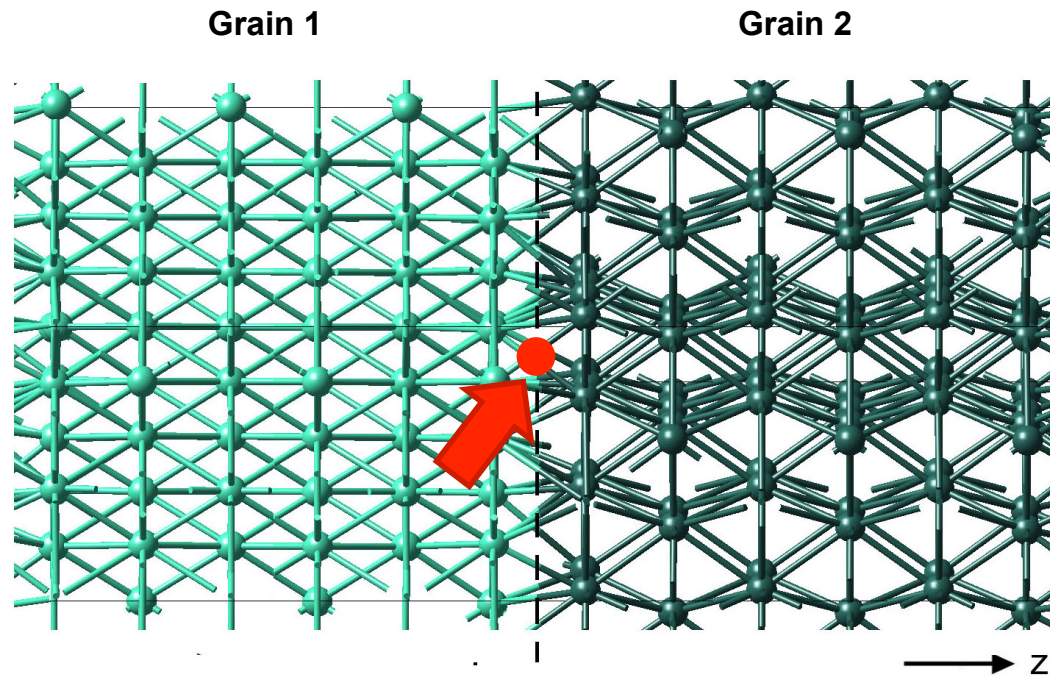
Zr(0001)/Zr(0001) S7
twist grain boundary

Zr GB and Surface Segregation

Cleavage of Zr Grain Boundaries

transgranular

intergranular
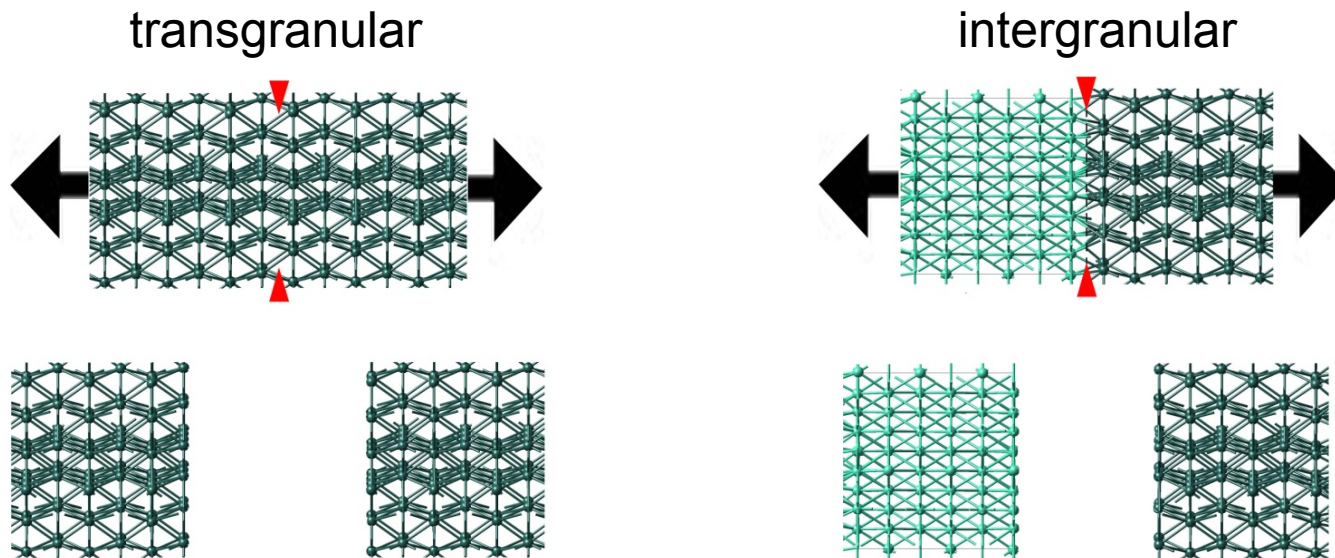
Computed work of separation

Cleavage energy of pure Zr along (0001) plane	**3.15** J m^{-2}
Cleavage energy of Zr along $\Sigma 7(0001)$ grain boundary	**2.86** J m^{-2}

Effect of Impurities

Change in work of separation of Zr grain boundary by impurities
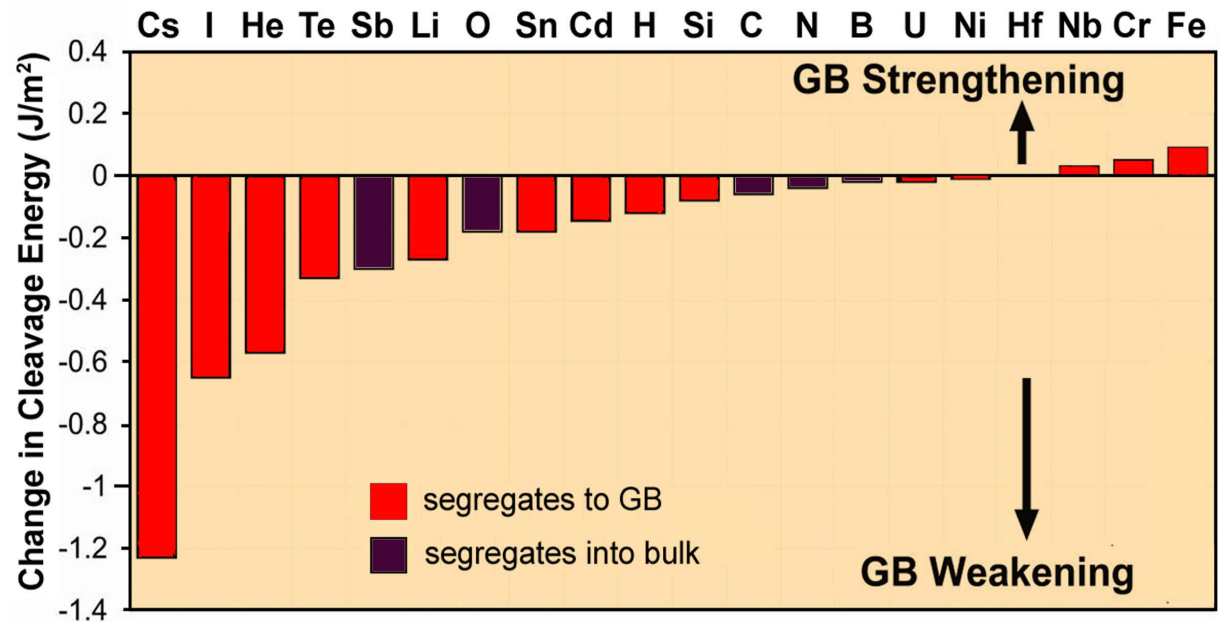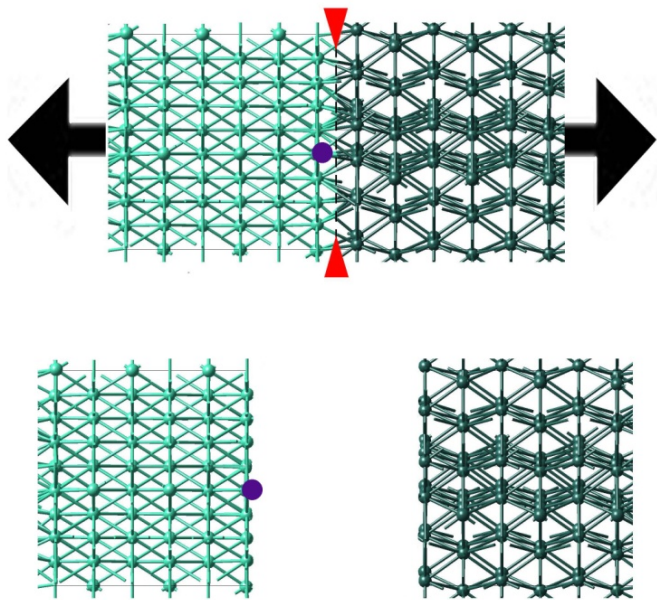
Embrittlement in Cu Micro-Structures

ELSEVIER

CrossMark
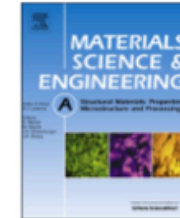
Temperature dependent transition of intragranular plastic to intergranular brittle failure in electrodeposited Cu micro-tensile samples

A. Wimmer [a], M. Smolka [b], W. Heinz [a], T. Detzel [c], W. Robl [d], C. Motz [e], V. Eyert [f], E. Wimmer [f], F. Jahnel [g], R. Treichler [g], G. Dehm [h,*]

[a] Kompetenzzentrum Automobil- und Industrie-Elektronik GmbH, A-9524 Villach, Austria
[b] Institute of Sensor and Actuator Systems, Vienna University of Technology, A-1040 Vienna, Austria
[c] Infineon Technologies Austria AG, A-9500 Villach, Austria
[d] Infineon Technologies Germany AG, D-93049 Regensburg, Germany
[e] Chair Experimental Methods of Material Science, University of Saarland, D-66123 Saarbrücken, Germany
[f] Materials Design SARL, F-92120 Montrouge, France
[g] Siemens AG, Otto Hahn Ring 6, D-81739 München, Germany
[h] Max-Planck-Institut für Eisenforschung GmbH, D-40237 Düsseldorf, Germany

- improve strength and ductility of Cu microstructures
- introduce additives to reduce grain size (Hall-Petch effect) ☺
- additives cause embrittlement at elevated temperatures ☹

ABSTRACT

Smaller grain sizes are known to improve the strength and ductility of metals by the Hall–Petch effect. Consequently, metallic thin films and structures which must sustain mechanical loads in service are deposited under processing conditions that lead to a fine grain size. In this study, we reveal that at temperatures as low as 473 K the failure mode of 99.99 at% pure electro-deposited Cu can change from ductile intragranular to brittle intergranular fracture. The embrittlement is accompanied by a decrease in strength and elongation to fracture. Chemical analyses indicate that the embrittlement is caused by impurities detected at grain boundaries. In situ micromechanical experiments in the scanning electron microscope and atomistic simulations are performed to study the underlying mechanisms.

48

Stress-Strain in Cu Microstructures
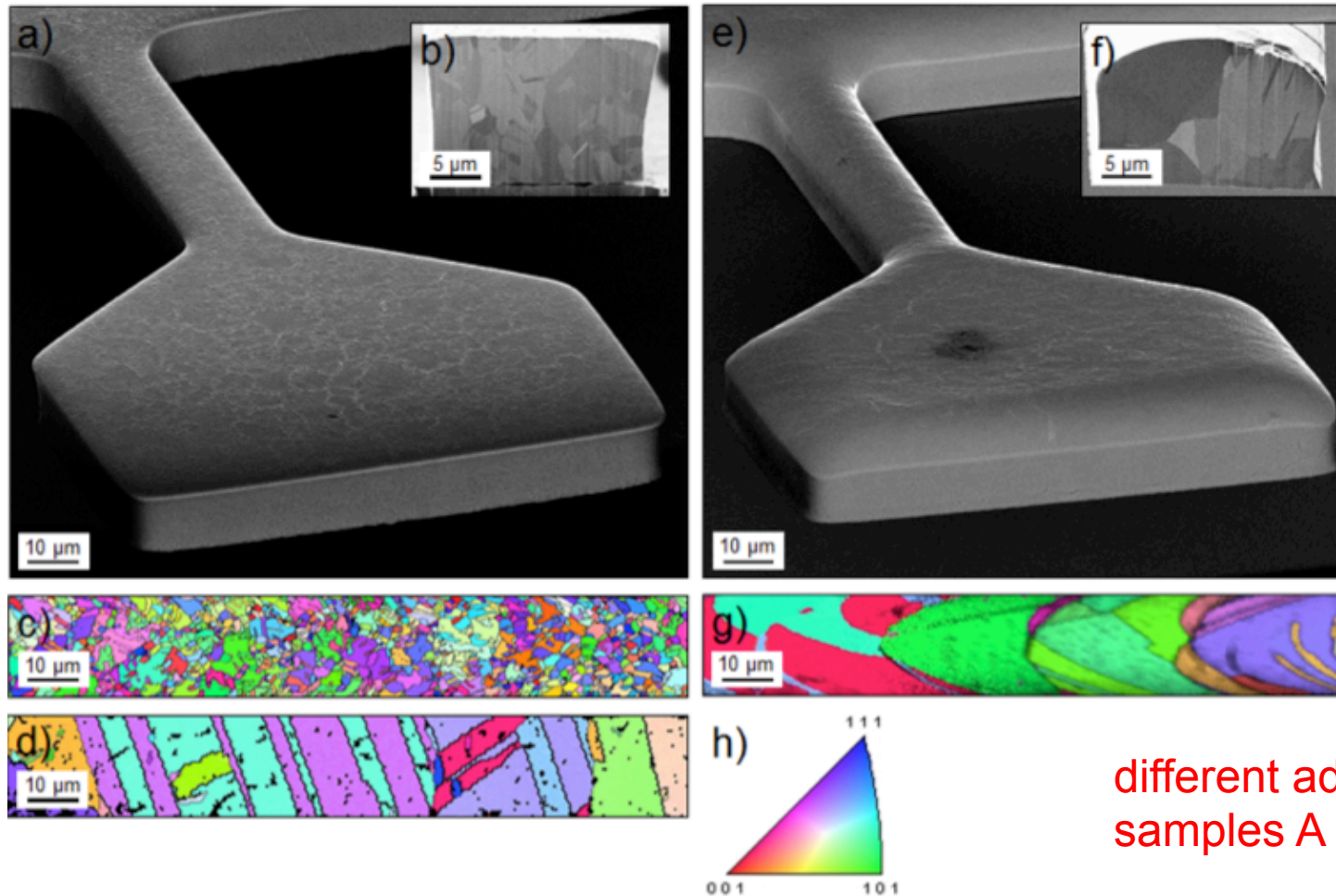
different additives in samples A and B!

- (a, b, c) sample type A (annealed at 673 K, medium grain size 2.7 ± 0.6 µm)
- (d) sample type A after additional annealing at 1073 K (15 ± 5 µm)
- (e, f, g) sample type B (10.1 ± 2.6 µm)

Stress-Strain in Cu Microstructures

a) sample type A (fine-grained)

Stress [MPa] vs Strain

Legend: 293 K, 473 K, 673 K

b) sample type B (coarse-grained)

Stress [MPa] vs Strain

Legend: 293 K, 473 K, 673 K
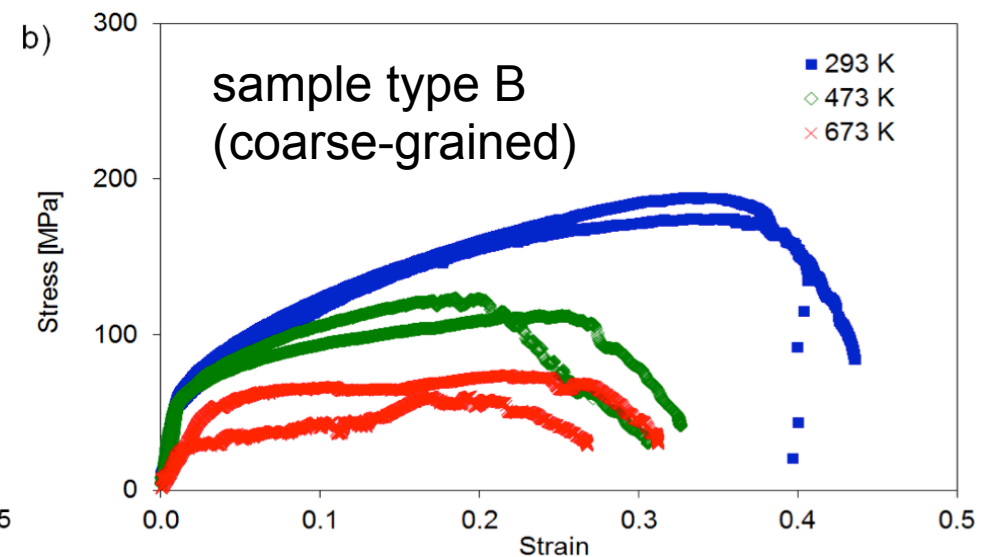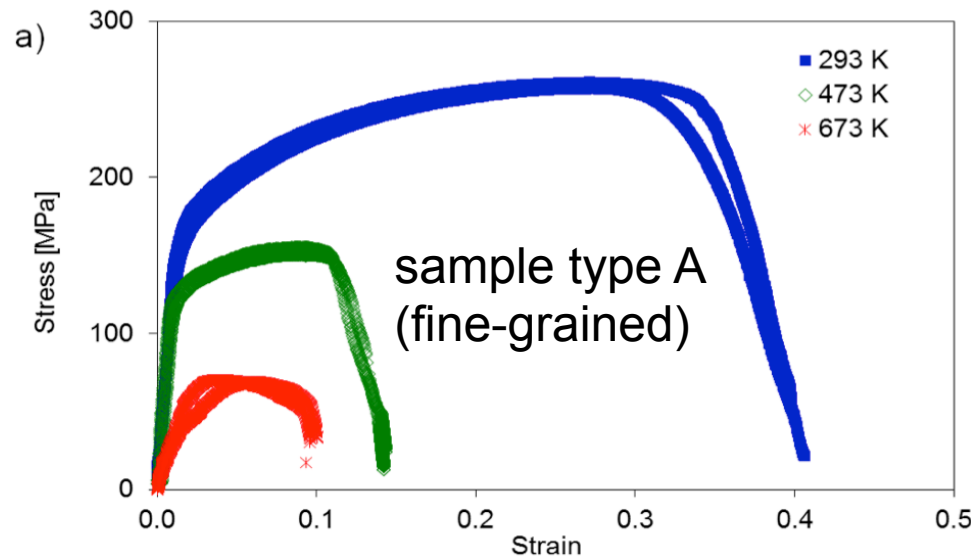
different additives in samples A and B!

293 K: coarse-grained → fine-grained
- yield stress and ultimate stress increase
- changes explained by Hall-Petch effect

473 K and 673 K:
- drastic reduction of elongation to fracture for fine-grained samples
- scattering of results for coarse-grained structures due to small number of grains

Stress vs Strain diagram:
- Strain Hardening
- Necking
- Ultimate Strength
- X Fracture
- Yield Strength
- Rise
- Run
- Young's Modulus = Rise/Run = Slope

50
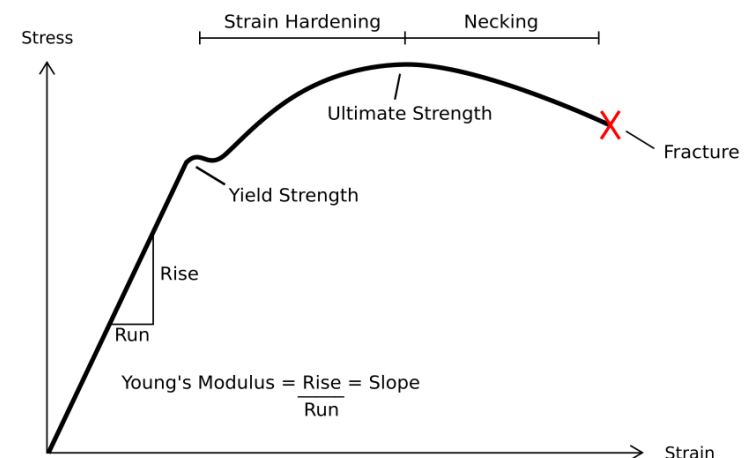
Stress-Strain in Cu Microstructures
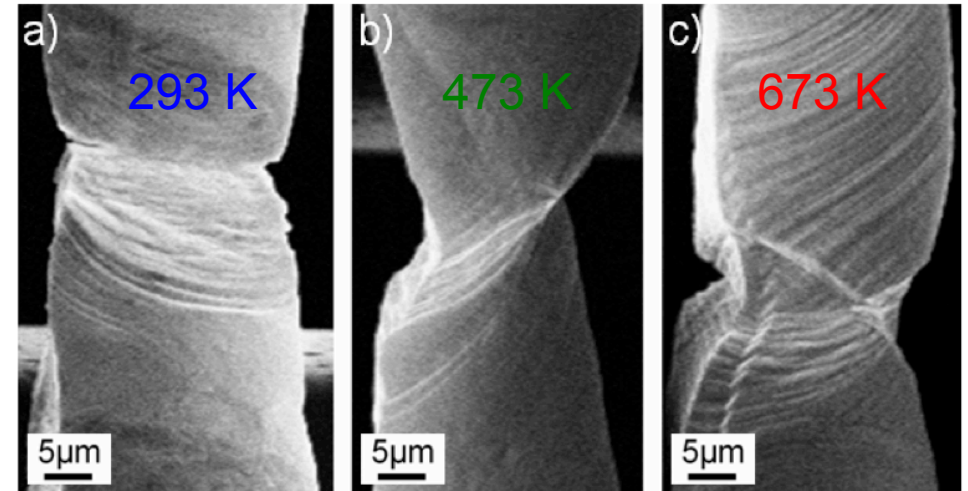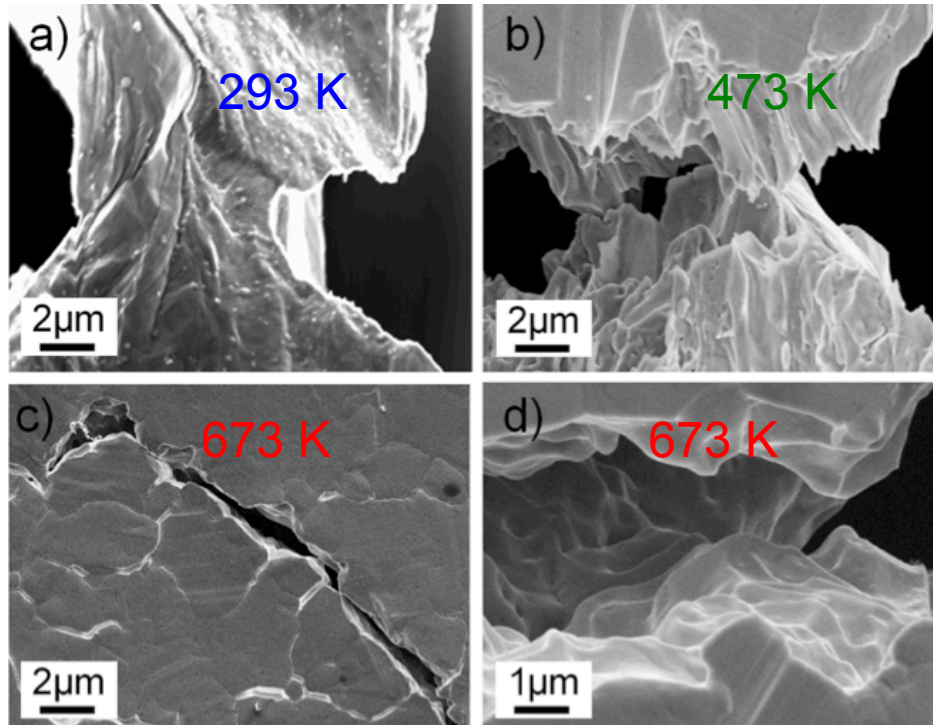
fine-grained samples A:
- strong plastic deformation
- grain-boundary embrittlement at elevated temperatures

coarse-grained samples B:
- glide steps across grains
- same morphology for all temperatures

Stress-Strain in Cu Microstructures

a) sample type A (fine-grained)

b) sample type B (coarse-grained)

— Cu
— Cl
— S
— H
— C
— O

c) O   d) Cl   e) S

20 µm
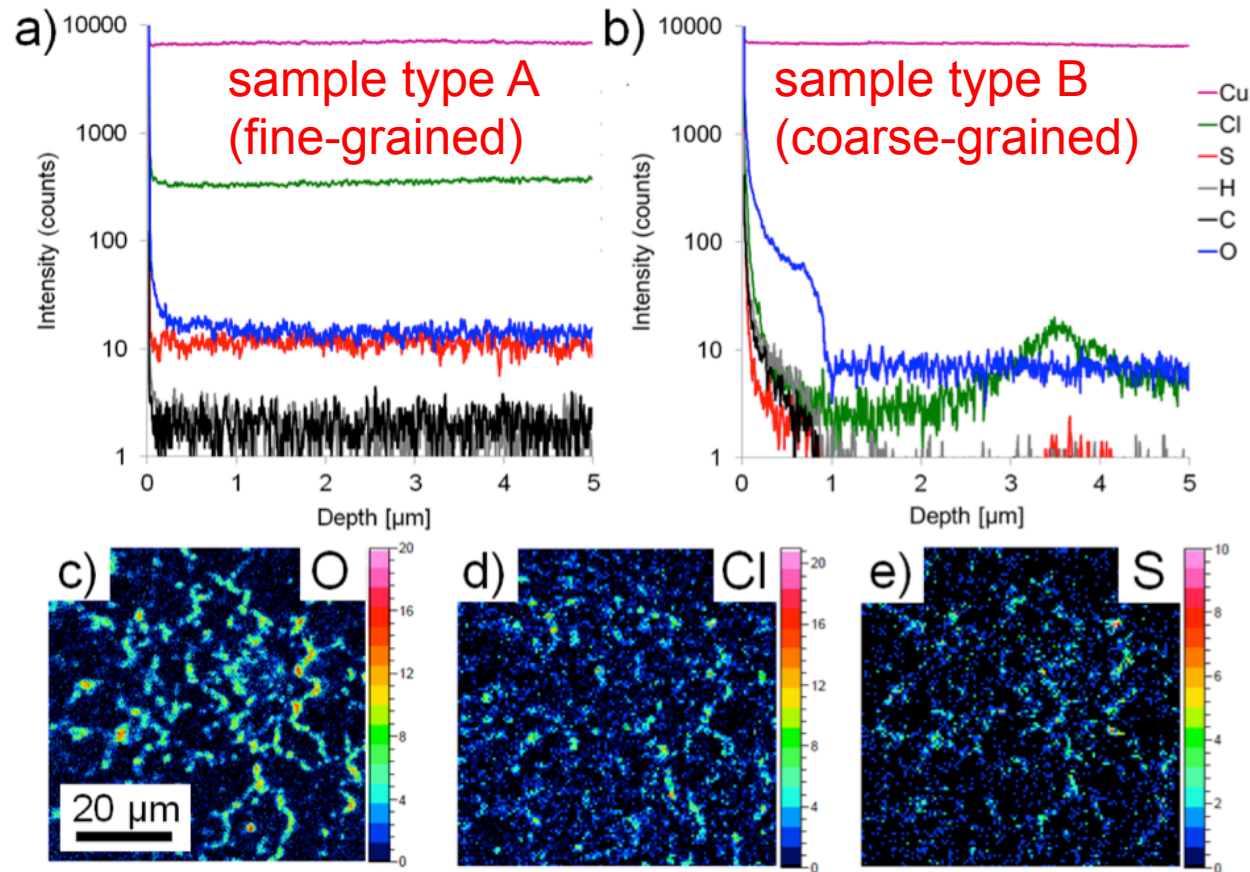
Atomistic Simulations
1. understand grain boundary and surface segregation; compute segregation energies
2. understand grain boundary weakening due to S and Cl
3. find elements which could compensate the detrimental effect of S and Cl but maintain the electronic and thermo-mechanical properties of Cu

- higher S, Cl content in fine-grained samples (additives)
- O, S, Cl enrichment at grain boundaries
- segregation of O, S, Cl to grain boundaries and surfaces

Stress-Strain in Cu Microstructures

Calculated energy release during segregation ΔE_{seg} of Cl and S in Cu.

Cl and S have strong tendency to segregate from the bulk to the GB and, even more so, to the surface

	ΔE_{seg} [kJ/mol]	
	Cl	S
GB segregation, $\Sigma 5$ (001)	-69.9	-54.3
surface segregation, (001)	-321.5	-145.3
GB segregation, $\Sigma 7$ (111)	-53.5	-56.3
surface segregation, (111)	-272.0	-129.9
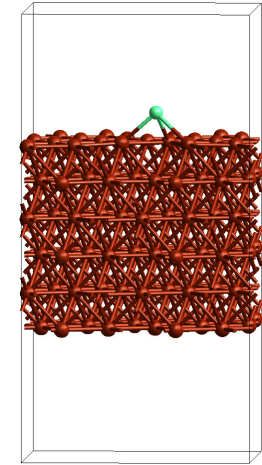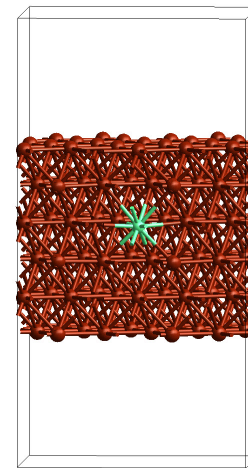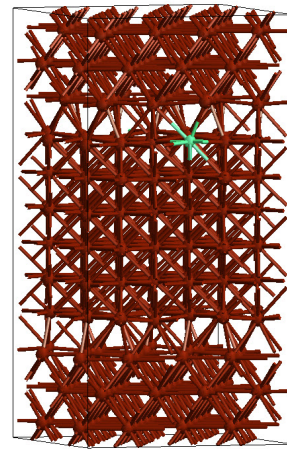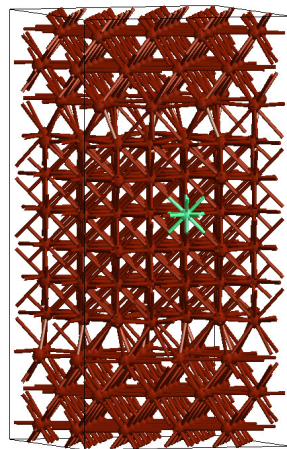
grain boundary segregation

surface segregation

Stress-Strain in Cu Microstructures

Calculated work of separation E_{sep} of $\sum 5$ and $\sum 7$ grain boundaries of pure Cu and Cu contaminated with Cl and S with planar impurity concentration c_{imp} in atoms per nm^2.

	c_{imp} [$1/nm^2$]	E_{sep} [J/m^2]		
		Pure Cu	Cl	S
$\sum 5$ (001)	0.77	1.08	0.82	1.01
$\sum 7$ (111)	0.62	1.13	0.89	1.04

- **Cl, more than S, has a pronounced weakening effect on grain boundary**
- **Formation of chlorides, more than sulfides, at the grain boundary may weaken the microstructure**
- **Objective: Find alloying elements, which already at low concentration**
  - **can be inserted into grain boundaries**
  - **compensate the detrimental role of Cl and S**
  - **maintain electronic and thermo-mechanical properties of Cu**

Microelectronics: Gate Stacks

Problem

Semiconductor devices

▶ How can one reduce the power consumption?

Complementary Metal Oxide Semiconductor

metal/semiconductor interface

oxide

doped semiconductor

Gate metal

Source

Drain

semiconductor

MOS

45 nm and less
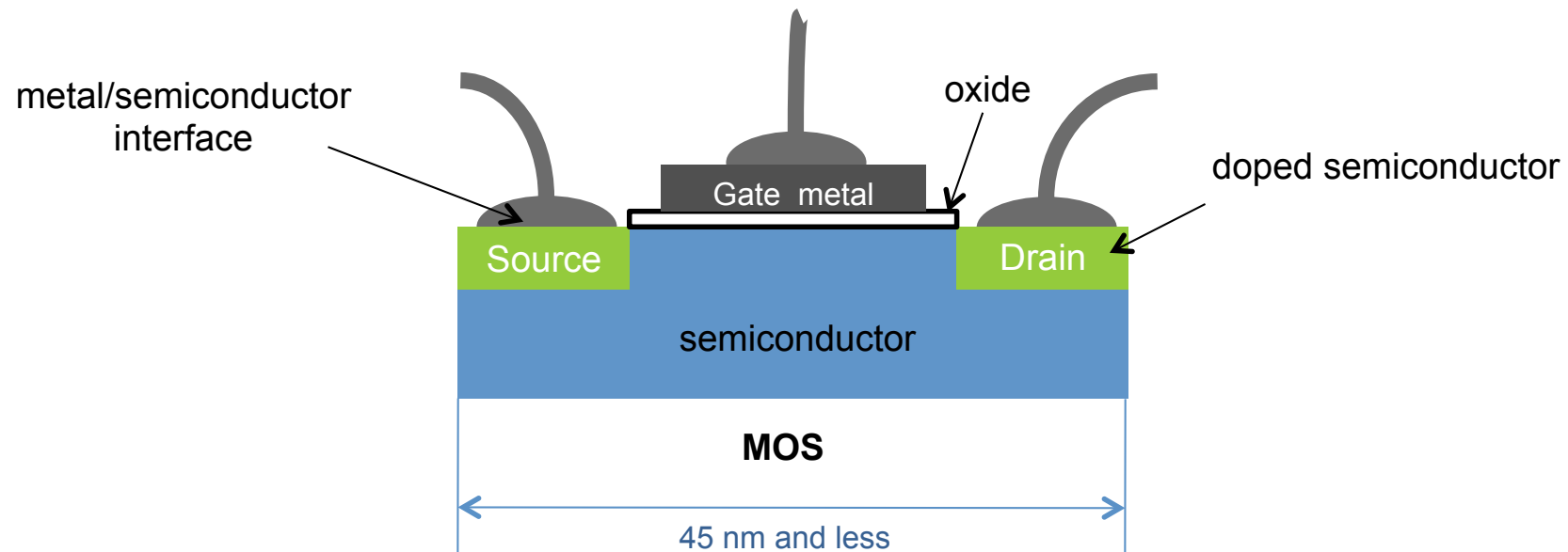
Next-Generation CMOS Devices

HfO$_2$/Ru/TaN gate stack
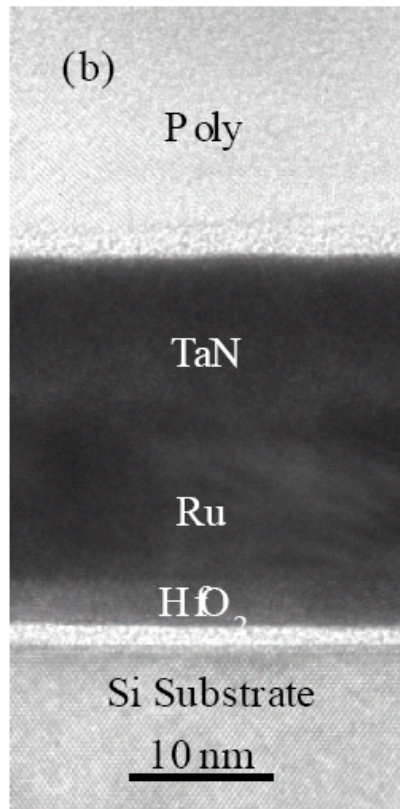
- SiO$_2$ cannot be used at thicknesses less than 15 Å (leakage current is too high)

- HfO$_2$ is replacement for SiO$_2$ as a dielectric

- **A critical design parameter is the work function of the metal – which metallic material should be used so that it can be tuned for PMOS and CMOS devices?**

ADVANCED FABRICATION PROCESSES FOR SUB-50 nm CMOS
Muhammad Mustafa Hussain
http://www.lib.utexas.edu/etd/d/2005/
hussainm51214/hussainm51214.pdf

Complete Gate Stack Model

| 1.7nm | 1.5nm | 1.4nm | 1.2nm |

Si · SiO$_2$ · HfO$_2$ · TiN · Al
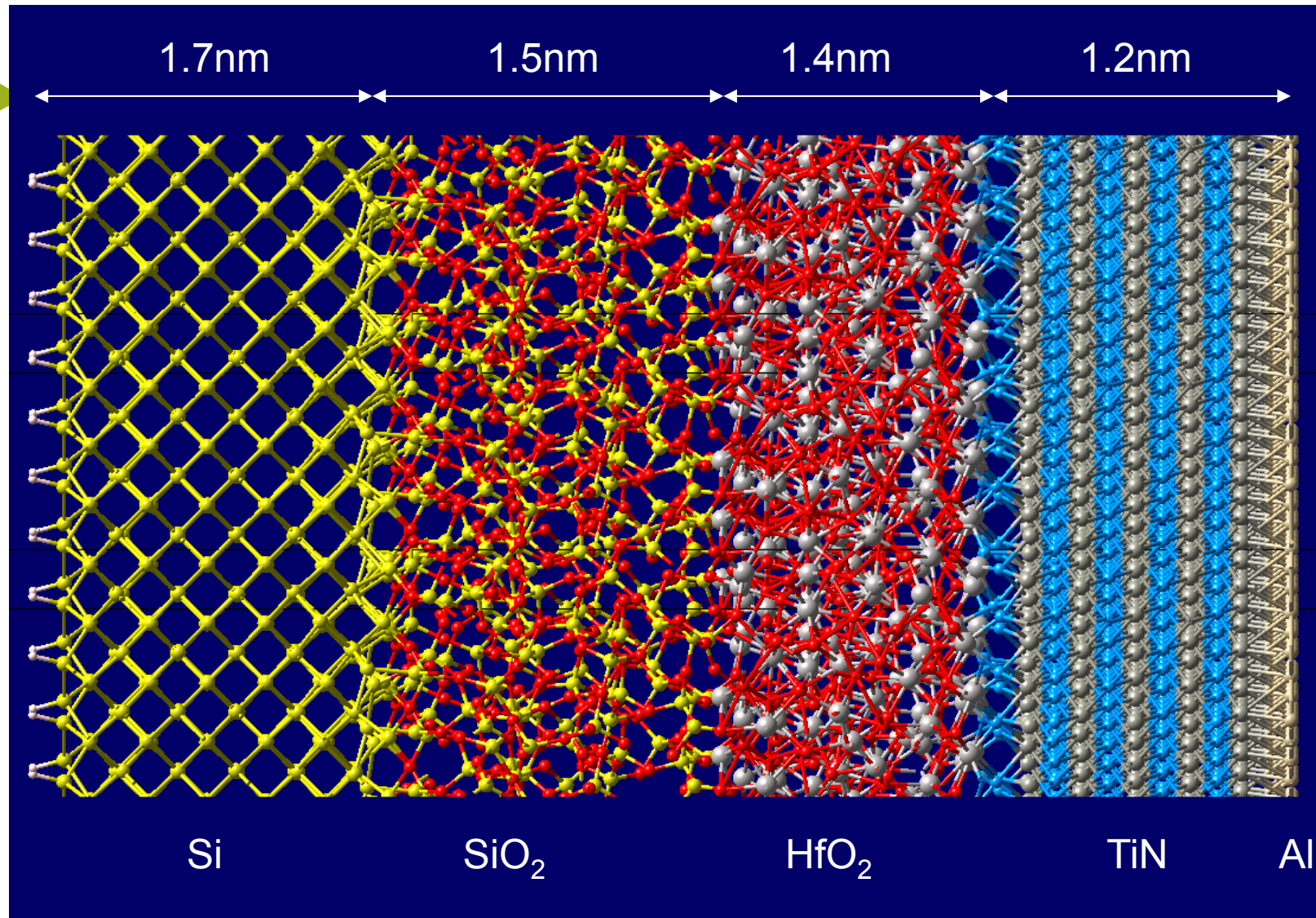
Modeling the TiN/HfO$_2$ Interface

Construction of Surface Models
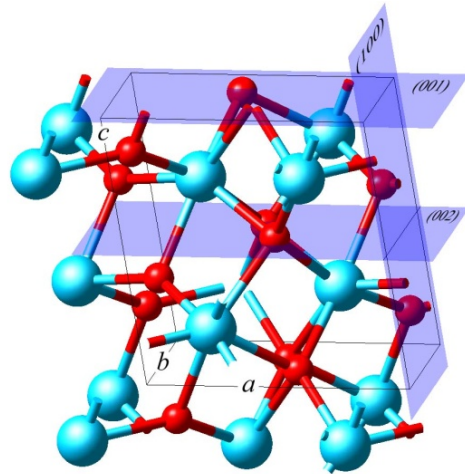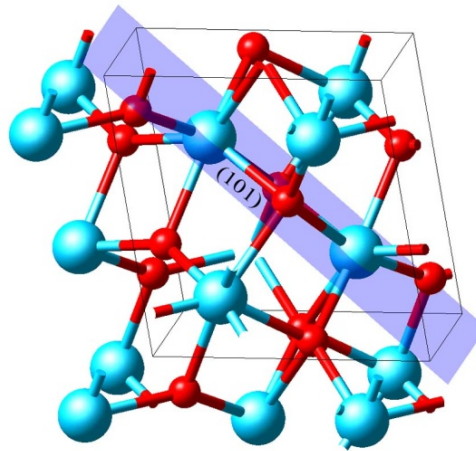
(100), (010),(001)   (110), (101),(101)   (111), (-111),(-1-11)
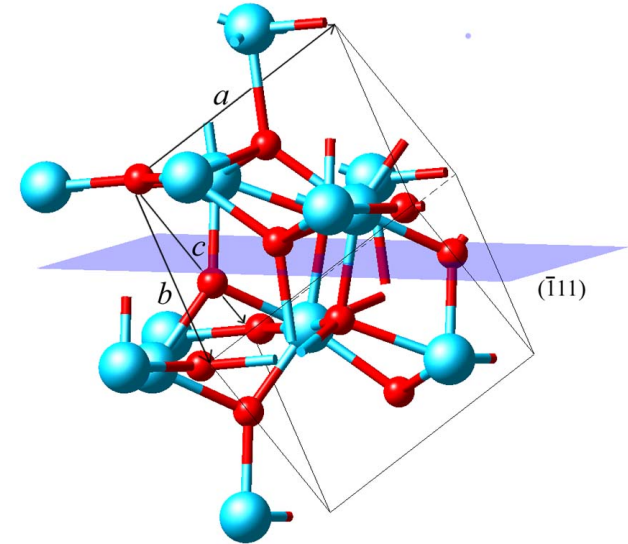
1. Define low-index Miller planes

2. Cut crystal with various surface terminations

3. Create slab models containing multiples of (HfO_2) units with identical upper and lower surfaces

Surface Energy of monoclinic ZrO$_2$ and HfO$_2$
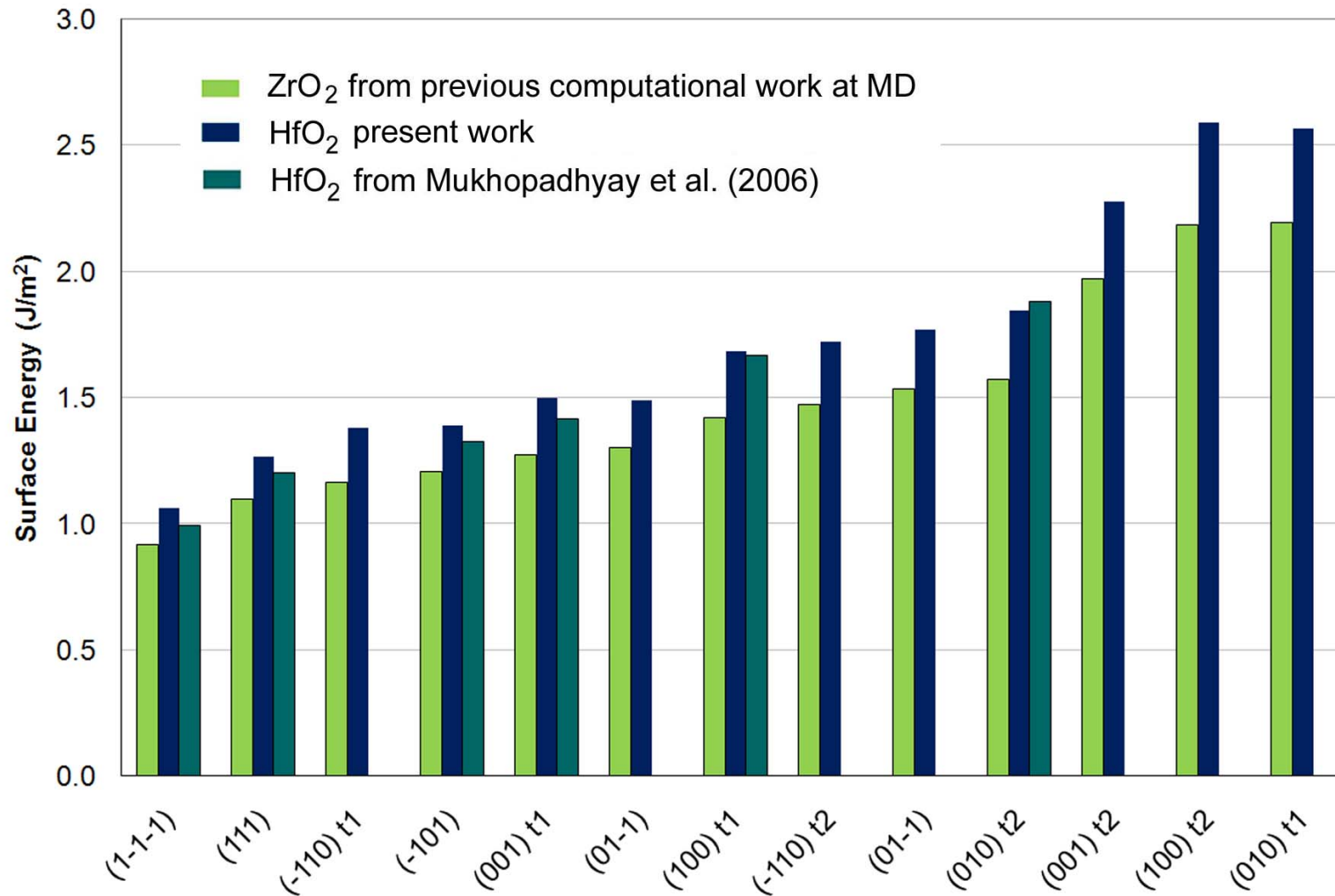
Relaxed HfO$_2$ ($\bar{1}$11) surface

side view of slab model

perspective view of top

top three layers (O-Hf-O)

top two layers (O-Hf)
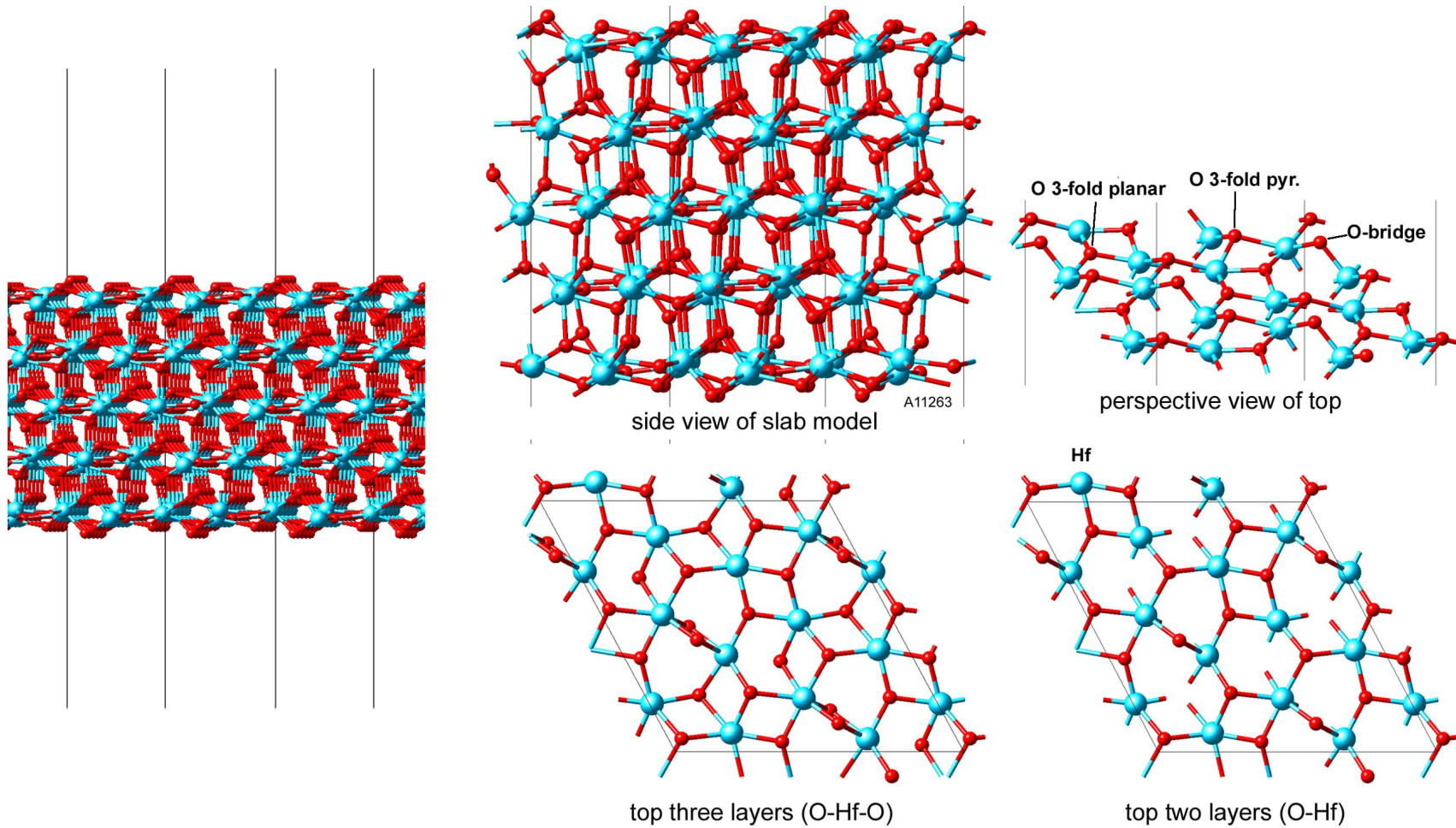
Computation of Interface Structure

HfO$_2$(-111)/TiN(111) Interface

1. Find supercell and orientation with best match of HfO$_2$(-111) and TiN(111) surfaces using MedeA-Interface builder

2. Create thin slab of HfO$_2$ surface

3. Deposit thin layer of TiN

4. Perform simulated annealing keeping bottom layers of oxide frozen

5. Add more layers of HfO$_2$ and TiN and relax all atoms in the system

Interface remains abrupt with some relaxation of O towards Ti and N towards Hf
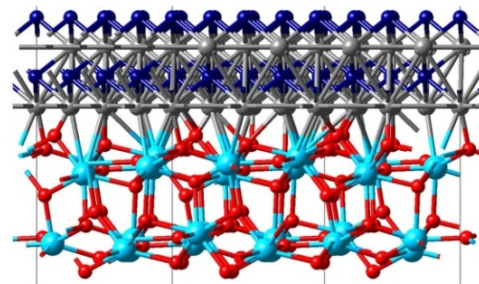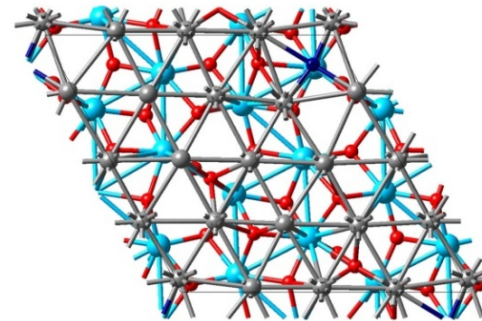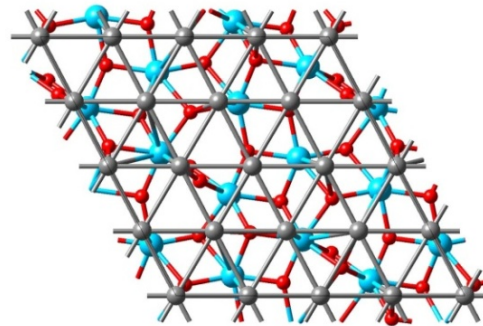
unrelaxed

annealed and relaxed

Annealing of TiN Film on HfO$_2$ Surface

TiN

HfO$_2$

Ti layers nearly flat even at interface

Some N atoms are displaced from octahedral TiN sites

O atoms at interface remain close to positions at free surface

N atom in 6-fold coordination migrated towards the interface

O atom at interface in 3-fold coordination bonding Hf and Ti

O atom at interface in 4-fold coordination bonding Hf and Ti

Hf atom at interface bonded to O and N

HfO$_2$/TiN Effective Work Function

O in TiN

HfO$_2$ TiN

(a)

(c) +550 meV

Work Function (eV)

[O] near interface (cm^{-3})

Experiment

Change in Average Potential (eV)

(c)

Distance to Interface (Å)

Simulation

▶ Experiments showed increase of EWF after annealing of stack under oxygen atmosphere

▶ Interpretation: oxygen inside TiN increase the work function

Reference: Hinkle *et al.*, Appl. Phys. Lett. **96**, 103502 (2010), cooperation TI & MD

HfO$_2$/TiN Effective Work Function

O in TiN

HfO$_2$ **TiN**

N at interface

- Interfacial O fills vacancies in HfO$_2$
- N builds up at interface
- O fills vacancies in TiN

(a)   (b)

O   Hf   Ti   N

(c) +550 meV

(c)   (d)

450 meV

Experiment   Simulation
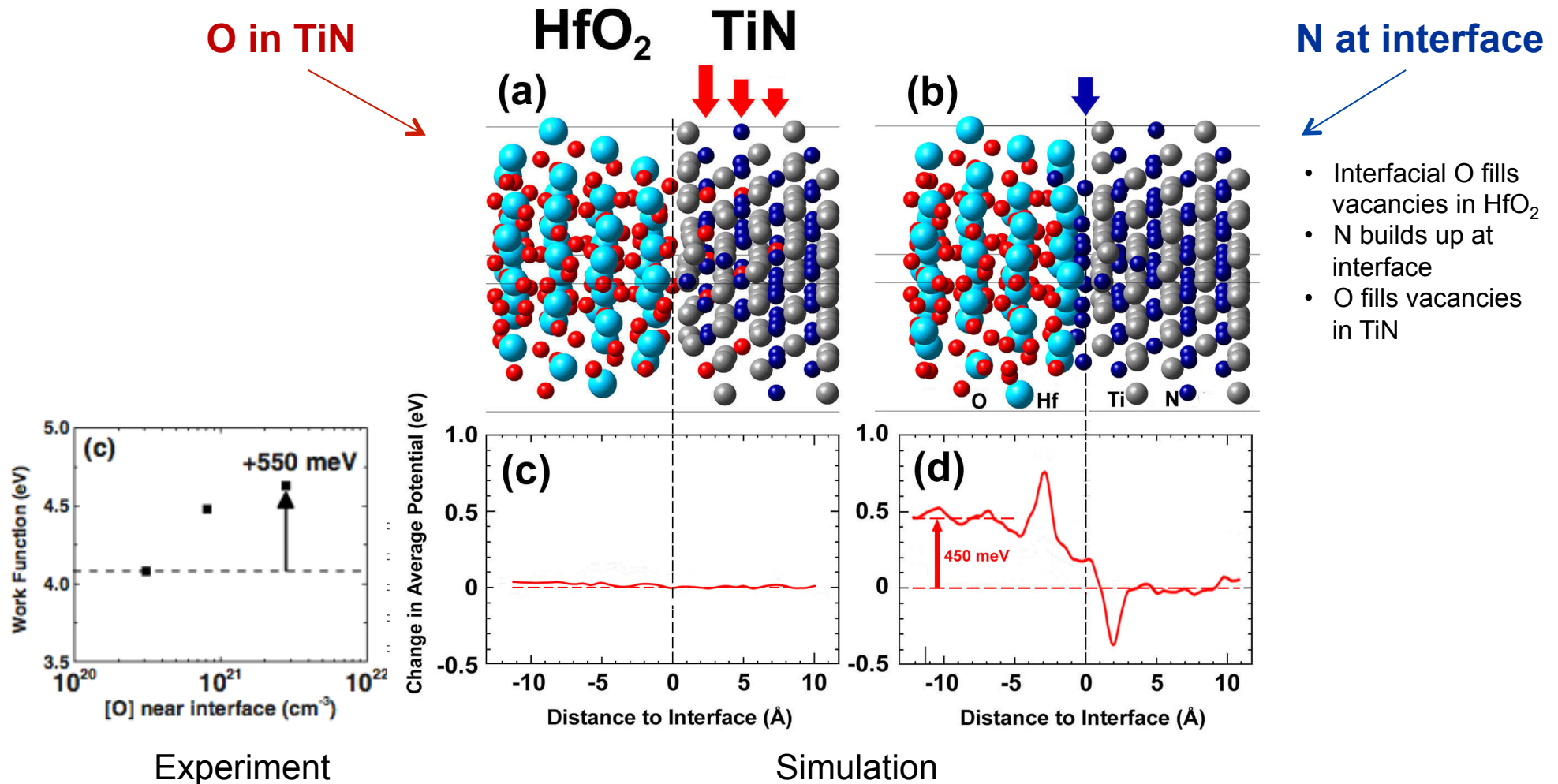
▶ Nitrogen replacing oxgyen at the interface plays the key role

Reference: Hinkle *et al.*, Appl. Phys. Lett. **96**, 103502 (2010), cooperation TI & MD

Interface HfO$_2$/TiN

Interfacial oxygen and nitrogen induced dipole formation and vacancy passivation for increased effective work functions in TiN/HfO$_2$ gate stacks

C. L. Hinkle,[1,2,a)] R. V. Galatage,[2] R. A. Chapman,[2] E. M. Vogel,[1,2] H. N. Alshareef,[3] C. Freeman,[4] E. Wimmer,[4] H. Niimi,[5] A. Li-Fatou,[5] J. B. Shaw,[5] and J. J. Chambers[5]

[1]*Department of Materials Science and Engineering, The University of Texas at Dallas, Richardson, Texas 75080, USA*
[2]*Department of Electrical Engineering, The University of Texas at Dallas, Richardson, Texas 75080, USA*
[3]*King Abdullah University of Science & Technology, Thuwal 23955-6900, Saudi Arabia*
[4]*Materials Design, Incorporated, Angel Fire, New Mexico 87710, USA*
[5]*Advanced CMOS, Texas Instruments Incorporated, Dallas, Texas 75243, USA*

Effective work function (EWF) changes of TiN/HfO$_2$ annealed at low temperatures in different ambient environments are correlated with the atomic concentration of oxygen in the TiN near the metal/dielectric interface. EWF increases of 550 meV are achieved with anneals that incorporate oxygen throughout the TiN with $[O] = 2.8 \times 10^{21}$ cm^{-3} near the TiN/HfO$_2$ interface. However, further increasing the oxygen concentration via more aggressive anneals results in a relative decrease of the EWF and increase in electrical thickness. First-principles calculations indicate the exchange of O and N atoms near the TiN/HfO$_2$ interface cause the formation of dipoles that increase the EWF. © 2010 American Institute of Physics. [doi:10.1063/1.3353993]

Schottky-Barriers

Importance

▶ Reduction of power consumption of electronic devices is a global imperative.

▶ In complementary metal oxide semiconductor (CMOS) devices some parts of the resistance are reduced by scaling to smaller sizes, but not the contact resistance at the source and drain. This contact resistance is becoming a critical bottleneck.

contact resistance
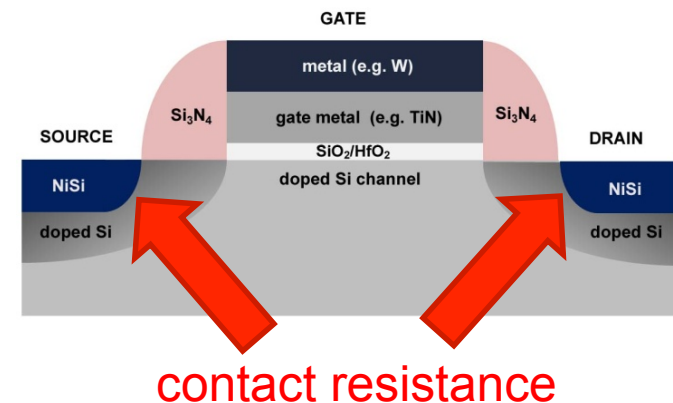
▶ The contact resistance is controlled by the Schottky barrier (SB) at the interface between the metallic (NiSi) and semiconducting (doped Si) regions.

▶ The critical interface can be simulated on the atomistic scale providing detailed understanding and guidance to innovative solutions.

Zooming in with MedeA®

▶ Realistic atomic-scale model of critical interface obtained from ab initio total energy calculations revealing bonding mechanisms
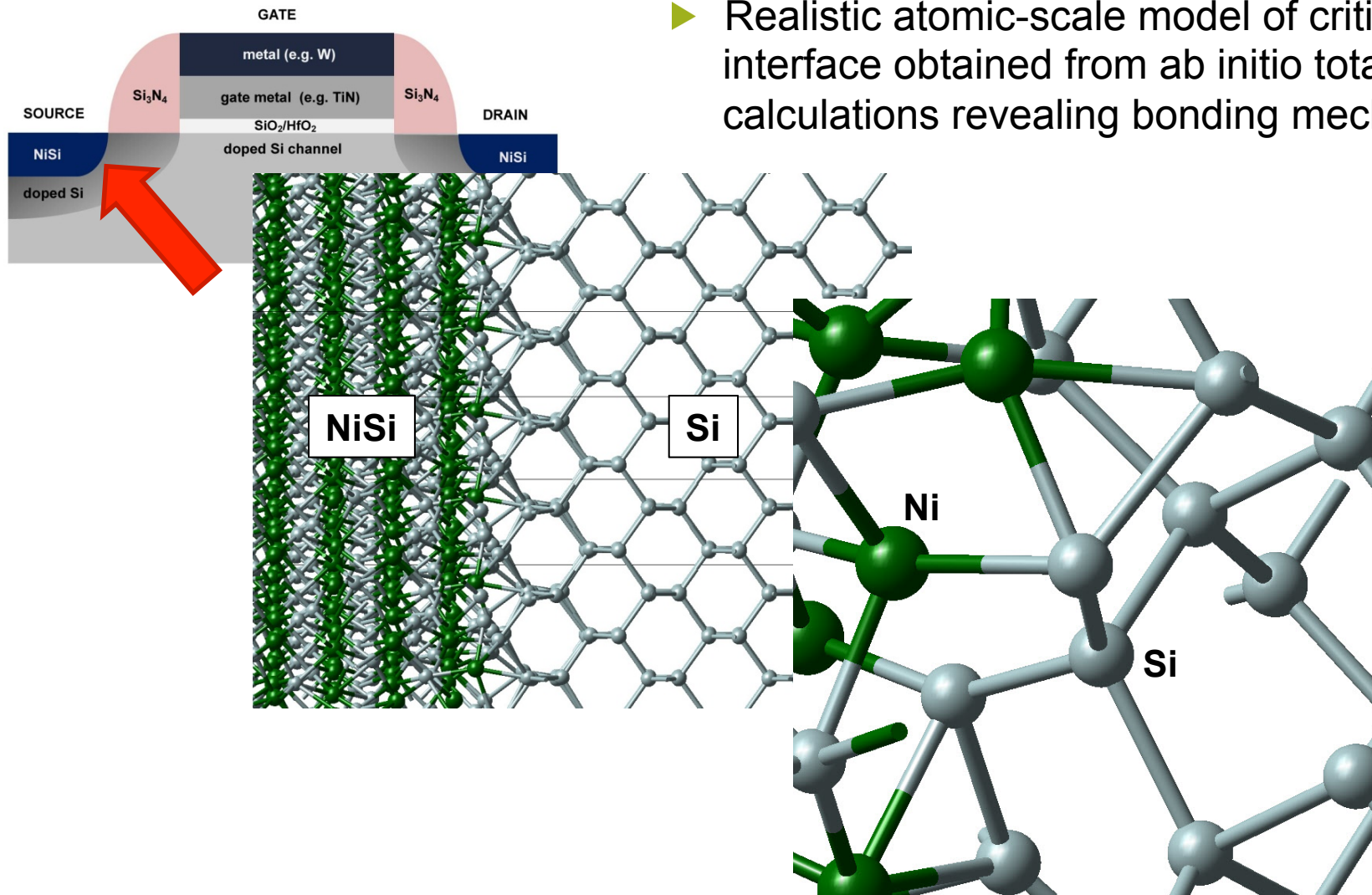
Simulating Formation of SB

Metal (NiSi)

Semiconductor (Si)

Energy

Fermi level

Density of states

conduction band

Band gap

valence band

Density of states
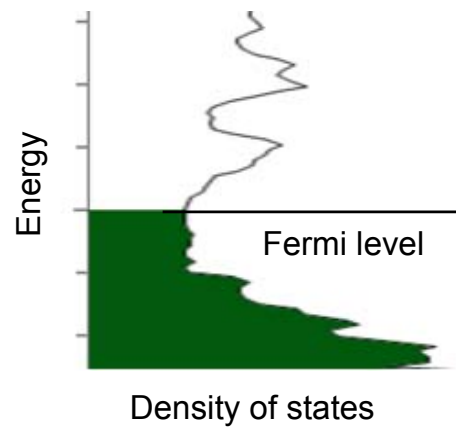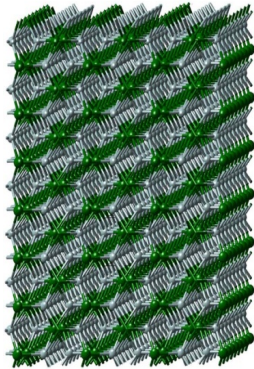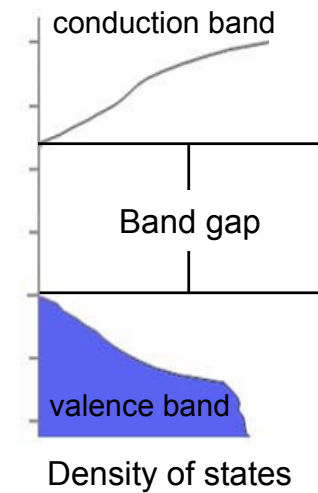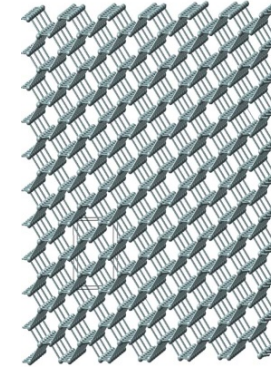
Simulating Formation of SB

Metal (NiSi)   Semiconductor (Si)

Schottky barrier height
(SBH)
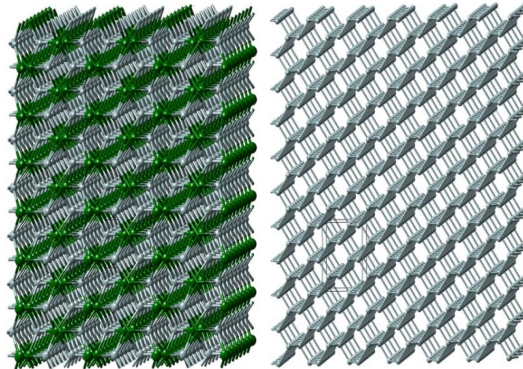
▶ What is the structure of the interface?

▶ What is the value of the SBH?

▶ What is the influence of dopants?

MedeA®-VASP Provides the Answers

NiSi   **Si**

- ▶ MedeA®-VASP provides detailed and reliable information on the structure and bonding of the interface
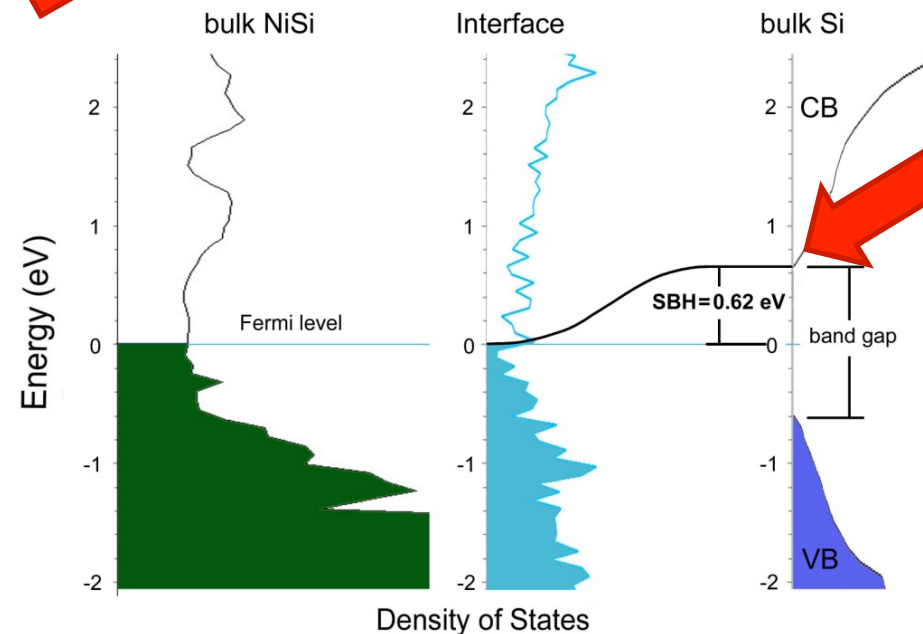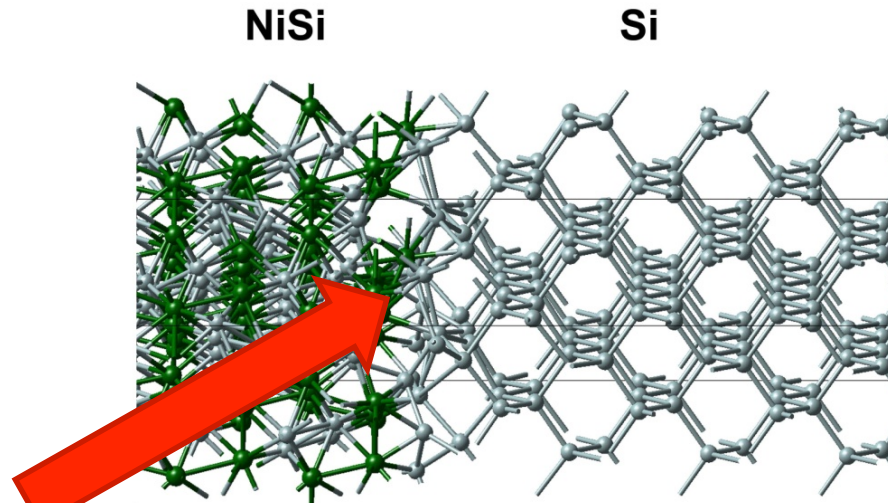
- ▶ MedeA®-VASP predicts the value of the SBH

bulk NiSi   Interface   bulk Si

SBH=0.62 eV

Fermi level

band gap

CB

VB

Energy (eV)

Density of States

MedeA®-VASP Provides the Answers
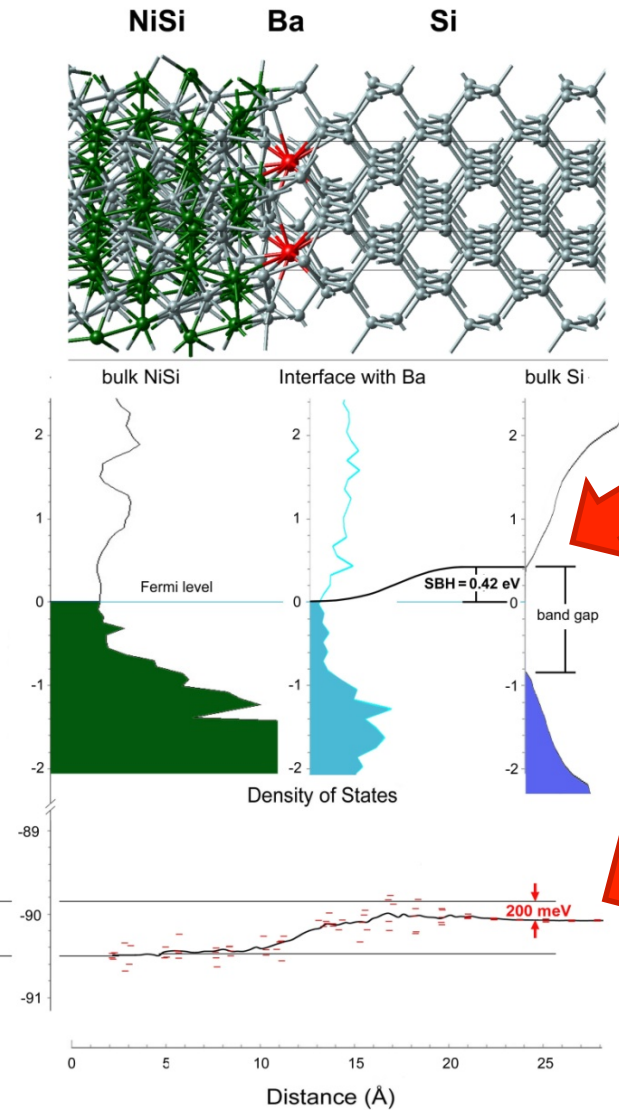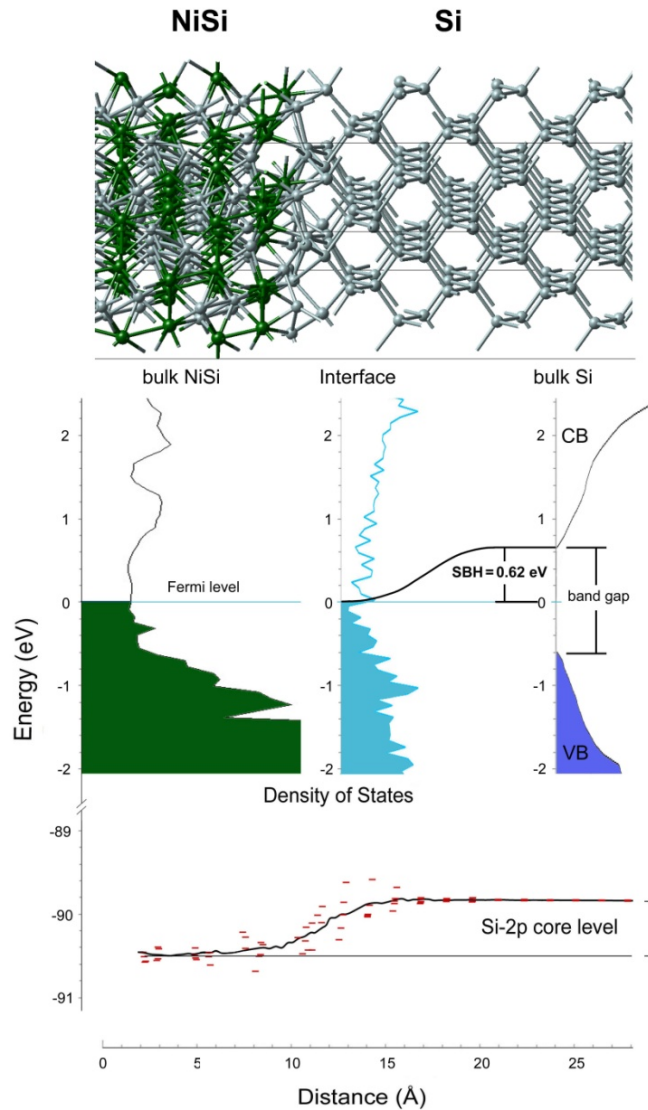
▶ MedeA®-VASP predicts the effect of dopants on the SBH

▶ MedeA®-VASP predicts core level shifts

Preferred Location of Dopants

▶ MedeA®-VASP predicts the preferred locations of dopant atoms

Tuning of SBH

Tuning of NiSi/Si Schottky barrier heights by sulfur segregation during Ni silicidation

Q. T. Zhao
Institut für Schichten und Grenzflächen (ISG1-IT), and Center of Nanoelectronic Systems for Information Technology (CNI), Forschungszentrum Jülich, 52425 Jülich, Germany

U. Breuer
Zentralabteilung für Chemische Analysen (ZCH), Forschungszentrum Jülich, 52425 Jülich, Germany

E. Rije, St. Lenk, and S. Mantl
Institut für Schichten und Grenzflächen (ISG1-IT), and Center of Nanoelectronic Systems for Information Technology (CNI), Forschungszentrum Jülich, 52425 Jülich, Germany

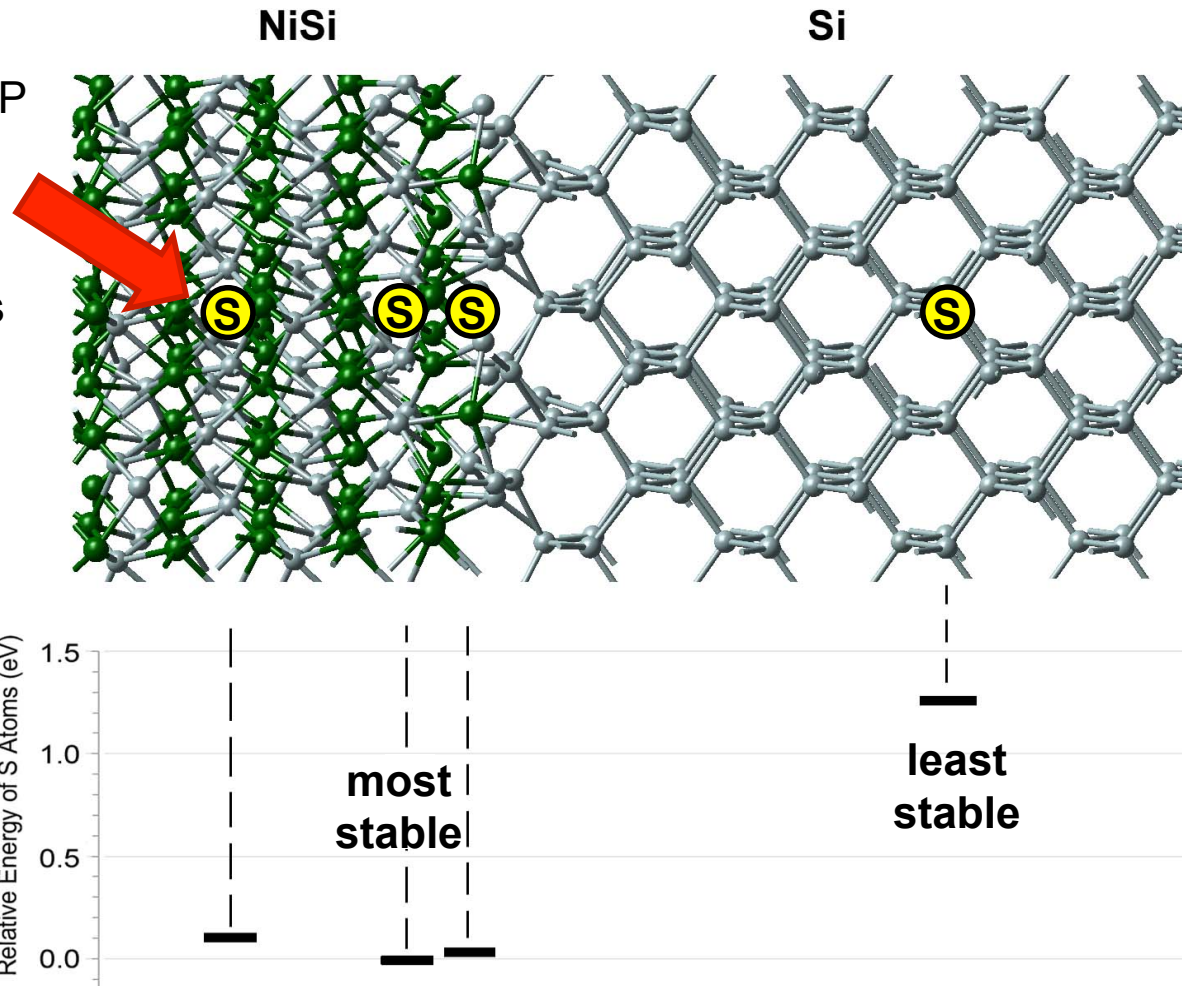The Schottky barrier height (SBH) of NiSi on Si(100) was tuned in a controlled manner by the segregation of sulfur (S) to the silicide/silicon interface. S was implanted into silicon prior to silicidation. During subsequent Ni silicidation, the segregation of S at the NiSi/Si interface leads to the change of the SBH. The SBH of NiSi decreased gradually on n-Si(100) from 0.65 eV to 0.07 eV and increased correspondingly on p-Si(100). © 2005 American Institute of Physics. [DOI: 10.1063/1.1863442]
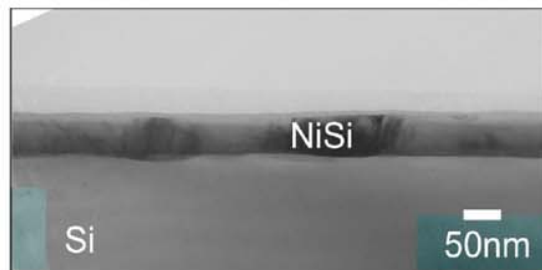

FIG. 1. XTEM image of a NiSi layer formed at 550 °C for 1 min on the n-Si(100) substrate implanted with 15 keV, 2×10^{14} S$^+$/cm^2 prior to Ni deposition.
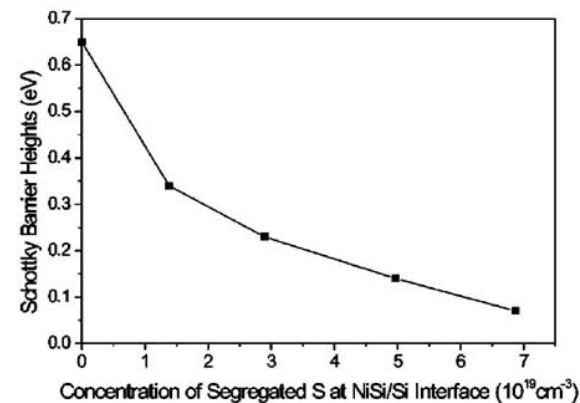

FIG. 6. SBH values of NiSi on n-Si(100) as a function of the concentration of the S atoms segregated at the NiSi/n-Si(100) interface.

(19) **United States**
(12) **Patent Application Publication** (10) Pub. No.: **US 2009/0134388 A1**
YAMAUCHI et al. (43) Pub. Date: **May 28, 2009**

US 20090134388A1

(54) **SEMICONDUCTOR DEVICE AND FABRICATION METHOD OF SAME**

(75) Inventors: **Takashi YAMAUCHI**, Kanagawa (JP); **Yoshifumi Nishi**, Kanagawa (JP); **Yoshinori Tsuchiya**, Kanagawa (JP); **Junji Koga**, Kanagawa (JP); **Koichi Kato**, Kanagawa (JP)

Correspondence Address:
OBLON, SPIVAK, MCCLELLAND MAIER & NEUSTADT, P.C.
1940 DUKE STREET
ALEXANDRIA, VA 22314 (US)

(73) Assignee: **KABUSHIKI KAISHA TOSHIBA**, Tokyo (JP)

(21) Appl. No.: **12/203,409**

(22) Filed: **Sep. 3, 2008**

(30) **Foreign Application Priority Data**

Nov. 26, 2007 (JP) 2007-304572

Publication Classification

(51) Int. Cl.
H01L 29/08 (2006.01)
H01L 21/06 (2006.01)

(52) U.S. Cl. **257/42**; 438/102; 257/E21.068; 257/E29.029

(57) **ABSTRACT**

A semiconductor device having a metal insulator semiconductor field effect transistor (MISFET) with interface resistance-reduced source/drain electrodes is disclosed. This device includes a p-type MISFET formed on a semiconductor substrate. The p-MISFET has a channel region in the substrate, a gate insulating film on the channel region, a gate electrode on the gate insulating film, and a pair of laterally spaced-apart source and drain electrodes on both sides of the channel region. These source/drain electrodes are each formed of a nickel (Ni)-containing silicide layer. The p-MISFET further includes an interface layer which is formed on the substrate side of an interface between the substrate and each source/drain electrode. This interface layer contains magnesium (Mg), calcium (Ca) or barium (Ba) therein. A fabrication method of the semiconductor device is also disclosed.
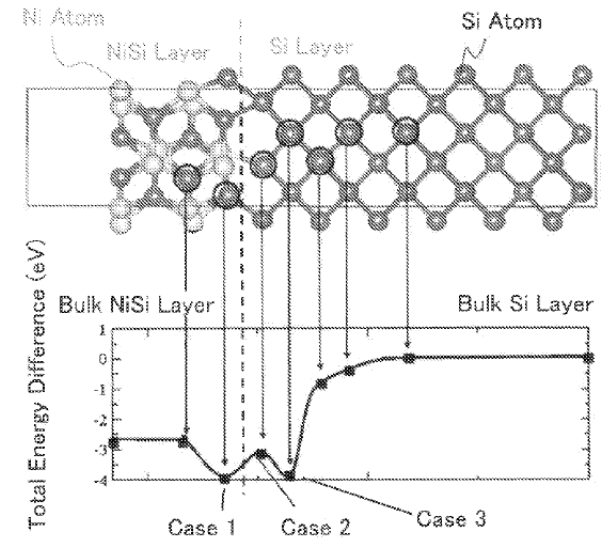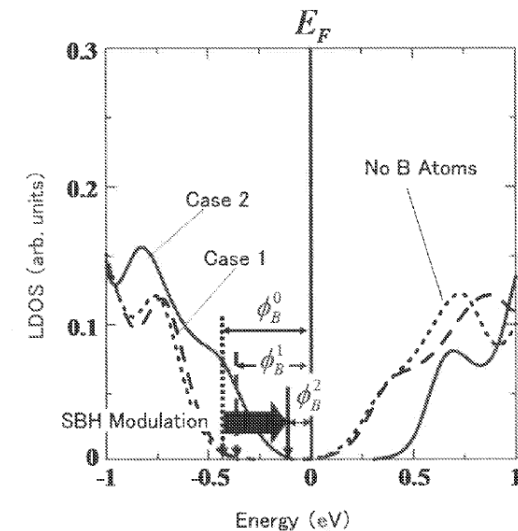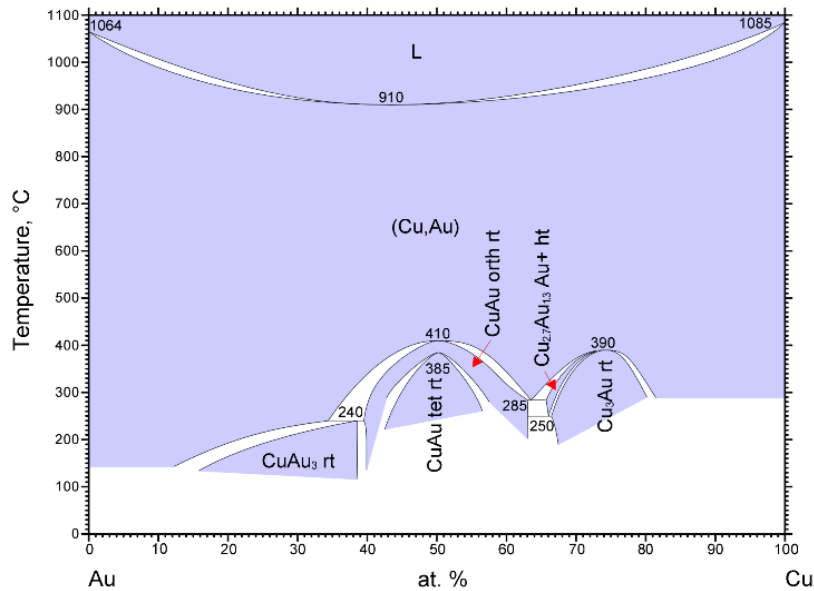
[0018] FIG. **47** is a graph showing SBH calculation results. Its lateral axis indicates the energy of an electron whereas the longitudinal axis indicates the local density of states (LDOS). For comparison purposes, calculation values in the case of an impurity segregation layer being absent are also shown in this graph. As apparent from FIG. **47**, in case a B atom entered to Case 2, SBH is lowered by 0.3 eV. This is ascertainable by measurement of the current-voltage characteristics of a NiSi/Si Schottky junction, which was formed for calculation of the values shown in FIG. **47**.
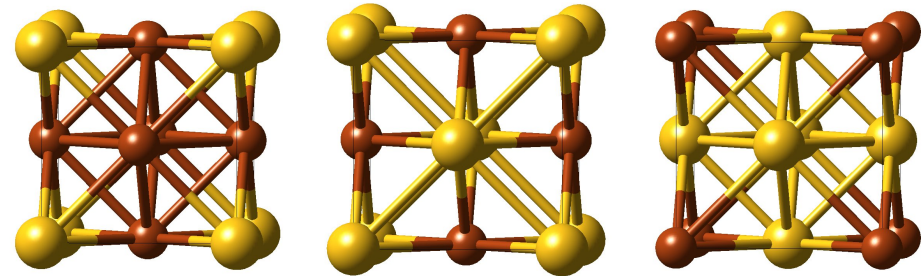
FIG.47

RELATED ART

Electrical Conductivity in Disordered Materials

Cu$_{1-x}$Au$_x$: Intermetallic Phases

ordered cubic phases (InfoMaticA):

disordered cubic phases (SQS):

Cu$_3$Au   CuAu   CuAu$_3$

- wide range of solubility
- ordered and disordered phases
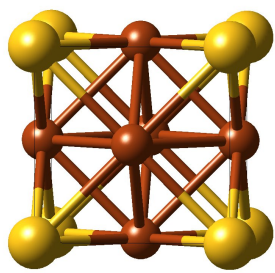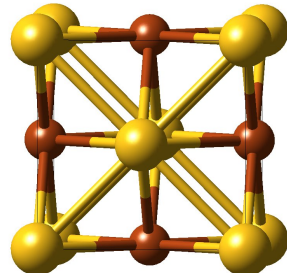
- ordered phases from literature (InfomaticA) and cluster expansion (CE)
- disordered phases modeled as special quasi-random structure (SQS)
  - mimic first few correlation functions of perfectly random structures

ordered cubic phases (InfoMaticA):
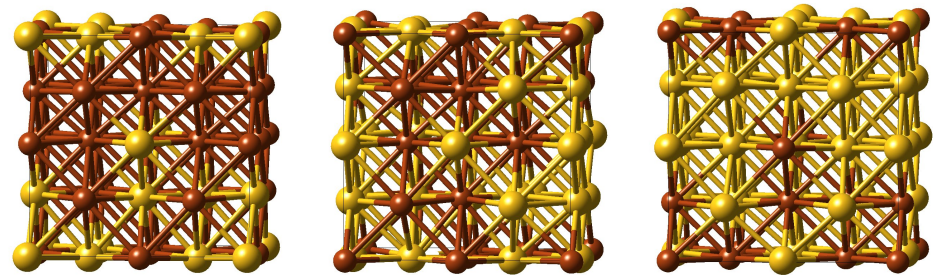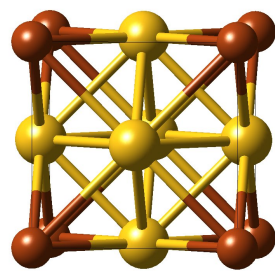
Cu₃Au   CuAu   CuAu₃

ordered tetragonal phases from cluster expansion (CE):
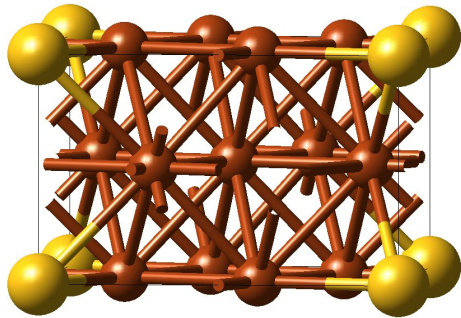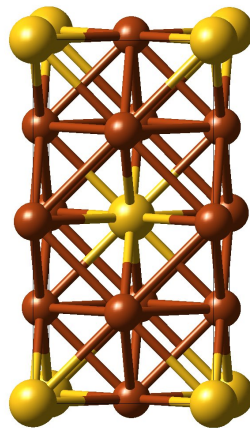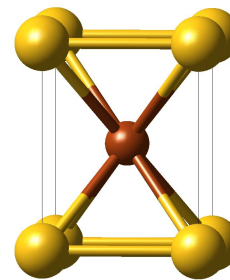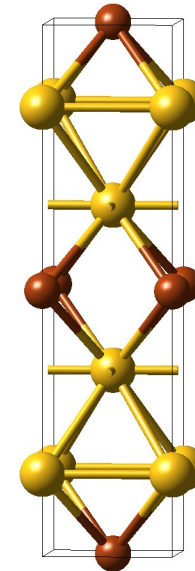
Cu₉Au   Cu₃Au   CuAu   CuAu₂   CuAu₈
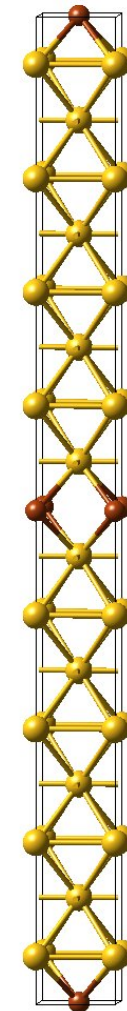
Cu$_{1-x}$Au$_x$: Electrical Resistivities

ungeordnete Legierungen

geordnete Legierungen

Widerstand

Ausbildung von Überstrukturen

Cu   Cu$_3$Au   CuAu   Au

At.-% Au
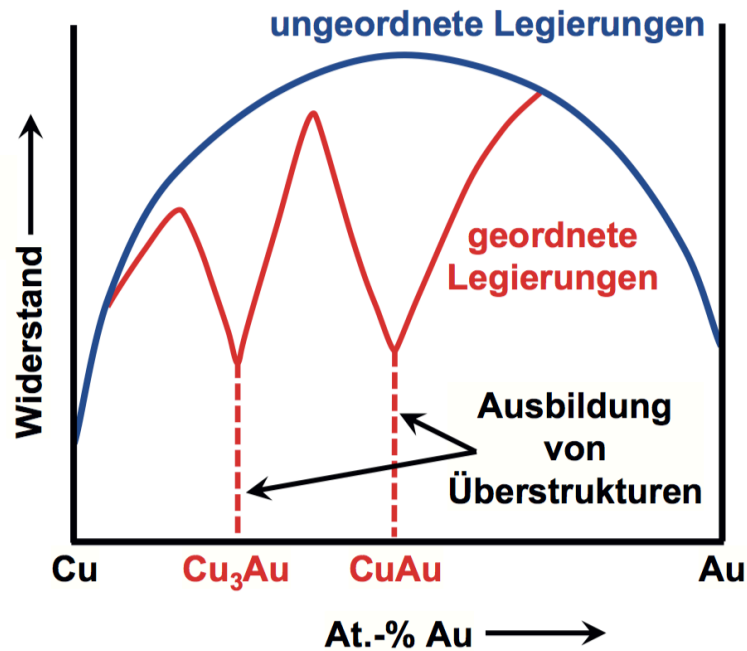
Pecher, Haarmann, Nachr. Chem. **61**, 1017 (2013);
Riedel, Janiak, *Anorg. Chem.* (de Gruyter, Berlin 2007)

Resistivity

disordered (SQS)

ordered (lit.)

ordered (CE)

At.-% Au
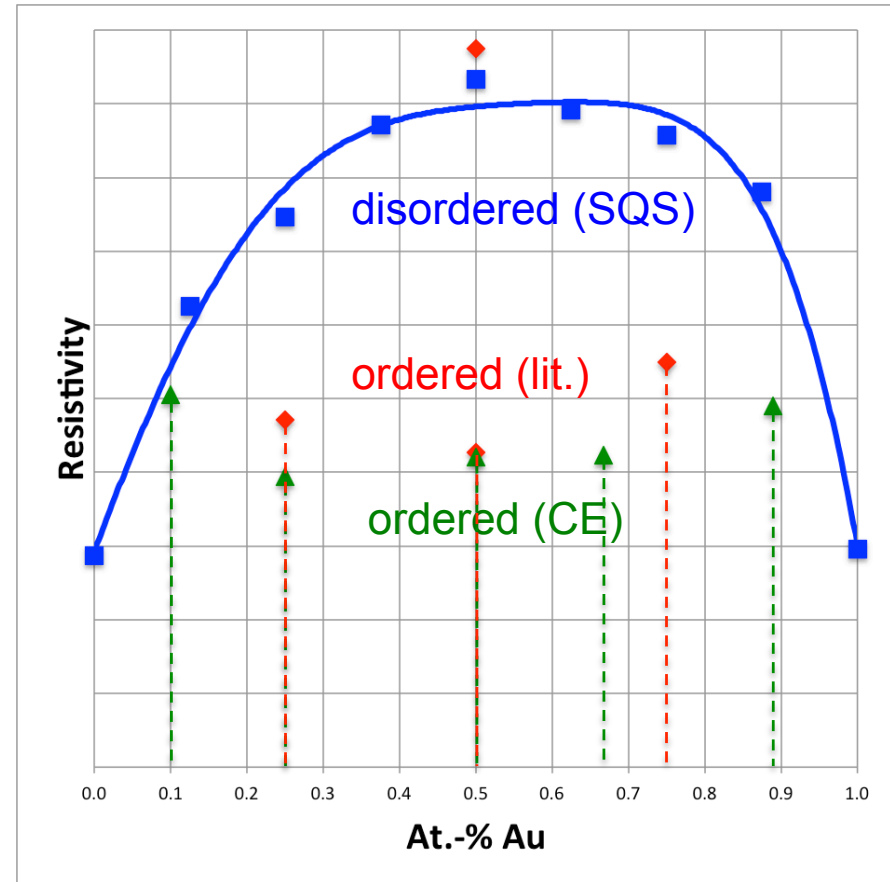
- ordered phases show systematically reduced electrical resistivities as compared to disordered alloys
- very good agreement of calculated data with experimental findings

Low-Strain Cathode Materials

Low-Strain Cathode Materials

Computational Design and Experimental Verification of Zero- and Low-strain Cathode Materials for Solid-State Li-ion batteries

Fabio Rosciano[1], Mikael Christensen[2], Volker Eyert[2], Alexander Mavromaras[2], Erich Wimmer[2]

[1]Toyota Motor Europe, Advanced Technology 1, Hoge Wei 33, Zaventem, Belgium
[2]Materials Design S.A.R.L., Montrouge, France

- electrode
- Solid electrolyte
- Discharge — **Expansion (ΔV)**
- Solid electrolyte
- Charge — **Contraction (-ΔV)**
- **Detached interface**
- Solid electrolyte
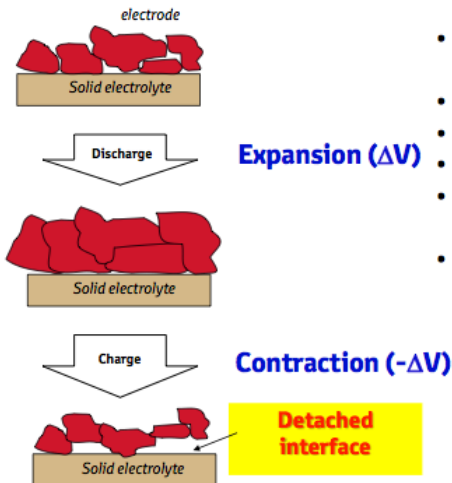
▶ Volume change of electrodes on charge/discharge major cause of degradation of Li-ion batteries

- stress generated at grain interfaces leads to destruction of solid-state batteries

▶ Use atomistic simulations to find high-voltage zero-strain cathode materials

- focus on compounds with spinel structure, start from $LiMn_2O_4$

presented at: International Battery Association, Brisbane March 2014

Optimization Strategy

$$\alpha \rightarrow V\alpha$$
$$\beta \rightarrow V\beta$$
$$V(x\alpha + y\beta) = x\,V\alpha + y\,V\beta$$

$$x\ LiM^1_2O_4$$
$$y\ LiM^2_2O_4 +$$
$$z\ LiM^3_2O_4 =$$
$$Li(M^1_xM^2_yM^3_z)O_4$$
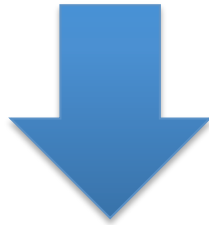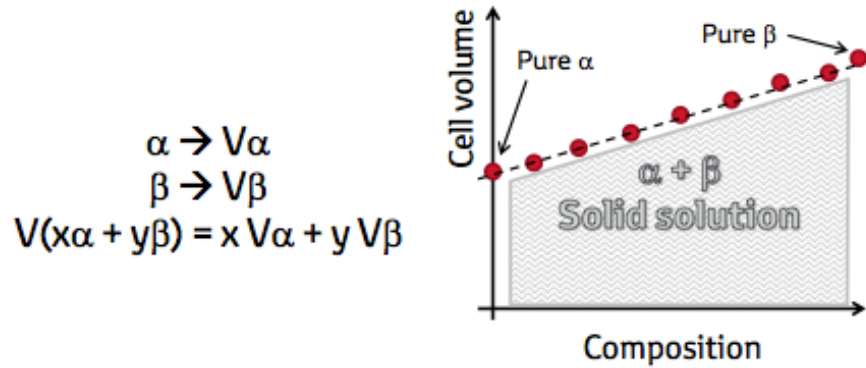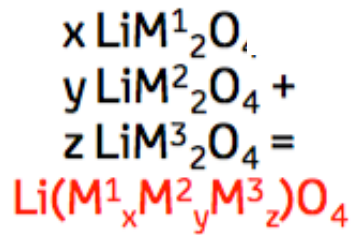
M = Mg, V, Cr, Mn, Fe, Co, Ni, Cu, Al
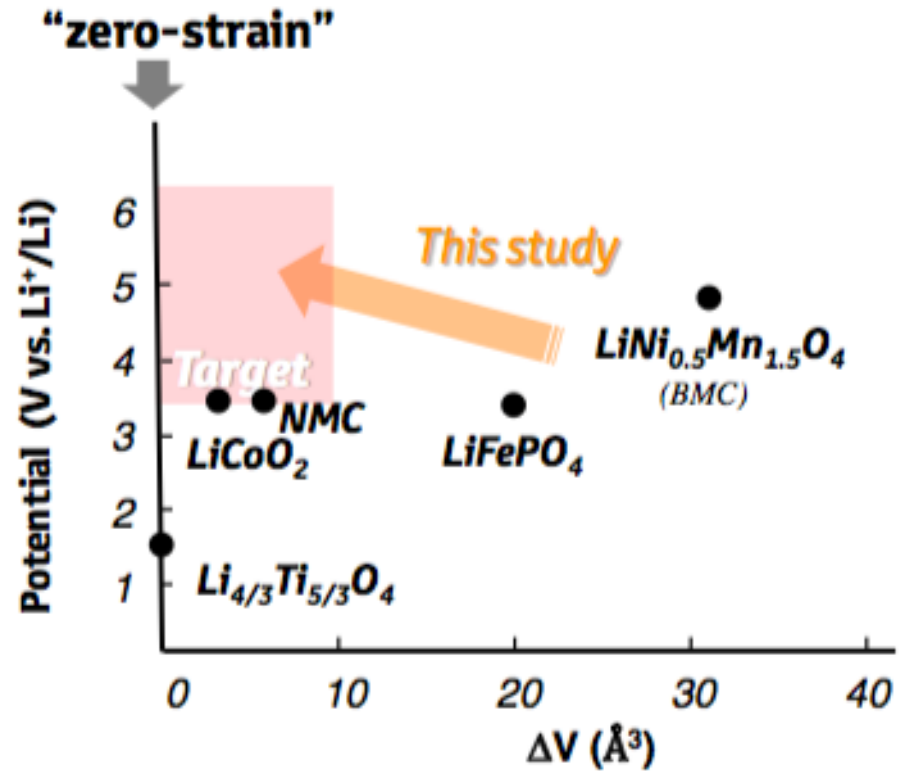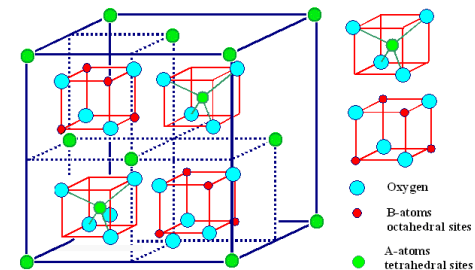
AB_2O_4 **spinel** The red cubes are also contained in the back half of the unit cell

Oxygen
B-atoms octahedral sites
A-atoms tetrahedral sites

Low-Strain Cathode Materials

Calculated volume change for LiM$_2$O4
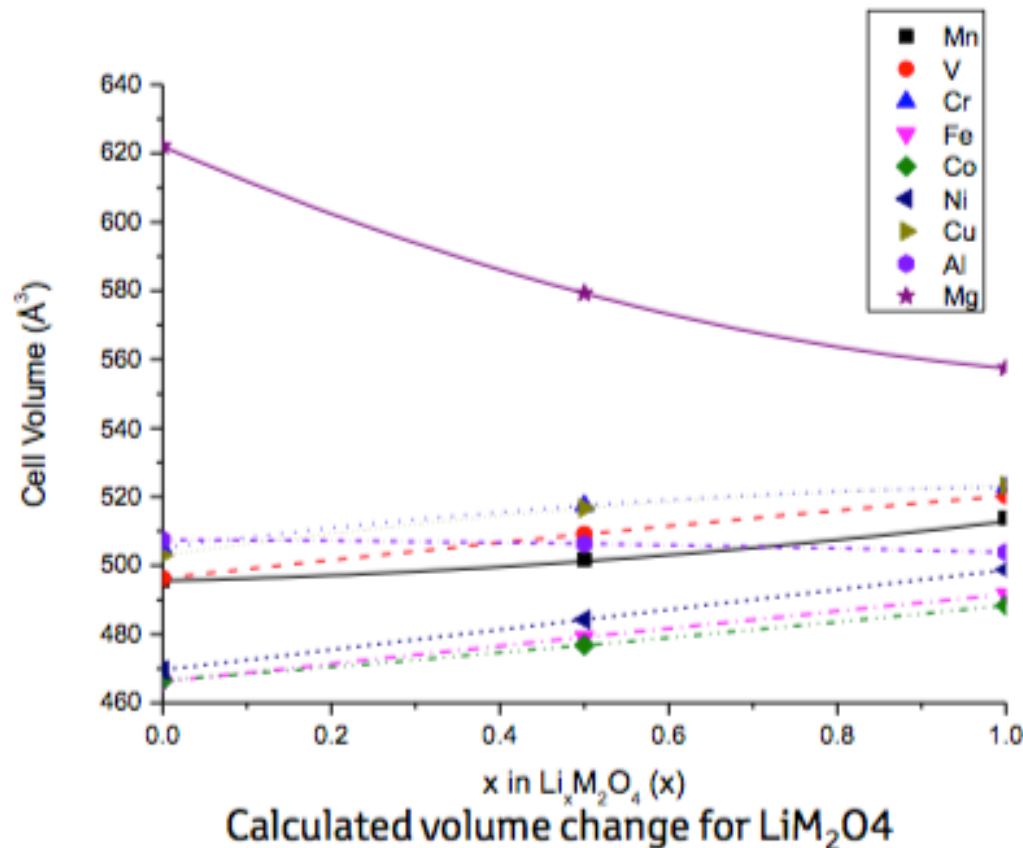
► Calculate volume for Li$_x$M$_2$O$_4$ with x=0,0.5,1 (M=Mg, Al, V, Cr, Mn, Fe, Co, Ni, Cu)

► Interpolate using 2nd degree polynomial

► Only Mg would allow for efficient volume change compensation

► Choose three components
  - Mn to provide structural stability
  - Mg to reduce volume change
  - Cr to compensate for electro-chemical inactivity of Mg

F. Rosciano, M. Christensen, V. Eyert, A. Mavromaras, E. Wimmer, IBA 2014

Low-Strain Cathode Materials
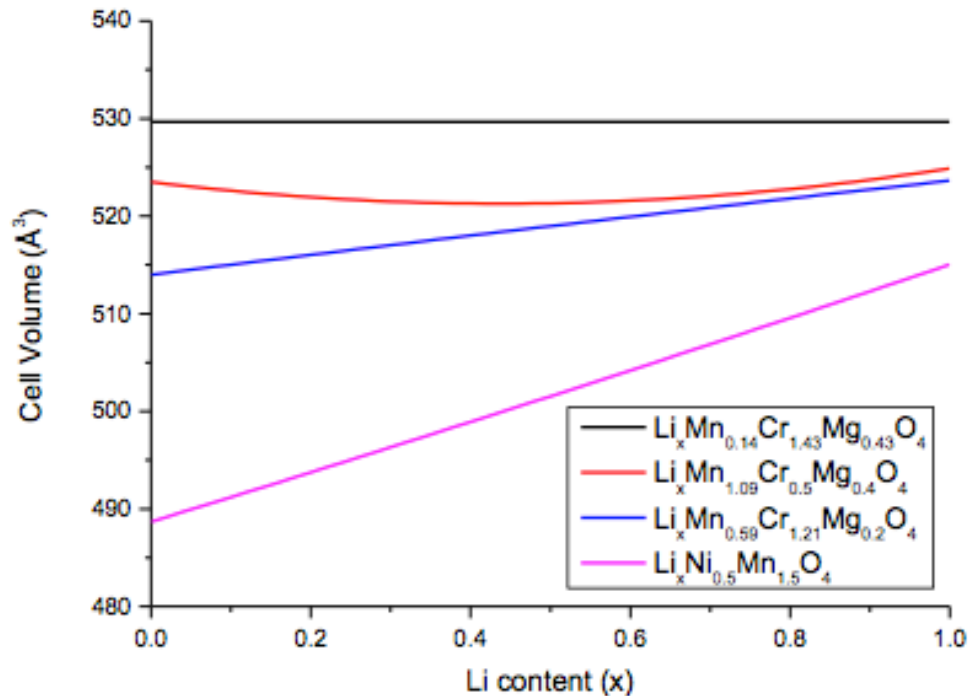
Calculated volume change for the optimized compositions

► **Choose three components**
  - Mn to provide structural stability
  - Mg to reduce volume change
  - Cr to compensate for electro-chemical inactivity of Mg

► **Mix according to three different principles**
  - free optimization to obtain true zero-strain material
  - optimization constraining Mn content ≥ 1
  - optimization constraining Mg content ≤ 0.2

► **Result**
  - $LiMn_{0.14}Cr_{1.43}Mg_{0.43}O_4$ with projected $\Delta V = 0 Å^3$
  - $LiMn_{1.1}Cr_{0.5}Mg_{0.4}O_4$ with projected $\Delta V = 3 Å^3$
  - $LiMn_{0.59}Cr_{1.21}Mg_{0.2}O_4$ with projected $\Delta V = 8 Å^3$
  - Benchmark: $LiMn_{1.5}Ni_{0.5}O_4$ with $\Delta V = 30 Å^3$

F. Rosciano et al., IBA 2014

Low-Strain Cathode Materials

- XRD pattern of $LiMn_{1.1}Cr_{0.5}Mg_{0.4}O_4$. A minor Li_2MnO_3 impurity is present (~3%)
- First charge of $LiMn_{1.1}Cr_{0.5}Mg_{0.4}O_4$
- Comparison of *ex situ* XRD patterns
- Detail of [400] peak shift for the spinel phase. Peak [200] of Aluminium is used as reference
- Comparison between experimental and simulation data for $LiMn_{1.1}Cr_{0.5}Mg_{0.4}O_4$
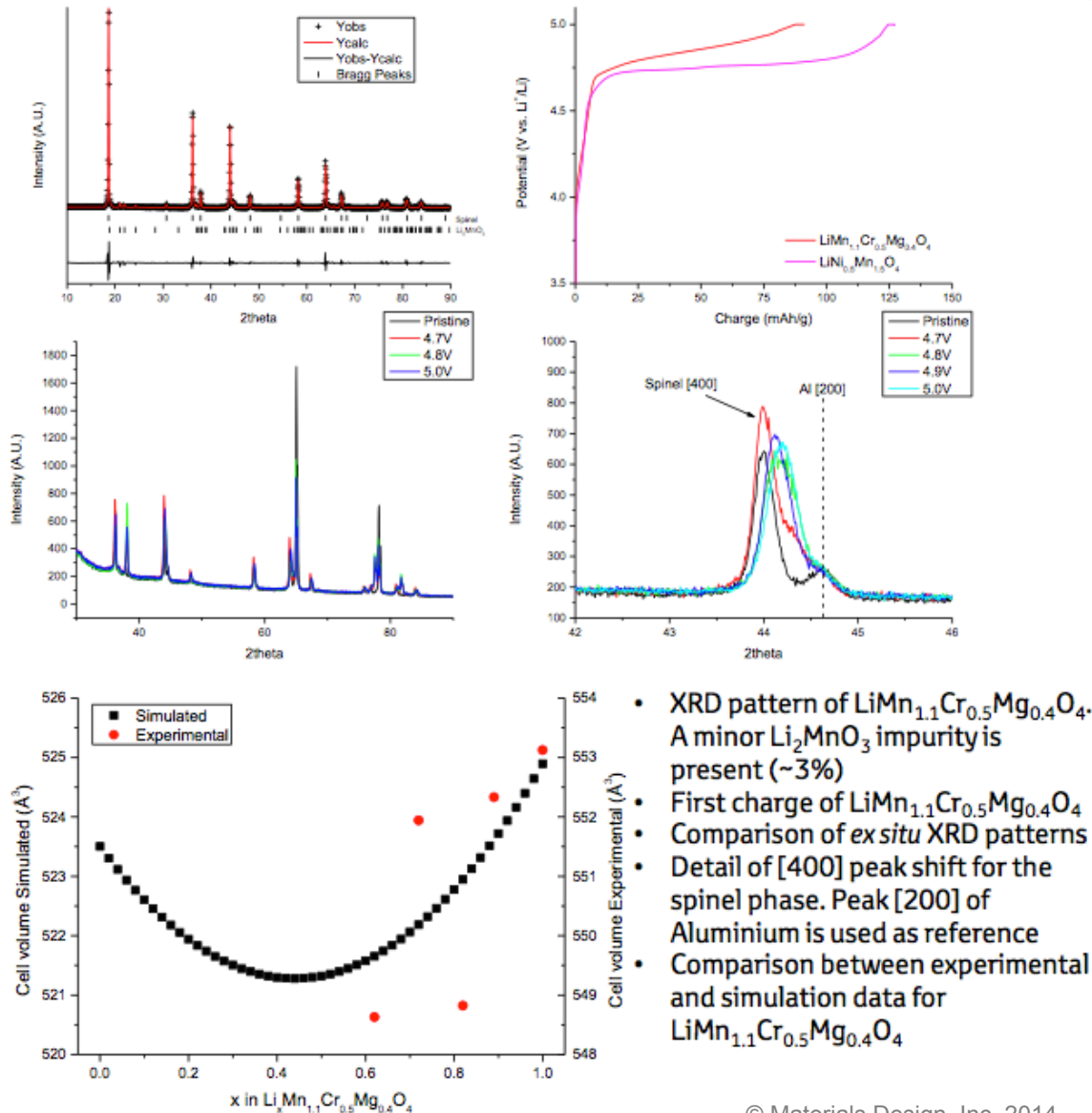
▶ $LiMn_{1.1}Cr_{0.5}Mg_{0.4}O_4$ could be synthesized in mostly pure form

▶ $LiMn_{1.1}Cr_{0.5}Mg_{0.4}O_4$ used to build electrochemical cells to study volume change on delithiation

▶ Measured volume change on lithiation/delithiation of $LiMn_{1.1}Cr_{0.5}Mg_{0.4}O_4$ in the range of $4Å^3$

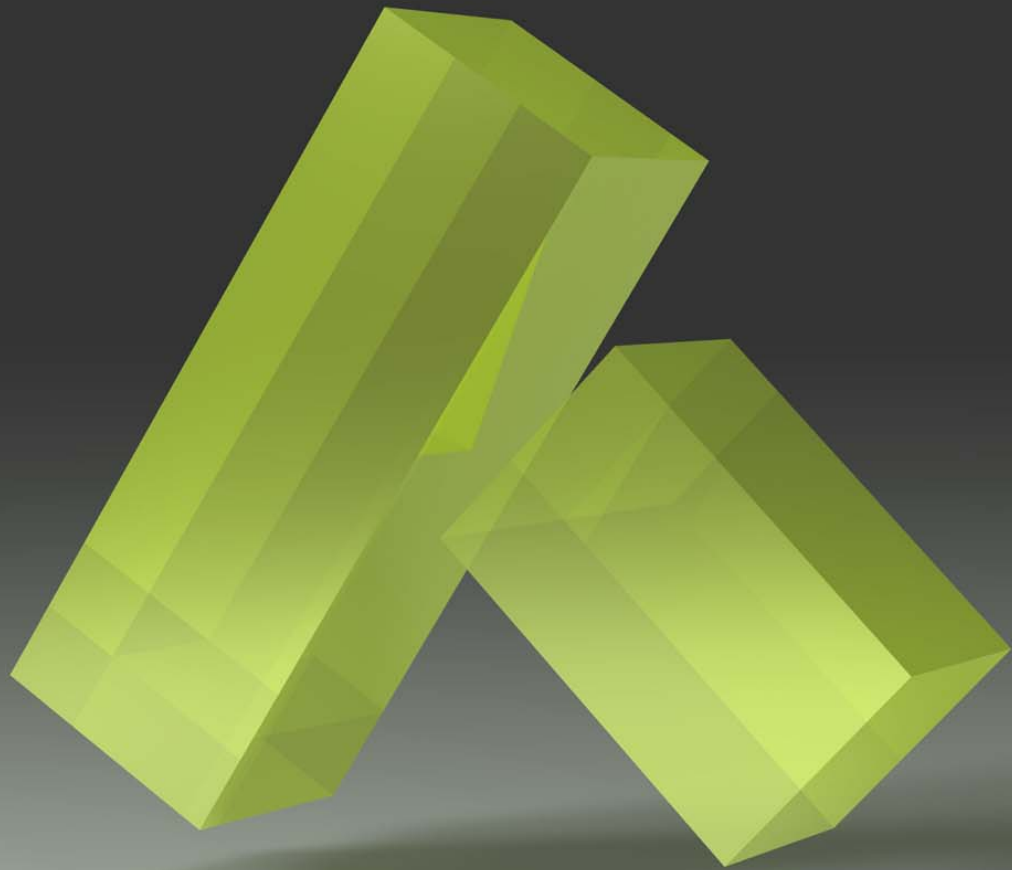F. Rosciano et al., IBA 2014

Summary and Perspectives

Summary

▶ DFT has become a standard in materials research

▶ A vast variety of properties can be calculated including

- structural, mechanical, thermodynamic, kinetic, electronic, optical, and magnetic properties

▶ Illustrative examples including

- H storage and diffusion in Ni

- Fracture at Zr grain boundaries

- Embrittlement of Cu microstructures

- Effective work function at the TiN/HfO_2 interface

- Schottky barriers (with impurities)

- Electrical conductivity of disordered intermetallics

- Low-strain cathode materials

Perspectives

▶ Current development efforts

- Simulation of alloys, e.g. ordering effects in $Cu_{1-x}Au_x$, $In_{1-x}Ga_xAs$
- Simulation of electronic and thermal conductivity

▶ Combined quantum mechanical and forcefield simulations

- Automated forcefields from quantum mechanical calculations
- Modeling kinetics
- Diffusion and segregation during processing and during operation

▶ Efficient use of large-scale computers

- Automation of simulation protocols (Flowcharts)
- Automated analysis of computed results
- BIG DATA, Materials Genome Initiative

▶ Combination with other engineering simulation software

Better materials with better simulations

www.materialsdesign.com